Network Dynamics in Olfactory Cortical Subregions

By

Matthew J. McGinley

A DISSERTATION

Presented to the Neuroscience Graduate Program,

Vollum Institute,

Oregon Health & Science University,

School of Medicine,

in partial fulfillment of

the requirements for the degree of

Doctor of Philosophy

June 2010

School of Medicine

Oregon Health & Science University

CERTIFICATE OF APPROVAL

This is to certify that the Ph.D. thesis of Matthew J. McGinley has been approved.

_____ (Gary Westbrook)

Mentor/Advisor

_____ (John Adelman)

Member/Chair

_____ (Craig E. Jahr)

Member

_____ (Larry Trussell)

Member

_____ (John T. Williams)

Member

TABLE OF CONTENTS

ACKNOWLEDGEMENTS

This dissertation would not have been possible without the help and support of many individuals. First, Gary Westbrook served as my advisor, providing resources to perform my work, enrichment opportunities outside of OHSU, as well as help with the writing process. I also warmly thank Lew Haberly and Sherry Feig at the University of Wisconsin for selfless assistance that was essential in getting started in the cortex of the olfactory system; this included help in development of a slice preparation used throughout the dissertation. Lew Haberly and Donata Oertel provided valuable feedback on the application for an NRSA grant which in part funded this work.

Members of the Westbrook lab provided much, and diverse, assistance, and my thesis committee gave valuable input. Hannah Monyer provided the opportunity to visit her lab to perform experiments on two of the transgenic mouse lines in Chapter 3. Two high school students in the Portland area: Neel Pandit and Brinda Gokul, provided assistance with immunohistochemistry on two other transgenic lines in Chapter 3. Finally, I would like to thank my partner, Sharon Anderson, and my parents, Paul and Jane McGinley, for unending and invaluable support.

ABSTRACT

There are three phylogenetic classes of cerebral cortex: archicortex (or hippocampus); neocortex (e.g. somatosensory and prefrontal cortex); and paleocortex, the cortex of the olfactory system. While archicortex and neocortex are among the most extensively studied brain regions, paleocortex has received comparatively little attention, particularly in the last two decades. As a result, physiological properties that are consider basic knowledge in other brain areas, such as distinguishing characterisitics of subregions and cell types, remain unknown in paleocortex. Interesting in its own right, paleocortex is also the evolutionary progenitor of neocortex. Therefore, insights into paleocortex have broad implications for cortical processing in general. Paleocortex has the technical advantages of its relatively simple layering and the compactness of the olfactory system. In this dissertation, I have sought to determine some of the basic physiological properties of the paleocortex, using whole-cell patch-clamp recordings in brain slices of juvenile mice. In Chapter 1, I developed a slice preparation containing several subregions of paleocortex, and used paired recordings to look at excitatory interactions across subregions. One subregion, the anterior olfactory cortex (AOC), had previously not been explored with whole-cell recording methods, so in Chapter 2, I characterized the intrinsic membrane and synaptic properties of pyramidal neurons in AOC. In chapter 3, I began to address the issue of cell types by characterizing the expression of 8 transgenic or knockin mouse lines. It is my hope that this dissertation will provide a foundation of tools and knowledge for further study of the paleocortex, as well as a few insights into its function.

BACKGROUND AND INTRODUCTION

The simple layering and vulnerability to seizures of the piriform cortex – the cortex of the olfactory system – make it useful for the study of cortical dynamics and epilepsy. Furthermore, the piriform cortex is the phylogenetic ancestor of neocortex (Jerison, 1990; Haberly, 1990), and therefore an interesting system in which to study basic questions of cortical function. The piriform cortex contains several subregions with functional specialization. Recent work has identified one subregion – the ventrorostral anterior piriform cortex ($APC_{V\text{-}R}$) – as particularly important for seizure initiation (Ekstrand et al., 2001a). The $APC_{V\text{-}R}$ is located immediately superficial to the physiologically defined "area tempestas," the site in the rat brain where the lowest concentrations of convulsants can elicit tonic-clonic seizures (Piredda and Gale, 1985). The "area tempestas," – also called pre-endopiriform nucleus (pEn) – and $APC_{V\text{-}R}$ are densely interconnected and share common immunocytochemical markers (Ekstrand et al., 2001a). The $APC_{V\text{-}R}$ projects heavily to the ventrolateral orbital cortex, an area of prefrontal cortex that integrates multimodal sensory input in primates (Rolls and Baylis, 1994).

This dissertation was motivated primarily by four network features that distinguish $APC_{V\text{-}R}$ from the remainder of piriform cortex. First, the dense interconnectivity between the $APC_{V\text{-}R}$ and pEn (Ekstrand et al., 2001a). Second, tufted cells in the olfactory bulb project selectively to the $APC_{V\text{-}R}$, and to the neighboring anterior olfactory nucleus (AON), whereas the main projection neurons of the olfactory

bulb – mitral cells – project to the entirety of olfactory cortex. Third, AON neurons project forward to the anterior piriform cortex – mostly to $APC_{V\text{-}R}$ – with an unusual termination pattern: on proximal dendrites adjacent to the cell bodies of piriform pyramidal neurons. And fourth, immunolabeling of axo-axonic terminals on axon initial segments, and of cholecystokinin positive (CCK+) basket cells, are lacking in the $APC_{V\text{-}R}$, while prominent in the remainder of piriform cortex (Ekstrand et al., 2001b). Axo-axonic and basket endings powerfully inhibit piriform cortical pyramidal cells. So their absence in $APC_{V\text{-}R}$ and pEn could promote epileptogenicity. These four previously established network features led me to the hypothesis that tufted cell excitation, and feedforward of tufted cell excitation via the AON, coupled with the absence of certain inhibitory interactions, contribute to the epileptogenicity of the $APC_{V\text{-}R}$. I also wondered what special roles these four properties play in normal cortical function.

The basic wiring of the olfactory system: pathways to cortex.

In the olfactory epithelium, where odorants are first detected, a given olfactory receptor neuron expresses a single molecular species of olfactory receptor. All receptor neurons expressing a given receptor species map their axons selectively to only a few glomeruli in the olfactory bulb (Buck, 1996). Processing in the olfactory bulb is complex. The bulb is layered, as follows (from superficial-to-inward): the glomerular layer, the external plexiform layer, the mitral cell body layer, the inner plexiform layer, and the granule cell layer (Figure 1). The glomerular layer contains the apical dendritic tufts of mitral and tufted cells, and also juxtaglomerular cells, including external tufted cells. The external plexiform layer contains a network of dendrites from granule, mitral, and tufted

cells, as well as the cell bodies of middle and internal tufted cells. The internal plexiform layer contains the dendrites of granule cells, whose somas are in the granule cell layer. The principal neurons of the bulb (mitral and tufted cells) receive input from a single glomerulus, but map their axons broadly and diffusely over olfactory cortical areas.

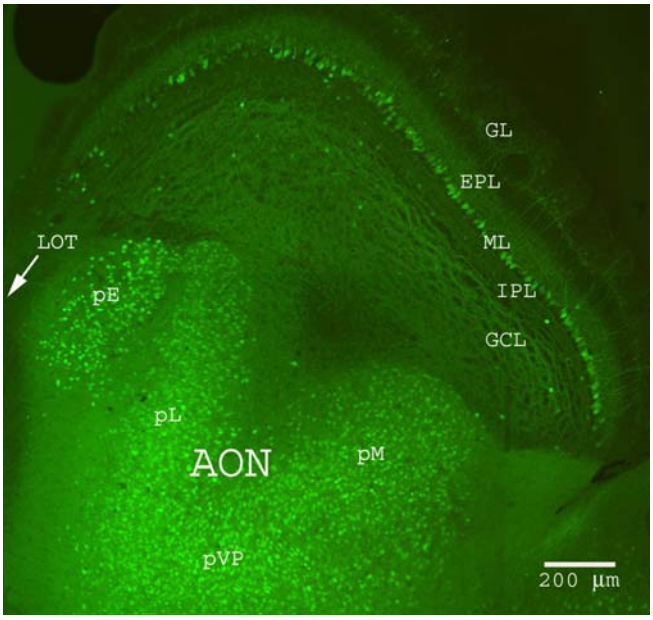

Figure 1. Confocal z-stack image of the olfactory bulb and anterior olfactory nucleus (AON) from a Thy-1 YFP transgenic mouse (line G, Guoping Feng). Layers of the olfactory bulb: GL- glomerular layer (contains the axonal terminations of olfactory receptor neurons, the apical dendritic tufts of mitral and tufted cells, and periglomerular and external tufted cells); EPL- external plexiform layer (contains a network of dendrites from granule and mitral cells, as well as the cell bodies and dendrites of middle and internal tufted cells); ML- mitral cell layer; IPL- internal plexiform layer (contains the dendrites of granule cells); GCL- granule cell layer. LOT- lateral olfactory tract. Subregions of the AON: pE- pars exterior, pL- pars lateralis, pVP- pars ventroposterioralis, pM- pars medialis. The slice was cut at an angle between coronal and horizontal.

The physiology of the piriform cortex

The piriform cortex, the largest olfactory cortical area, provides a model for the more complex (six layered) neocortex, and for associative learning (Haberly and Bower, 1989; Johnson et al., 2000; Neville and Haberly, 2004). Piriform cortex is also layered. *Layer Ia* contains afferent fibers from the olfactory bulb via the lateral olfactory tract (LOT). *Layer Ib* contains association fibers from other parts of the piriform cortex and from other cortical areas. *Layer II* contains the cell bodies of pyramidal cells, and *Layer III* contains associational fibers and synapses, and the axons of piriform cortical pyramidal cells (Figure 2). The piriform cortex is often divided into anterior and posterior

subregions, based on the path of the LOT. The LOT covers the AON and coalesces into a visible band over the surface of the anterior piriform cortex, and ends at the border with the posterior piriform cortex (Price and Sprich, 1975).

The physiology of afferent and associational synapses, and temporal patterns of activity, in piriform cortex, have been studied using whole-cell and extracellular recording techniques. Stimulation of the LOT triggers a monosynaptic EPSP, generated in *layer Ia*, followed by a disynaptic EPSP, generated in *layer Ib* by the associational fiber system (Ketchum and Haberly, 1993). Afferent and associational synapses in piriform cortex show long-term potentiation (LTP) with properties similar to the CA1 region of hippocampus (Jung and Larson, 1994; Collins, 1994). LTP at associational synapses is easier to induce and more prominent in its expression than LTP at afferent synapses (Collins, 1994; Kanter and Haberly, 1990), consistent with the larger complement of NMDA receptors at associational than at afferent synapses (Franks and Isaacson, 2005). Associational and afferent synapses can also be distinguished by the influence of $GABA_B$, mGluR, and cholinergic receptors on synaptic transmission (Hasselmo and Bower, 1991; Hasselmo and Bower, 1992; Tang and Hasselmo, 1994). However, none of these studies distinguished between mitral and tufted cell inputs.

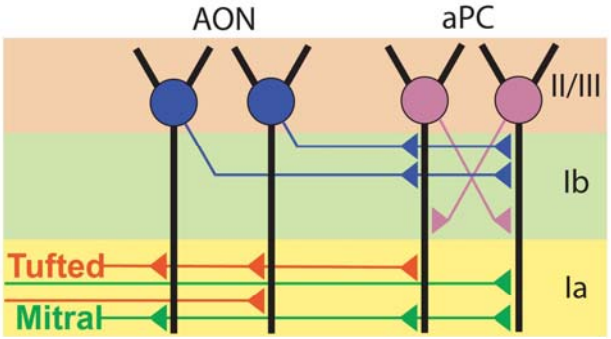

Figure 2. Diagram illustrating the layering of synaptic connections in paleocortex, including the selective termination of tufted cells in AON (AOC) and $APC_{V\text{-}R}$, the proximal location of AON inputs to piriform pyramidal neurons, and the associational connectivity within APC.

Receptive fields in piriform cortex consist of diffuse ensembles of cells, and are plastic (Wilson, 2001). At the behavioral level, experience shapes the detection of odors differently in anterior than in posterior piriform cortex, as anterior piriform encodes synthetic odorant identity whereas posterior piriform encodes odor similarity or quality (Kadohisa and Wilson, 2006). The cellular mechanisms that underlie the receptive fields of piriform cortical neurons are not known. A recent study indicates that single fiber LOT input to the piriform cortex has a wide range of response amplitudes, with some inputs leading to very large responses (Franks and Isaacson, 2006). The diffuse anatomical mapping from olfactory bulb to cortex is recapitulated in responses to individual odorants in AON and piriform cortex – in c-fos expression and 2-photon calcium imaging – in which there is a trend such that activity is progressively more diffuse as one moves caudally across the cortex (Illig and Haberly, 2003; Stetler and Axel, 2008). *In vivo* recordings indicate that receptive fields are broader in AON neurons than mitral cells (Boulet et. al., 1978; Lei et al., 2006), but narrower in anterior piriform neurons (Wilson, 2001).

The AON in olfactory cortical processing

The olfactory cortex and piriform cortex are often taken to be synonymous. In reality, the olfactory cortex consists of several brain areas. One of these, the anterior AON, is the predominant olfactory structure that bilaterally integrates exclusively olfactory information (Brunjes et al., 2005). It is located in the olfactory peduncle, between the olfactory bulb and anterior piriform cortex. The entire AON receives strong input from the ipsilateral olfactory bulb, and is typically divided into five or six

subregions on the basis of projection patterns and cytoarchitecture (Figure 1; Haberly and Price, 1978; Brunjes et al., 2005). The *pars externa* forms a border between the olfactory bulb and the remainder of the AON (Figure 1), receives topographically organized input from the bulb, and projects exclusively to the contralateral bulb, in a topographical fashion (Scott et al. 1985). The medial subdivision of AON, *pars medialis* projects exclusively to the ipsilateral bulb, also with topographical specificity. The remaining subdivisions are the *pars lateralis*, *pars dorsalis*, and the *pars ventroposterioralis,* which is sometimes broken down into *pars ventralis* and *pars posteroralis*. These subregions project bilaterally to the olfactory bulbs, with unique patterns of termination in terms of overall topography and layer specificity (Davis and Macrides, 1981) and have been collectively termed the anterior olfactory cortex (AOC; Haberly, 2001). The subregions of AON that comprise the AOC have prominent feedforward projections to the ipsilateral anterior piriform cortex (Haberly and Price, 1978). The *pars ventroposterioralis* projects to the periglomerular region of the olfactory bulbs (Luskin and Price, 1983a).

There have been several proposals for the function of the AON in olfaction. Anatomical and immunohistochemical data suggest that the AON inhibits the olfactory bulb, coordinates the functions of olfactory bulbs bilaterally, and excites the piriform cortex (Alheid et al. 1984; Reyher et al., 1988). Although odors are deconstructed into a combinatorial representation of their chemical features in the first stages of processing, odors are perceived as singular percepts, indicating that encoded molecular features must be integrated downstream of the olfactory bulb (Buck, 1996). The AON receives almost exclusively olfactory input, from the olfactory bulb and the piriform cortex. In contrast, the piriform cortex receives substantial input from non-olfactory brain regions,

suggesting that it plays a more complicated associational role, integrating olfactory information with other modalities (Johnson et al., 2000). Based on these suggestions, AON has been proposed as the "primary cortex" of the olfactory system (Haberly, 2001). The development of the commissural pathways, which connect heavily with the AON, allows for bilateral recall of memories that were trained on only one side, suggesting a role for the AON in plasticity of olfactory representation (Haberly and Price, 1978; Kucharski and Hall, 1987). In addition to the throughput afferent pathway to piriform cortex, feedforward, lateral, and feedback pathways connect the piriform cortex and olfactory bulb. Some of these pathways are direct synaptic linkages (Pinching and Powell, 1972; Luskin and Price, 1983a&b; Lodovichi et al., 2003; Hayar et al., 2004). Based on the evidence that AON is a major crossroads of olfactory information (Yan et al., 2008), perhaps the AON is a substrate for the close tie between olfactory perception and memory (Wilson and Stevenson, 2003). Yet, there have been only a few physiological studies to include the AON, and none at the level of whole-cell recording (Nakajima and Iwasaki, 1973; Boulet et al., 1978; McNamara et al., 2004; Lei et al., 2006).

Feedforward excitation from AON to piriform cortex

The piriform cortex is an elaborate associative network, with inputs from diverse non-olfactory brain regions as well as from within piriform cortex. Synapses of mitral and tufted cells are segregated from associational fibers on apical dendrites of pyramidal cells in the piriform cortex. Specifically, olfactory bulb input impinges on the far distal dendrites in layer Ia. Associational inputs in piriform cortex havev an orderly

arrangement in layer Ib, with increasingly distal dendrites receiving input from progressively rostral cortex, carrying more olfactory and less extrinsic information (Figure 2; Luskin and Price, 1983b). AON input to piriform cortex, in contrast, arises from the most rostral source, but arrives at synapses directly adjacent to the cell bodies of piriform cortical pyramidal cells, suggesting that AON feedforward excitation of olfactory bulb is a special, perhaps driving, input to APC. This circuit has similarities to input from the entorhinal cortex, which terminates directly on CA3 pyramidal neurons on their distal dendrites and is also fed forward via the dentate gyrus to the proximal dendrites of CA3 neurons via the perforant path. Also analogous to the hippocampus, piriform pyramidal neurons form associative connections with each other on their proximal dendrites throughout an intermediate dendritic layer (*layer Ib*; Haberly, 2001). The strength of input to $APC_{V\text{-}R}$ is of particular interest owing to the high susceptibility of $APC_{V\text{-}R}$ to epileptogenesis (Piredda and Gale 1985).

The role of tufted cells

Ramón y Cajal distinguished three types of tufted cells – external, middle, and internal – on the basis of the location of their cell bodies in the layers of the olfactory bulb (Cajal, 1911; Figure 1). External tufted cell bodies are located in the glomerular layer. They coordinate activity within each glomerulus, and project predominantly to specific locations in the granule cell layer of the contralateral olfactory bulb (Pinching and Powell, 1972; Hayar et al., 2004; Belluscio et al., 2004) whereas a few ascend to the ipsilateral cortex (Haberly and Price, 1977). Middle and internal tufted cells (hereafter referred to collectively as tufted cells) have their cell bodies in the external plexiform

layer and, along with mitral cells, form the predominant ascending pathway to the ipsilateral olfactory cortex (AON, piriform cortex, olfactory tubercle, and lateral entorhinal cortex; Haberly and Price, 1977; Orona et al., 1984). Tufted cells project exclusively to the AON and the ventrorostral portion of the APC ($APC_{V\text{-}R}$), whereas mitral cells project across the entire rostro-caudal extent of piriform cortex (Haberly and Price, 1977, Scott et al. 1985).

Mitral and tufted cell inputs are often lumped together in studies of piriform cortex (Franks and Isaacson, 2005; Franks and Isaacson, 2006; Suzuki and Bekkers, 2006). Yet, several lines of evidence suggest that tufted cells are more strongly activated by odorants than mitral cells. Extracellular and intracellular recordings initially showed that tufted are more excitable in response to olfactory nerve stimulation than cells identified as mitral projecting to more caudal regions of the piriform cortex (Schneider and Scott, 1983). Tufted cells respond to odorants with more vigorous firing than mitral cells (Nagayama et al., 2004). Furthermore, in slices, tufted cells are less inhibited by neighboring glomeruli than mitral cells (Christie et al., 2001). I hypothesized that the central projection of tufted cells excites AON and $APC_{V\text{-}R}$ more strongly than mitral cells excite the remainder of olfactory cortex, thus driving feedforward excitation in the olfactory cortex. The selective regional projection of tufted cells suggests that they play a special role in feedforward excitation and epileptogenic network dynamics.

The '*area tempestas*' and epileptogenesis in olfactory cortex.

The ventrorostral anterior piriform cortex ($APC_{V\text{-}R}$) is reciprocally connected with the pre-endopiriform nucleus (pEn), originally called "area tempestas," where picomolar

amounts of GABAergic antagonists can elicit tonic-clonic seizures (Piredda and Gale, 1985). The $APC_{V\text{-}R}$ can initiate epileptic activity that propagates to the entorhinal cortex and hippocampus (de Curtis, et al., 1994). Interactions between the entorhinal cortex and the hippocampus, and their involvement in the *propagation* of tonic-clonic seizure activity, have been studied *in vivo* and *in vitro*, including in response to stimulation of the LOT (Gnatkovsky and de Curtis, 2006). The propagation of epileptiform discharges in piriform cortex is mediated by longitudinal associational fibers, and this has been recapitulated in a rat brain slice that contains these fibers (Biella et al., 1996; Demir et al., 2001).

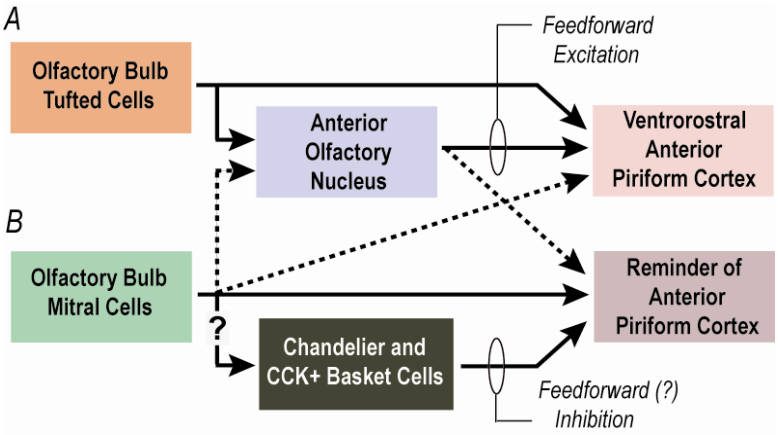

Interneurons in olfactory cortical epileptogenesis

GABAergic interneurons are known to play a role in seizure propagation in the neocortex and hippocampus (Trevelyan et al., 2007). There is a rich network of GABAergic interneurons in the piriform cortex, with cell body populations and terminations in all three cortical layers (Neville and Haberly, 2004). Notably, the $APC_{V\text{-}R}$ lacks the axo-axonic “cartridge” endings of chandelier neurons, and contains low levels

of CCK-positive cell bodies (Figure 3, Ekstrand et al., 2001a&b). Cartridge and basket endings (both GABAergic) encase the initial segments and cell bodies of pyramidal cell axons, respectively, and therefore can powerfully shunt action potential initiation (Freund and Buzsáki, 1996). On the other hand, recent evidence has suggested that axo-axonic and basket inputs may be excitatory (Szabadics et al., 2006; Woodruff et al., 2006). Perhaps the absence of these inhibitory connections contributes to the susceptibly of $APC_{V\text{-}R}$ to seizure initiation.

Summary

In Chapter 1, I studied the integration of AON into activity generated in $APC_{V\text{-}R}$ and pEN. I restricted study to *pars lateralis* of AON, because of its convenient location directly under the LOT, and its interconnectivity with piriform cortex. For simplicity of description, I hereafter will refer to *pars lateralis* of AON simply as AON, or AOC, unless otherwise specified. Excitatory interactions between AON and piriform cortex are addressed in Chapter 1, including the somewhat surprising finding of evidence for strong feedback, but not feedforward, excitation in the circuit. In Chapter 2, I examined the synaptic properties of lateral olfactory tract inputs to the AON, the extent of local connections, and the intrinsic membrane properties of AON principal neurons. Chapter 3 describes efforts to target perisomatic targeting interneurons for whole cell recording using mutant mouse lines. The selective projection of tufted cells was a primary motivation for this dissertation, and efforts to selectively target tufted cell axons for electrical stimulation are also discussed in Chapter 3.

Widespread coherent activity in an excitatory synaptic network

Matthew J. McGinley and Gary L. Westbrook

Vollum Institute

Portland, OR 97239

Address correspondence to:

Matt McGinley

Vollum Institute, L474

3181 SW Sam Jackson Park Road

Portland, OR 97239

Email: matthew.j.mcginley@gmail.com

Acknowledgements

We thank Lew Haberly and Sherry Feig for help in developing the slice preparation and critical conversations regarding olfactory cortex. We also thank Gordon Pipa for suggestions regarding analysis and statistics and Peter Huybers for Matlab code. This work was supported by F31-NS058196 (MJM), a Max Planck Research Award (GLW) and NIH grant NS26494 (GLW).

Author Contributions

M.J.M. designed the study, collected the data, performed the analyses, and wrote the paper. G.L.W. designed the study and wrote the paper.

Abstract

Sensory input to the olfactory cortex is highly distributed, but how activity is shaped within the cortex is not well understood. Here, we examined the topology of the excitatory network within olfactory cortex using an impulse-response approach and paired whole-cell voltage-clamp recordings. Neurons in anterior olfactory cortex, the most rostral cortical subregion, were recorded in pairs with neurons in the piriform network. A network burst of excitation was triggered by low amplitude electrical stimulation of lateral olfactory tract inputs from the olfactory bulb. Principal neurons in anterior olfactory cortex received powerful feedback that was driven by the piriform network. The latency and waveforms of network bursts were strikingly coherent across millimeters of olfactory cortex. These results suggest that widespread and overlapping, rather than columnar, interactions dominate excitatory functional connectivity in olfactory cortex. An excitatory network with widespread interactions may facilitate olfactory coding given the high dimensionality of olfactory space.

Introduction

In response to an odorant, sensory activity, as detected by 2-deoxyglucose, c-fos expression, multiunit recording, or calcium imaging, is distributed broadly throughout the olfactory cortex (Cattarelli, et al., 1988; Illig et al., 2003; Rennaker et al., 2007; Stettler and Axel, 2009). At the single cell level, neurons in piriform cortex, and neighboring anterior olfactory cortex, have broad receptive fields (Haberly et al., 1969; Lei et al., 2006). Furthermore, axons of pyramidal neurons in piriform cortex ramify widely within the olfactory cortex, with patchiness apparent on only a very broad scale (Johnson et al., 2000). These patterns suggest that sensory processing in the olfactory cortex relies on spatially distributed and overlapping neuronal ensembles (Haberly, 2001) rather than the modular organization typical of sensory cortex (Mountcastle, 1997).

However, physiological and anatomical features discriminate subregions of the olfactory cortex. For example, odorant identity and similarity may be separately encoded in anterior and posterior piriform cortex, respectively (Kadohisa and Wilson, 2006), suggesting specialized functional networks. Likewise, neuronal responses in piriform cortex appear to be specific for categories of odorants (Yoshida and Mori, 2007). From an anatomical perspective, the anterior olfactory cortex (AOC; also called anterior olfactory nucleus, AON) has fewer layers than the more caudal three-layered piriform cortex (Behan and Haberly, 1999). The endopiriform nucleus and adjacent pre-endopiriform nucleus (pEN), which together underlie the piriform cortex, have denser local connectivity compared to the overlying piriform cortex (Behan and Haberly, 1999; Ekstrand et al., 2001). The pEN has been identified as the

‘area tempestas,’ a sensitive epileptogenic locus (Piredda and Gale, 1985) that has dense reciprocal connectivity with the overlying ventro-rostral anterior piriform cortex ($APC_{V\text{-}R}$; Ekstrand et al., 2001).

To study functional connectivity of the olfactory cortex, we isolated the excitatory network using a tailored brain slice preparation that included the AOC, and several subregions of the piriform network: ventro-caudal anterior piriform cortex ($APC_{V\text{-}C}$), $APC_{V\text{-}R}$, and pEN, as well as connections between them. We took an impulse-response approach to probe the functional connectivity of the excitatory network by utilizing a dynamic circuit property shared by the hippocampus, neocortex, and piriform cortex: the generation of transient, all-or-none, network bursts of excitation with $GABA_A$ receptors blocked (Wong and Traub, 1983; Connors, 1984; Demir et al., 2001). We evoked network bursts with single weak stimuli to the lateral olfactory tract (LOT). We then analyzed the coherence between synaptic excitation in pairs of neurons, using a multitaper spectral analysis method that was optimized for high spectral resolution (Thomson, 1982; Percival and Walden, 1993; Huybers, 2004; Zoubir, 2009). Our results demonstrate a remarkable degree of coherence in excitatory activity across broad subregions, suggesting that distributed and overlapping connectivity dominates the excitatory network of olfactory cortex.

Results

Network bursts of synaptic excitation in olfactory cortex

In order to analyze the flow of excitation in olfactory cortex, we developed a slice preparation containing the anterior olfactory cortex (AOC), ventral anterior piriform cortex (APC_V) and subjacent pre-endopiriform nucleus (pEN) (**Figure 1A**; **Supplementary Figure 1**). We first recorded from pyramidal cells in the AOC, the most rostral cortical subregion contacted by axons from the olfactory bulb. Low intensity stimulation of the lateral olfactory tract (LOT; 0.05 - 0.1 Hz) evoked short latency inward currents (V_h = -75 mV, n= 10; **Figure 1B**). To isolate the excitatory synaptic network we blocked $GABA_A$ receptors with picrotoxin (50 μM), which unmasked a long-latency burst of inward current in response to LOT stimulation (**Figure 1B**, blue trace). These bursts were biphasic with decay time constants of 12.6 ± 1.1 and 185 ± 22 ms (n=9; **Figure 1B**, red curve). To isolate more discrete bursts of fast synaptic activity within the network, we added the NMDA receptor antagonist CPP (5 μM). NMDA receptor blockade did not affect the amplitude of bursts, but eliminated the slow phase, and revealed a slow outward current (**Figure 1C**) that could be blocked by the $GABA_B$ antagonist CGP55845 (10 μM, data not shown). Burst amplitudes were 491 ± 41 pA in control conditions (n=37) and 504 ± 14 pA in the presence of CPP (n=9, p=0.78).

Network bursts had an all-or-none threshold that was independent of the presence of short latency monosynaptic current in the recorded cell (**Figure 1C**, arrowhead**; Figure 1D**). Increasing the stimulus intensity, beyond threshold, shortened the latency to the bursts but did not increase their amplitude (n= 10, **Figure 1D**). As expected, the short-latency monosynaptic current gradually increased as stimulus intensity increased (n = 17, **Figure 1D**) indicative of graded direct input

from LOT fibers. The all-or-none characteristic, long-latency, and irregular shape of the bursts are consistent with network-generated activity. Network bursts occurred in all cells in all subregions tested with graded LOT stimulation: AOC (n= 50), APC_V, (n=30) and pEN (n=17). We used the bursts as an impulse response of the network to map excitatory interactions across olfactory cortical subregions. Network bursts in paired recordings had strikingly similar latencies for a given trial, even though the neurons were separated by as much as several millimeters (**Figure 1E**). Even more obvious, the shapes of bursts were much more similar between cells on a particular trial, compared to bursts in the same cell on repeated trials, as shown for a pair of cells in AOC and $APC_{V\text{-}C}$ (**Figure 1E**). This behavior suggested that neurons in the different subregions have a substantial amount of shared activity.

Initiation and propagation of network bursts

We first analyzed the latency to the onset of bursts, as well as the difference in latency between cells (lag) on each trial, in paired recordings across several subregions (**Figure 2A**). Burst onset was defined as the time when inward currents deflected from, and did not return to, baseline prior to large amplitude bursts (**Figure 2B**, arrowheads). For AOC / $APC_{V\text{-}R}$ pairs, the latency to the onset of bursts ranged from 20 to 90 ms from trial-to-trial (**Figure 2C**), but was highly correlated between cells on individual trials (ρ =0.97, p <10e-10, N=6 pairs, n=178 trials). Furthermore, the start of bursts in the AOC neuron lagged the neuron in $APC_{V\text{-}R}$ by 7.5 ±1.6 ms (p < 0.005; n=7, **Figure 2B,C,F**) and there was a trend for the AOC neuron to lag slightly more at longer latencies, reflected in the slope of the linear fit to the latency-

latency scatter plot (**Figure 2C,F**). For paired recordings between a neuron in AOC and a neuron in the more caudal $APC_{V\text{-}C}$ (**Figure 2D**), stimulus latencies were also highly correlated (ρ =0.95, p < 10e-10, N=7 pairs, n=180 trials). There was no consistent lag between regions (p=0.16; n=7; **Figure 2D,F**) whether stimulation was above AOC or above $APC_{V\text{-}C}$ (open vs. closed symbols, **Figure 2D,F**). Furthermore, there was not a trend in the lag across latency, as reflected in the near unity slope of the linear fit to the latency-latency scatter plot (**Figure 2D,F**). Latencies were again highly correlated between AOC and pEN (ρ = 0.51, p < 10e-10, N=9 pairs, n=139 trials; **Figure 2E**), and there was a consistent lag between regions (10.5 ± 1.5 ms, p < 0.0002; n=9; **Figure 2E,F**). The small slope in the latency-latency plot indicated that burst currents started much earlier in pEN neurons when latencies were long in the AOC neuron (**Figure 2E,F**). Our results indicate that network bursts first become detectable in pEN, irrespective of the site of stimulation.

The above analysis captures the timing of the start of burst activity, but not the timing of activity during each burst. To analyze intra-burst timing, we used cross-correlations of bursts in cell pairs from different subregions. Cross-correlations exhibited a single broad peak, as shown for an AOC-$APC_{V\text{-}R}$ pair (**Figure 3A,B**). The peak was consistently offset from 0 ms, indicative of a lag in the overall burst waveform between subregions (**Figure 3B**, vertical dashed line**)**. The bursts in AOC lagged all other subregions of the olfactory cortex, even though the site of stimulation was closest to AOC (**Figure 3C**). AOC lagged $APC_{V\text{-}R}$ by 10.0 ± 0.8 ms (n=10, p<5e-7), $APC_{V\text{-}C}$ by 4.8 ± 2.0 ms (n=8, p<0.03), and pEN by 4.9 ± 1.4 ms (n=9, p<0.01). Although the onset of burst activity was earliest in pEN, as shown in Figure 2, the

burst envelope in $APC_{V\text{-}R}$ led other subregions, as indicated by the lag at peak cross-correlation (**Figure 3C,** $F_{3,30} = 5.2$, $p < 0.005$). In paired recordings of two neurons in AOC, burst currents always occurred earlier in the more caudally located AOC neuron (3.6 ± 1.4 ms, n=4, p = 0.08), further evidence of the flow of activity from the piriform network toward AOC (**Figure 3C**). Consistent with the contribution of pEN in initiating network activity, burst currents were much larger in pEN neurons than in the other subregions (p < 1e-6; **Supplementary Figure 2A,C**). Action potential firing during network bursts was also more intense in pEN than in other subregions (p < 5e-5; **Supplementary Figure 2B,D**). Furthermore, the first spike in a burst tended to occur in pEN (**Supplementary Figure 2E,F**). The relative timing of burst start time and cross-correation peak lag, taken together, suggest that the mechanism of burst generation involves synaptic interactions between the $APC_{V\text{-}R}$ and pEN.

When the AOC and piriform network were separated with micro-cuts (**Figure 4A**), network bursts did not occur in AOC even with strong stimulation of the LOT (n=25 (control); n=9 (cut); **Figure 4B,C**, left). In contrast, bursts were present in $APC_{V\text{-}R}$ pyramidal neurons (**Figure 4B**, right), and had similar amplitudes (n=8 (control); n=2 (cut); **Figure 4C**, right). The absence of bursts in AOC neurons did not result from a reduction in afferent input, because stimulation of LOT in cut slices evoked short latency currents (**Figure 4B**, left, arrowhead) that were not different in amplitude from control slices (n=6 (control); n=7 (cut); **Figure 4C**, left; p = 0.44). Thus, the piriform network is required for network bursts in AOC.

Widespread coherence of network burst currents

In addition to the consistency in latencies, the shape of burst waveforms appeared remarkably consistent in pairs on the same trial, suggesting tightly coupled synaptic interactions between subregions. As mentioned previously, this similarity was first apparent when visually comparing the shapes of bursts between cells on a single trial to the shapes in the same neuron across trials of identical stimulation (see **Figure 1E**). We sought to quantitatively evaluate this similarity. Cross-correlation was not appropriate because peaks in cross-correlation can occur even when completely independent cell ensembles are simultaneously stimulated and thus do not necessarily indicate network interactions between subregions (Brody, 1999a). Therefore we calculated the covariation and coherence between burst currents. Covariation, by removing off trial cross-correlation, provides a way to determine if correlated activity between pairs is independent, or if it reflects shared synaptic activity (Brody, 1999b). Coherence identifies the degree of shared spectral content, thus providing insight into the fine temporal structure of correlated activity (Thomson, 1982; Huybers, 2004; Senkowski et al., 2008; Wehr and Laurent, 1999).

We first assessed the coherence and covariation in network bursts for the adjacent subregions, AOC and $APC_{V\text{-}R}$. For a set of trials from an example pair shown in **Figure 5A1**, there was a peak in coherence at low frequencies (< 75 Hz), and smaller peaks that persisted at higher frequencies (**Figure 5A2**), as well as a single broad peak in covariation (**Figure 5A2**, inset). Because burst latencies were highly correlated between these subregions (see Figures 2 and 3), we wondered whether latency covariation could account for the observed coherence and covariation. To accomplish this, we used a simplex optimization routine to align the

bursts across trials, and eliminate the latent period (**Figure 5B1**; see **Methods**; **Supplementary Code**; Brody, 1999b). Aligned traces showed no apparent reduction in the coherence (**Figure 5B2**), but covariation was reduced to nearly insignificant levels (**Figure 5B2**, inset). Therefore, the coherence between subregions could not be attributed to latency covariation.

To further isolate the trial-specific coherence of burst waveforms, we calculated the mean burst for each cell, and subtracted the mean from each individual trace, resulting in 'residual' currents (**Figure 5C1**). As expected, residual currents showed reduced coherence below 75 Hz, because the consistent envelope of the response, that dominated coherence at low frequencies, was eliminated. However, coherence above 75 Hz was minimally affected by mean subtraction (**Figure 5C2**). Therefore, the coherence at higher frequencies reflects the trial-specific fine timing of synaptic events.

We assessed the significance of coherence by comparing the bursts with a preceding baseline period. Population results for baseline and signal coherence, for paired recordings between neurons in AOC and $APC_{V\text{-}R}$, are shown in **Figure 6A**. For raw bursts and latency adjusted bursts, coherence between AOC and $APC_{V\text{-}R}$ was significantly above baseline up to 500 Hz ($p < 0.05$; **Figure 6A**). The inset shows coherence in the 0–40 Hz range. Coherence of residual currents was reduced below 75 Hz, but was still above baseline ($p < 0.05$; **Figure 6A)**. Along with the reduction in coherence magnitude, the consistency of the phase across trials was reduced at low frequencies for residual currents (**Supplementary Figure 3A**). Similar coherence and phase consistency were observed for paired recordings between AOC and $APC_{V\text{-}C}$

(**Figure 6B**; **Supplementary Figure 3B**), even though the neurons were separated by 3–4 millimeters in these recordings. Thus, the peaks in the coherence spectra in the 75–500 Hz range provided a robust measure of shared synaptic input, which persisted across broad subregions of the olfactory cortex.

Discussion

We used paired whole-cell recording to assay the functional connectivity of excitatory synapses in the olfactory cortex. Threshold lateral olfactory tract (LOT) stimulation evoked network burst synaptic currents in disinhibited slices with remarkably similar latencies and waveforms across pairs on each trial. Bursts originated in $APC_{V\text{-}R}$ / pEN and then spread to more rostral and caudal regions. These results suggest a highly interconnected excitatory network that extends throughout the AOC and piriform cortex. Such a distributed and overlapping excitatory synaptic network may be a unique characteristic of olfactory cortex compared to sensory neocortex.

Probing the excitatory synaptic network in olfactory cortex

Coordinated excitatory activity *in vivo* may be driven or modulated from other brain areas (Ketchum and Haberly, 1993; Neville and Haberly, 2003), and shaped by inhibition (Hasenstaub et al., 2005; Luna and Schoppa, 2008) as well as intrinsic membrane properties (Suzuki and Bekkers, 2006). In order to isolate the excitatory synaptic network within the olfactory cortex, we blocked inhibition and tailored a brain slice to include the anatomical subregions of the olfactory cortex that receive

the most input from the olfactory bulb. A single weak stimulation of the LOT generated a short burst of activity that served as a probe of the underlying network topology, much as impulse functions are used in systems analysis.

Although the network bursts clearly do not exactly recapitulate cortical activation *in vivo*, the effectiveness of weak stimulation indicates that network bursts are not a pathological response to supramaximal stimulation, but rather provide a trigger for activity that reflects the architecture of the intrinsic excitatory circuitry. Such bursts are not unique to these conditions, as burst activity in the piriform network can be generated after *in vivo* kindling, induction of synaptic plasticity, disinhibition, or in normal conditions with paired stimulation (Hoffman and Haberly, 1991; Hoffman and Haberly, 1996; Demir et al., 2001; Tseng and Haberly, 1989). Block of inhibition has been used to good advantage in other brain regions to focus on network dynamics and function, revealing spiral waves in neocortex (Huang et al., 2004) and laminar features of the excitatory circuit in motor cortex (Weiler et al., 2008). Analysis of the timing of network bursts provides a map of the functional connectivity between subregions of the olfactory cortex. The network bursts originated in pEN and propagated by $APC_{V\text{-}R}$ to other subregions. This pattern is consistent with the dense anatomical connectivity between pEN and $APC_{V\text{-}R}$ (Ekstrand et al., 2001), the seizure susceptibility of pEN (Piredda and Gale, 1985), and the hyperexcitability of the surrounding endopiriform nucleus (Demir et al., 2001; Hoffman and Haberly, 1991; Hoffman and Haberly, 1996; Tseng and Haberly, 1989). Thus, features of the functional excitatory connectivity in pEN are likely to contribute to normal cortical function as well as seizure generation.

Coherence analysis of synaptic currents

Cross-correlation between paired measurements of network bursts was useful in our experiments in revealing latency characteristics, and thus patterns of flow of excitatory synaptic activity between olfactory cortical subregions. However, spurious peaks in cross-correlation can arise from a variety of causes (Brody, 1999a). Specifically, simultaneous stimulation of two cells can cause peaks in cross-correlation, indicating synchrony, even in the complete absence of network interactions (Brody, 1999a). Thus, additional analysis is needed to examine network interactions. We observed peaks in covariation, the trial-specific component of cross-correlation, indicating interaction between neurons across subregions (Brody, 1999b). However, much of the covariation could be accounted for by latency, and thus provides limited information about the fine timing of synaptic interactions between subregions. In addition, cross-correlation and covariation have limitations because they are derived from the 'periodogram.' In general, the periodogram is a biased estimator of the true spectral density; has large variance; suffers from spectral leakage; and requires large sample sizes (Thomson, 1982; Percival and Walden, 1993).

Our use of a coherence analysis method with improved spectral characteristics addressed the shortcomings of cross-correlation and covariation. Coherence analysis has been applied extensively to paired EEG, MEG, unit, and field recordings (Senkowski, 2008), but much less frequently for cellular level signals (Wehr and Laurent, 1999). The combination of an improved coherence analysis with the high

temporal resolution and signal-to-noise ratio of paired voltage clamp data is ideally suited to extract information on fine timing in synaptic networks. To improve the spectral characteristics in our coherence analysis, we developed an estimator based on the multitaper method (Thomson, 1982). The method incorporated adaptive weighting to reduce variance and bias in power spectra (Thomson, 1982), correction for the upward bias inherent in coherence calculations (Huybers, 2004), and a robust bootstrap statistical procedure (Zoubir, 2009). We also developed a flexible method for dealing with averaging across trials (**Supplementary Code**). The coherence between olfactory cortical subregions was striking in that it was present between widely separated regions and across a wide range of frequencies, in all pairs tested. In relating the spectral components of the coherence to the time domain, coherence below 75 Hz could be attributed to the envelope of the burst responses, as subtraction of the average response reduced the amplitude of coherence in this frequency range. More interestingly, coherence above baseline was apparent throughout the 75-500 Hz range, reflecting network interactions of action potentials and synaptic events. The significant coherence in this frequency range thus provides a unique measure of excitatory interactions, indicating the high degree of functional network interconnectivity across subregions of olfactory cortex.

Widespread coherence in excitatory networks

What features of networks lead to widespread bursts and what features lead to widespread coherence during bursts? Much more is known about the former than the latter. Excitatory associational connections between pyramidal neurons are a

prominent feature of the piriform cortex (Johnson et al., 2000; Haberly, 2001), and this circuit feature is a likely factor in facilitating burst generation (Demir et al., 2001). Interestingly, the piriform cortex and the burst-prone CA3 region in hippocampus are thought to have the densest associational connectivity in the brain (Haberly, 2001). Indeed, the hippocampus, as well as neocortex, generates all-or-none network burst activity (Wong and Traub, 1983; Connors, 1984; de la Prida, 2006). Theoretical work has shown that networks of sparsely connected neurons can generate burst activity, such as the network bursts we observed, when certain criteria are met. Specifically, when connectivity in the network has a density above a certain threshold (Golomb, 1998); the strength of individual connections are low (Golomb and Hansel, 2000); and background firing rates are low (Kumar et al., 2008). Burst generation is not a ubiquitous feature of olfactory cortex, because isolated AOC had no network bursts, even with strong stimulation.

Networks that generate all-or-none bursts may or may not exhibit widespread coherence. Rather, only certain network architectures are consistent with what we observed in olfactory cortex. Axons of pyramidal neurons in piriform cortex have highly distributed patterns (Johnson et al., 2000), but pairs of neurons across subregions were not monosynaptically connected (data not shown). Thus, the olfactory cortex cannot be viewed as an all-connects-to-all network. If the olfactory cortex was strongly organized into distributed subnetworks, paired recordings would be expected to sample across subnetworks, and thus not exhibit widespread coherence (Voges et al., 2009). Therefore, the occurrence of widespread coherence seems to suggest a lack of strong subnetwork architecture in the excitatory network of

olfactory cortex. The short lags between bursts in different subregions, and known anatomical features (Johnson et al., 2000; Haberly et al., 2001; Behan and Haberly, 1999), are not consistent with 'lattice' architecture, the extreme representation of modular or columnar organization (Mountcastle, 1997).

These constraints raise the possibility that the organization of excitatory connections in the olfactory cortex is random (Stettler and Axel, 2009). Simulated random networks support widespread coherence and have the capacity for associative memory (McGraw and Menzinger, 2003), a proposed function of the olfactory cortex (Johnson et al., 2000; Haberly et al., 2001). However, the tendency of the deep subregions of the piriform network to drive activity, indicated by strong and early synaptic activation, indicates that the excitatory network in olfactory cortex is not a random network. Rather, neurons in the pEN and EN may act as 'hubs,' generating more connections to other neurons in the olfactory cortex than are generated by neurons in other subregions. Furthermore, the known dense interconnection within pEN and EN creates a second level of hub architecture, preferentially connecting the primary hubs to each other, a hallmark of so-called power-law or scale-free networks (Barabasi and Albert, 1999). The driving role of pEN (current results; see also Ekstrand et al., 2001 and Piredda and Gale, 1985) may indicate a third level of hub organization. Scale-free networks can support widespread coherence and bursts (Lind et al., 2004). Computationally, scale-free networks are resistant to random failures (McGraw and Menzinger, 2003) and provide an efficient mechanism for widespread interactions within a network, without necessarily utilizing modular (i.e. small-world) organization (Lind et al., 2004).

Implications for Olfactory Cortical Processing

The piriform cortex is considered the principal target area of axons from the olfactory bulb. However, mitral and tufted cell axons also reach the more proximal anterior olfactory cortex as well as other olfactory-related regionsm such as olfactory tubercle and tinea tecta (Brunjes et al., 2005). Our coherence measurements indicate that AOC is integrated into the excitatory synaptic network of the olfactory cortex. AOC pyramidal cells receive direct input from olfactory bulb, have associational connections (McGinley, unpublished), and send a projection to the piriform cortex (Brunjes et al., 2005). Although this organization might suggest a feedforward role for AOC, our results point to strong feedback excitation from the piriform network to the AOC, likely contributing to the feedback loop to olfactory bulb and contralateral olfactory areas (Davis and Macrides, 1981).

On a more general level, the spatial organization of processing in olfactory cortex remains an enigma. In many sensory systems the cohorts of cortical neurons that process a particular feature of sensory space show modular clustering, particularly in primary neocortex (Mountcastle, 1997). For example, primary visual cortex is organized into orientation columns, ocular dominance columns, pinwheels, and hypercolumns or ‘blobs’, auditory cortex into isofrequency laminae and binaural columns, and barrel cortex into discrete columns that receive input from a single vibrissae (Mountcastle, 1997). In contrast, the widespread coherence we observed suggests a distributed and overlapping excitatory network in the olfactory cortex. We expect that when inhibition is intact, coherence will be temporally restricted to

smaller, though distributed, ensembles, providing a substrate for population coding (Averbeck et al., 2006). Distributed and overlapping cortical ensembles may be essential to olfactory coding in order to accommodate the high dimensionality of chemical space (Dravnieks, 1985).

Experimental Procedures

Slice Preparation

Slices of the olfactory cortex were prepared from C57BL/6J mice of age P21-P28 (300 μm, Leica VT 1200S). All animal handling and experimental procedures were approved by the IACUC at OHSU. The age was chosen to bypass early developmental changes in properties of excitation in olfactory cortex (Schwob et al., 1984; Franks and Isaacson, 2005). After decapitation, the brain was cut coronally at the level of the superior colliculus and sagitally at the midline. The right hemisphere was removed from the skull and mounted on a plastic block specially machined at angles such that the circuitry of the olfactory cortex was preserved in the slices (**Figure 1A**; **Supplementary Figure 1A,B**). Dissection and slicing were conducted in ice cold and carbogenated saline (in mM): 83 NaCl, 26.2 $NaHCO_3$, 2.5 KCl, 1 mM NaH_2PO_4, 3.3 $MgSO_4$, 0.5 $CaCl_2$, 22 glucose, 72 sucrose. Slices were incubated at 33^oC in dissection solution for 35-45 minutes, and then held at room temperature until transfer to the recording chamber. In cut experiments (**Figure 4**), the AOC and piriform network were separated immediately after slicing, under a dissecting microscope, using two toothpicks with small needles embedded in their tips.

Electrophysiological Recording

Pyramidal neurons in layer IIb of piriform cortex, multipolar neurons in pEN, and principal neurons in AOC were targeted for whole cell patch clamp recording using IR-DIC optics through a 40x objective on a Zeiss Axioscope microscope. Principal neurons from the broad cell body layer of AOC (layer II) were targeted based on their large diameter tapering dendrite(s) coursing toward the pial surface, and tear-drop shaped cell bodies. AOC principal neurons exhibited membrane properties that are typical of pyramidal neurons (McGinley, unpublished). Piriform pyramidal neurons were selected from the deep half of layer II (layer IIb) based on morphology, and exhibited membrane properties consistent with previous studies (McGinley, unpublished; see Suzuki and Bekkers, 2006). The presence of basal dendrites was not confirmed in all cases, so it is possible some piriform neurons were semilunar cells (Suzuki and Bekkers, 2006). Multipolar cells in pEN were selected based on morphology, and exhibited characteristic intrinsic membrane properties (McGinley, unpublished; see Suzuki and Bekkers, 2006 and Tseng and Haberly, 1989). Occasional neurons which exhibited narrow action potentials with deep and sharp after hyperpolarizations and unusually high firing rates, typical of GABAregic cortical interneurons, were excluded from the analysis (McGinley, unpublished; see, i.e., Hasenstaub et al., 2005).

Data were acquired at 25 kHz and low-pass filtered online at 10 kHz using a Multiclamp 700B amplifier (Molecular Devices). Most recordings were further lowpass filtered offline (2 kHz) after calculating the series resistance from short voltage pulses. Series resistances were 11.8 ± 0.4 MΩ (n= 230). Neurons with high

series resistance (>20 MΩ) or unstable recordings were excluded from further analysis. The internal solution in all recordings contained (in mM): 135 K-gluconate, 5 NaCl, 10 HEPES, 12 phosphocreatine, 3 MgATP, 0.3 NaGTP, 0.1 EGTA, 0.025 $CaCl_2$. The pH was adjusted to 7.3, resulting in a final osmolarity of 285 mOsm. The bath solution during recordings contained (in mM): 119 NaCl, 26.2 $NaHCO_3$, 2.5 KCl, 1 NaH_2PO_4, 1.0 $MgSO_4$, 2.0 $CaCl_2$, and 22 glucose (300 mOsm). 5 μM R-CPP, 100 μM picrotoxin, or 10 μM CGP55845 were used in some experiments to block NMDA, $GABA_A$ or $GABA_B$ receptors, respectively. Series resistance was corrected in current clamp recordings. To allow for accurate monitoring of the series resistance, and because of the use of a potassium-based internal solution, whole cell compensation was not employed in voltage clamp recordings. A potassium-based internal was used in order to allow for cell identification based on intrinsic membrane properties, as above. Electrical stimulation was performed using a bipolar steel electrode placed in the LOT (Frederick Haer Co., Bowdoinham, ME). The site of electrode placement was in the LOT above the AOC, unless otherwise specified (**Figure 2D**, open symbols).

Data Analysis and Statistics

Coherence was estimated using a multitaper method with adaptive weighting (Thomson, 1982; Percival and Walden, 1993) and a correction for the spurious upward bias of coherence measurements (Huybers, 2004). Coherence is constrained to be between 0 and 1, but spurious coherence greater than zero is inevitable for even uncorrelated signals. Thus, we corrected all coherence estimates by subtracting the

coherence that would be expected by chance for two random uncorrelated white noise processes (Huybers, 2004). Coherence analysis was carried out with custom written code (**Supplementary Code**), which incorpored code provided with permission by Peter Huybers (Huybers, 2004) using Matlab 7.8 with Signal Processing Toolbox 6.11. Between 7 and 13 tapers were used, depending on sweep length, resulting in a consistent 'resolution bandwidth,' f_0, of 28-33 Hz, where $f_0 = (T+1)/(N \cdot dt)$; T = the number of tapers, N = number of data points per sweep, and dt = time between adjacent data points (Percival and Walden, 1993). The resolution bandwidth is the frequency domain equivalent of temporal resolution, conceptually similar to having averaged spectra with a sliding window of width, f_0.

The peak covariation was minimized, as a function of latency, using custom written code (**Supplementary Code**) based on a simplex algorithm (Matlab Optimization Toolbox 4.2). For a given trial, we deleted the same amount of time for each cell to maintain the relative timing. We considered the possibility that the minimization procedure over-corrected for the contribution of latency, but alignment of the burst to their point of maximum rise gave similar reductions in covariation (data not shown). Paired recordings were used for coherence analysis if both neurons had particularly low series resistances (< 12 MΩ), and sufficient repetitions (> 15; 24 ± 2.5; N=8).

Variability across trials within pairs, of coherence and phase uncertainty estimates, are presented (**Figure 5**) and calculated, respectively, as 95% confidence intervals using the BCa bootstrap algorithm with 1000 bootstrap replicates (Matlab Statistics Toolbox 7.1; see ref. 22) and implemented with custom written code

(**Supplementary Code**). Statistical differences across pairs, of coherence and phase uncertainty estimates, were assessed using Kruskal Wallis ANOVA followed by the Mann Whitney-U test with a Newman-Keuls correction for multiple comparisons, and presented as mean ± 1 S.D. (**Figure 6**; **Supplementary Figure 3**). Estimates of covariation are presented as mean ± 2 S.D., calculated according to Brody (Brody, 1999b). All other data are presented as mean ± 1 S.E.M. Statistical comparisons used Student's t-test, when comparing only two groups, or ANOVA with Tukey's post-hoc test for pair-wise comparisons when comparing multiple groups. Kruskal-Wallis ANOVA with Conover's post-hoc was used for comparisons of network burst current amplitudes due to skewed distributions. The F statistic is reported where ANOVA was used, the χ^2 value reported for Kruskal-Wallis ANOVA. All relevant statistical tests were two-sided. Correlation (ρ) was calculated as Pearson's correlation coefficient (OriginPro 8, OriginLab Corporation, Northampton, MA).

Figure Legends

Figure 1 Network-generated bursts of synaptic current in principal neurons of the olfactory cortex. **(A)** Transmitted light image of a fixed slice (top) and the schematic (bottom) showing the stimulation and recording sites for panels B-E. Abbreviations: OB, olfactory bulb; $APC_{V\text{-}R}$, ventrorostral anterior piriform cortex; $APC_{V\text{-}C}$, ventrocaudal anterior piriform cortex; pEN, pre-endopiriform nucleus; *I, II, III,* layers of piriform cortex; LOT, lateral olfactory tract. **(B)** Superimposed responses of an AOC neuron to LOT stimulation (30V): before (black trace), during (grey traces) and after (blue trace) wash in of picrotoxin. The red curve is a fit with a sum of two

exponentials (τ_f = 14.3 ms, τ_s = 280 ms). Inset, LOT stimulation (7V) in a different AOC neuron, voltage clamped at -40 mV, showed inward, followed by outward (GABAergic) currents, similar to piriform pyramidal neurons (Luna and Schoppa, 2008). **(C)** Repeated LOT stimulation at the threshold for burst generation (12V) in picrotoxin and CPP generated supra-threshold responses (blue trace) exhibiting three phases: short-latency monosynaptic current (arrow), a burst of inward currents, and slow outward current. Sub-threshold responses exhibited only the short latency component (black trace, arrow). Inset histogram of burst amplitudes at threshold shows the all-or-none character. **(D)** LOT stimulation for a range of shock strengths (lower panel, 9–50V) evoked graded mono-synaptic and all-or-none burst responses in another AOC neuron (upper panel). Weak stimulation failed to elicit synaptic current (9V, dark green trace). Stronger stimulation (10V, red trace) triggered a burst of inward current at a latency of 30 ms. Further increases in shock strength (other traces) increased the amplitude of monosynaptic current and shortened the burst latency without decreasing its amplitude. Color code connects upper and lower panels. Same pharmacological conditions as in panel C. **(E)** Five examples of paired burst responses to repeated LOT stimulation (8V, trial # at left) for a typical paired recording of a neuron in AOC (black traces) and a neuron in $APC_{V\text{-}C}$ (red traces). Same pharmacological conditions as in panel C.

Figure 2 Network bursts initiate in the pEN. **(A)** The schematic shows the location of recording and stimulating electrodes for paired recordings between a neuron in AOC (black electrode) and a neuron in $APC_{V\text{-}R}$ or pEN (red electrodes). **(B)** Example traces

from two paired recordings between a neuron in AOC (black traces) and a neuron in $APC_{V\text{-}R}$ (top red trace) or pEN (bottom red trace) show the latency to burst onset (arrowheads; top: AOC, 33.0 ms, $APC_{V\text{-}R}$, 23.3 ms; bottom: AOC, 57.1 ms, pEN, 12.5 ms). **(C)-(E)**, Scatter plots for paired recordings of the burst onset latency for the neuron in AOC plotted against the onset latency in $APC_{V\text{-}R}$ (**C**), $APC_{V\text{-}C}$ (**D**), or pEN (**E**). Stimulus intensities were above the threshold for bursts, over a wide range (7–50V). Each symbol/color corresponds to multiple trials from a single pair. The stimulating electrode was placed in the LOT above AOC, except for open symbols in panel D, in which stimulation was in the LOT above $APC_{V\text{-}C}$. **(F)** The lag in start time (difference in latency; left) and slope of linear fits to latency-latency scatter plots (right) are shown for paired recordings between a neuron in AOC and a neuron in another subregion, as indicated on the x-axis.

Figure 3 Cross-correlations of network bursts indicate that AOC lags the piriform network. **(A)** The example traces show a paired recording of a neuron in AOC (top) and a neuron in $APC_{V\text{-}R}$ (bottom). Same traces as Figure 2b, top. The vertical dashed lines demarcate the 200 ms window used for calculation of cross-correlations, chosen to begin after termination of monosynaptic current and end after completion of burst currents. Longer segments were used for some pairs, to accommodate the large variability in onset latency (see Figure 2). **(B)** The cross-correlation of the traces in panel A exhibited a single broad peak with maximum at a lag of 10.6 ms. A positive lag corresponds to later bursts in AOC. **(C)** The lag at peak cross-correlation is plotted for paired recordings between a neuron in AOC and another location indicated

below the x-axis. AOC ‘c’ refers to the more caudally located neuron (closer to piriform) in paired recordings in which both neurons were in AOC. Network bursts in AOC neurons consistently lagged behind simultaneously recorded currents in neurons from the piriform network, and in particular behind $APC_{V\text{-}R}$. The lag from $APC_{V\text{-}C}$ to AOC was only marginally different from 0 ms, whether stimulation was above AOC (4.8 ± 2.0 ms, n=8, p=0.05) or above $APC_{V\text{-}C}$ (1.5 ± 0.5, n=3, p=0.1). The lags were not statistically different between stimulation sites (p = 0.16), thus results were grouped in the plot and for subsequent statistics.

Figure 4 Burst currents in anterior olfactory cortex (AOC) require the piriform network. **(A)** Micro-cuts (red dashed lines) were performed as illustrated, to separate the AOC from the piriform network and perform stimulation and recording in isolated sub-slices. **(B)** Evoked currents from an AOC (left) and $APC_{V\text{-}C}$ neuron (right) from example intact (black) and isolated (red) sub-slices. In intact slices, monosynaptic current (arrowheads) was followed by a burst of inward current in AOC (left) and $APC_{V\text{-}C}$ neurons (right). Burst currents were absent in AOC neurons from cut slices (left), whereas in $APC_{V\text{-}C}$ burst currents were not affected by removal of the AOC and the olfactory bulb (right). **(C)** The summary plots show that removal of the piriform network eliminated bursts without affecting the amplitude of monosynaptic currents in AOC, whereas removal of the AOC did not eliminate bursts in $APC_{V\text{-}C}$ (right).

Figure 5 Bursts in AOC and $APC_{V\text{-}R}$ show coherence that can not be attributed to latency covariation or correlated average responses. **(A1)** Superimposed burst

currents from multiple trials of LOT stimulation for a pair of neurons in AOC (top) and APC_{V-R} (bottom) for 7 repetitions of stimulation of the LOT show correlated latencies and fine timing of synaptic events. **(A2)** Coherence (black line) and 95% confidence interval (grey band) for the currents from panel A1 and 30 additional trials. The inset shows the covariation between the same synaptic currents. The red curves indicate ±2 standard deviations. **(B1)** Bursts from panel A1 were effectively aligned after minimization of the covariation with respect to between-trial latency covariation (see **Methods** and **Supplementary Code**). **(B2)** Coherence was not reduced after alignment of bursts, whereas covariation (inset) was reduced to nearly insignificant levels. **(C1)** Residual current traces were calculated by taking each trace and subtracting off the average burst waveform in each cell, for the currents in panel B1. **(C2)** Coherence of residual currents was not reduced as a result of mean subtraction.

Figure 6 Robust coherence between AOC and subregions of the piriform cortex. **(A)** Coherence for AOC and APC_{V-R} pairs (n=4) was above baseline up to 500 Hz. The color of the line (mean) and lighter colored band (±1 SD) indicate: raw, latency adjusted, residual, or baseline currents, according to the inset at top left. The right inset shows the 0–40 Hz range at higher temporal resolution. Coherence in line noise (60 Hz and odd multiples) is blanked for clarity (see **Supplementary Figure 3**). The magnitude of the power spectrum of the noise was an order of magnitude smaller than burst current signals, out to 1 kHz. Therefore, line noise contributed little to coherence between bursts (data not shown). **(B)** Coherence estimates for recordings

from AOC and $APC_{V\text{-}C}$ pairs (n=4) were calculated and are displayed as in panel A. Results were similar to those of AOC and $APC_{V\text{-}R}$ pairs, even though the AOC and $APC_{V\text{-}C}$ neurons were 3–4 mm apart.

Supplementary Figure 1 Anterior olfactory cortex, ventral anterior piriform cortex, and pre-endopiriform nucleus in a tailored brain slice preparation. **(A)** The angle of section for slices was tailored to be perpendicular to the surface of the brain and parallel to the long axis of the lateral olfactory tract, using a specially machined acrylic block (ϕ = 15 degrees, φ = 40 degrees). The isolated front hemisphere was laid on the block so that the dorsal edge, at the sagital plane, was parallel to the upper edge of the block. **(B)** Montage of DIC images from a typical live 300 μm slice (top). Edges of individual images in the montage are blurred for clarity of the overall image. Bottom is a diagram labeling the brain regions present in the slice: OB; olfactory bulb; OP, olfactory peduncle (contains several olfactory structures including parts of the AON not under investigation); pE, pars externa of AON; LOT, lateral olfactory tract; AOC, anterior olfactory cortex (mostly pars lateralis of AON, and possibly some pars ventroposterialis); $APC_{V\text{-}R}$, ventrorostral anterior piriform cortex; $APC_{V\text{-}C}$, ventrocaudal anterior piriform cortex; PPC, posterior piriform cortex; OC, orbital cortex; ec; external capsule; pEN, pre-endopiriform nucleus; VEN, ventral endopiriform nucleus; CPu, caudate-putamen complex; GP, globus palidus. Regions indicated in color (except the olfactory bulb) were under investigation in the current study.

Supplementary Figure 2 Network bursts are driven from the pre-endopiriform nucleus (pEN). **(A)** An example current trace of evoked network bursts from a representative cell in each subregion. Scale bars at bottom right. **(B)** An example voltage trace during network bursts from a current clamp recording of the same cells in panel A, at the same shock strengths. Blue lines indicate a membrane potential of -75 mV. **(C)** Summary data of the amplitude of network burst currents in each recording region. Network burst currents in pEN were substantially larger than those in other regions. **(D)** Summary data of the number of spikes evoked during network bursts in each recording region. More spikes occurred in pEN than in each of the other regions. **(E)** Histogram of spike lag vs. current lag for several paired recordings of a cell in AOC and a cell in another subregion. Spike lag was calculated as the difference between the time of reaching action potential threshold for the first spike in each cell in a pair. Each plotted point is an average across trials for a cell pair. Error bars indicate ±1 S.E., calculated across trials in a paired recording. Positive lag corresponds to a later first spike in AOC. Current lags were calculated as in Figure 2. **(F)** Summary data for spike lag and spike acceleration. Spike acceleration is the spike lag minus the current lag for each cell pair. Error bars were calculated across pairs. Neurons in pEN have earlier spikes than neurons in AOC, whereas other regions do not (gray bars). Neurons in pEN have earlier spikes than AOC with respect to their currents (spike acceleration), whereas neurons in the other regions of the piriform network do not. The spike acceleration in pEN is consistent with the large amplitude of burst currents. Differences between subregions in intrinsic membrane properties of

principal neurons do to contribute to the observed differences in spike timing or number (McGinley, unpublished).

Supplementary Figure 3 Coherence and phase uncertainty across pairs and regions indicate widespread coherence in the olfactory cortex. **(A1)** Coherence estimates for AOC / $APC_{V\text{-}R}$ pairs, repeated from Figure 6A but with line noise in baseline coherence left unblanked. **(A2)** Phase uncertainty for the coherence estimates in panel A1. **(B1)** Coherence estimates AOC / $APC_{V\text{-}C}$ pairs, repeated from **Figure 6B** as in panel B1. **(B2)** Phase uncertainty for the coherence estimates in panel B1.

Figure 1

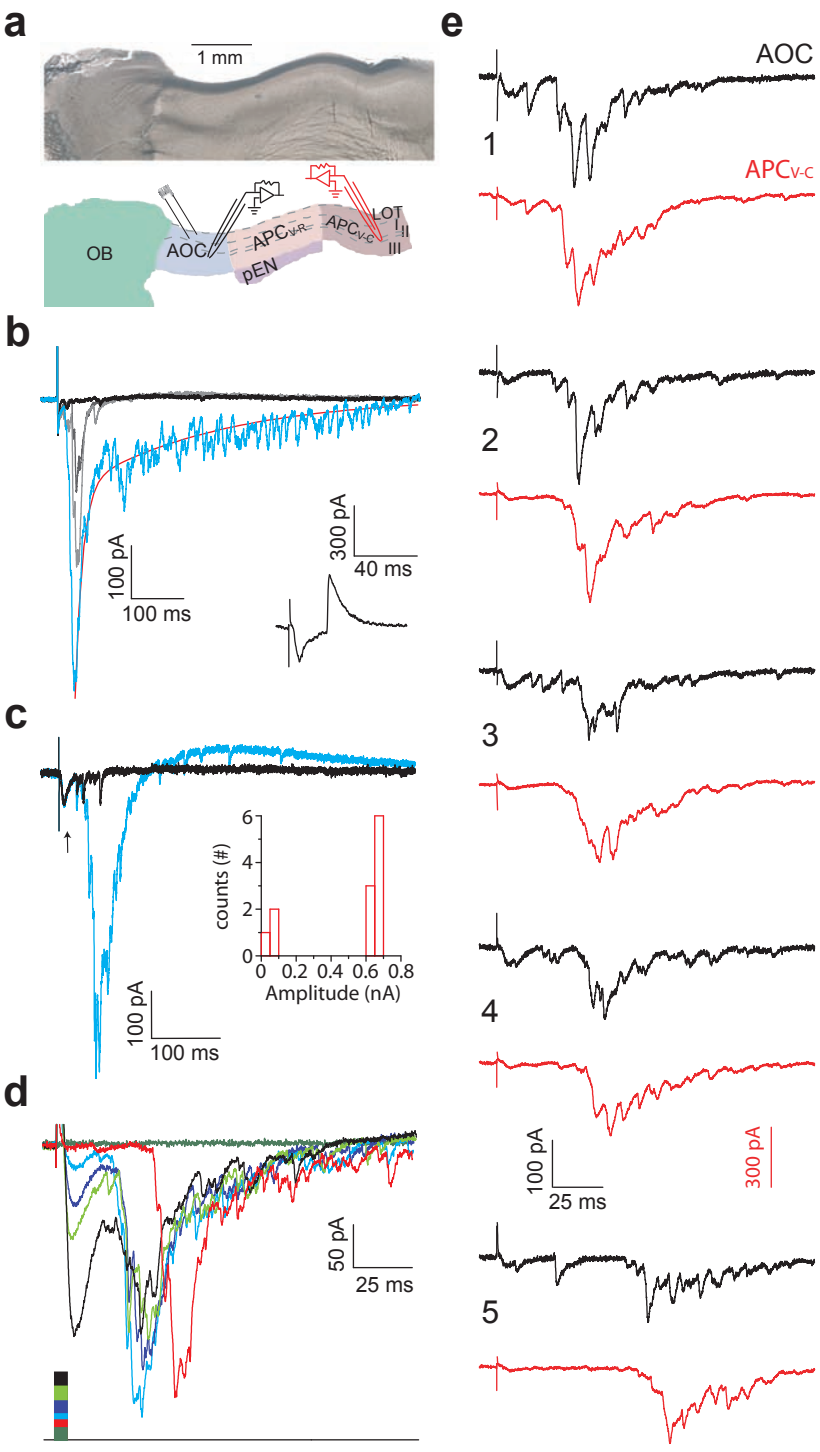
a
1 mm
OB
AOC
APCV-R
APCV-C
pEN
LOT
II
III
b
100 pA
100 ms
300 pA
40 ms
c
counts (#)
Amplitude (nA)
100 pA
100 ms
d
50 pA
25 ms
e
AOC
1
APCV-C
2
3
4
100 pA
25 ms
300 pA
5

Figure 2

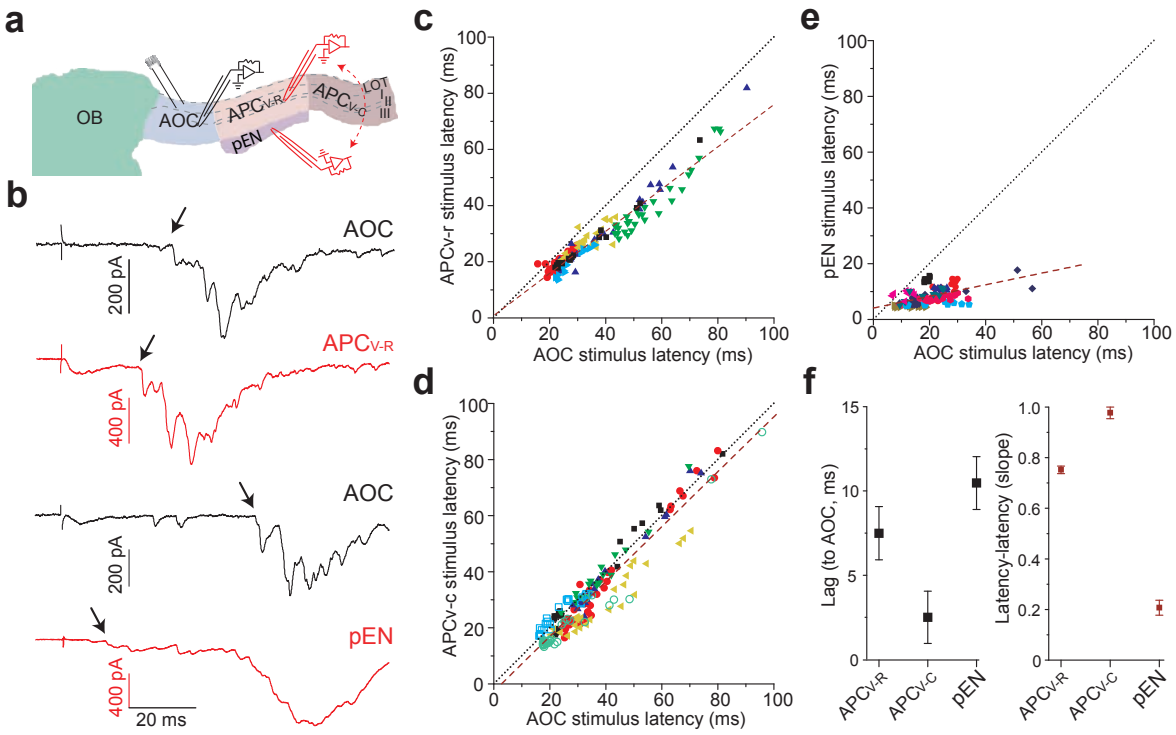
a
OB
AOC
APCV-R
APCV-C
pEN
LOT
II
III
b
AOC
200 pA
APCV-R
400 pA
AOC
200 pA
pEN
400 pA
20 ms
c
APCv-r stimulus latency (ms)
AOC stimulus latency (ms)
d
APCv-c stimulus latency (ms)
AOC stimulus latency (ms)
e
pEN stimulus latency (ms)
AOC stimulus latency (ms)
f
Lag (to AOC, ms)
Latency-latency (slope)
APCV-R
APCV-C
pEN

Figure 3

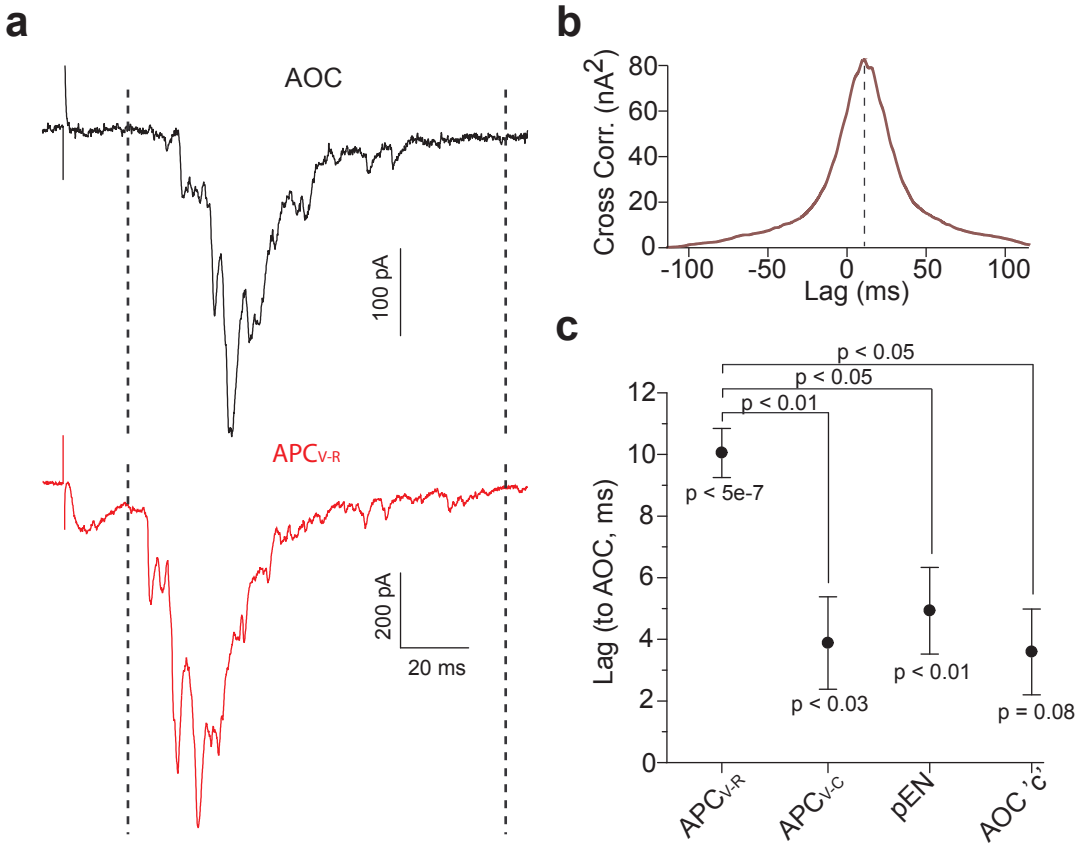
a
AOC
100 pA
APCV-R
200 pA
20 ms
b
Cross Corr. (nA2)
80
60
40
20
0
-100
-50
0
50
100
Lag (ms)
c
p < 0.05
p < 0.05
p < 0.01
p < 5e-7
p < 0.03
p < 0.01
p = 0.08
Lag (to AOC, ms)
12
10
8
6
4
2
0
APCV-R
APCV-C
pEN
AOC 'c'

Figure 4

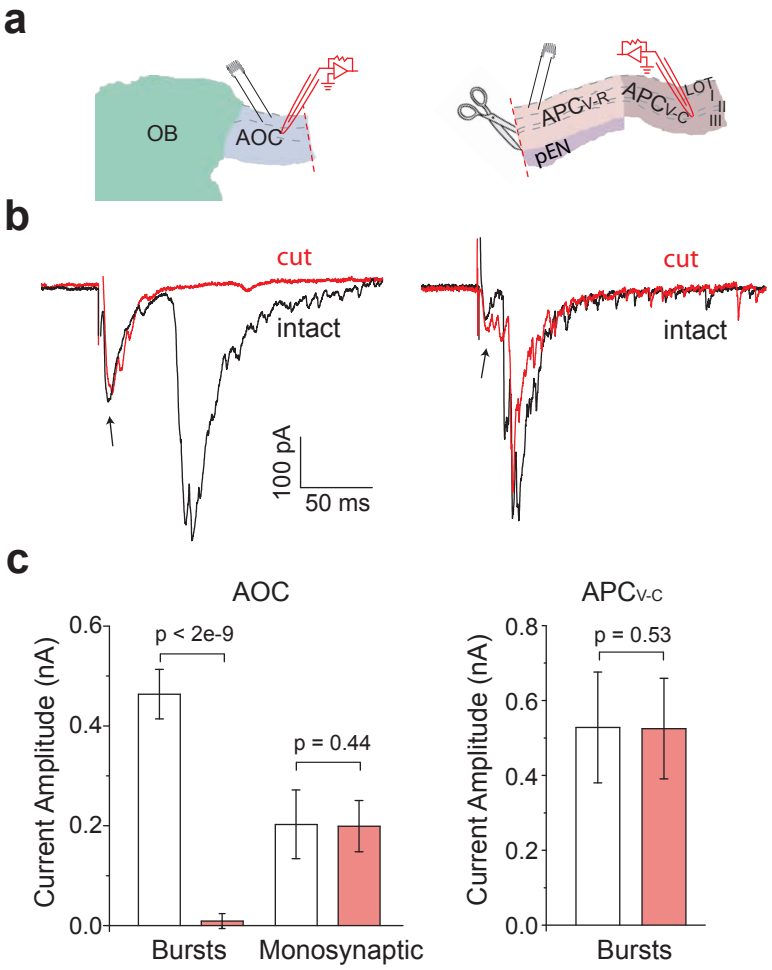
a
OB
AOC
APCV-R
APCV-C
LOT
I
II
III
pEN
b
cut
intact
100 pA
50 ms
cut
intact
c
AOC
p < 2e-9
p = 0.44
Current Amplitude (nA)
0.6
0.4
0.2
0.0
Bursts
Monosynaptic
APCV-C
p = 0.53
Current Amplitude (nA)
0.8
0.6
0.4
0.2
0.0
Bursts

Figure 5

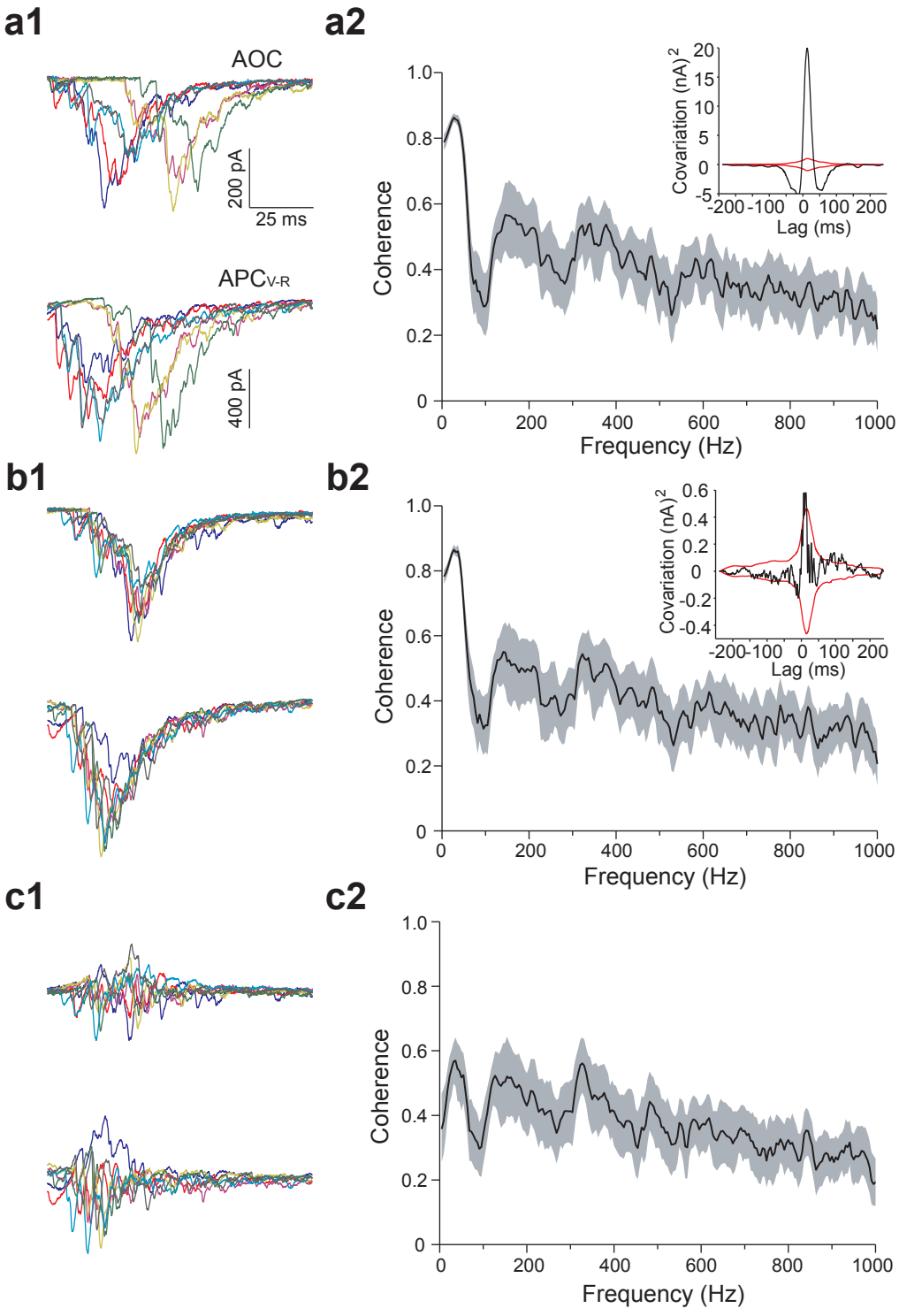
a1
AOC
200 pA
25 ms
APCV-R
400 pA
a2
Coherence
Frequency (Hz)
Covariation (nA)2
Lag (ms)
b1
b2
Coherence
Frequency (Hz)
Covariation (nA)2
Lag (ms)
c1
c2
Coherence
Frequency (Hz)

Figure 6

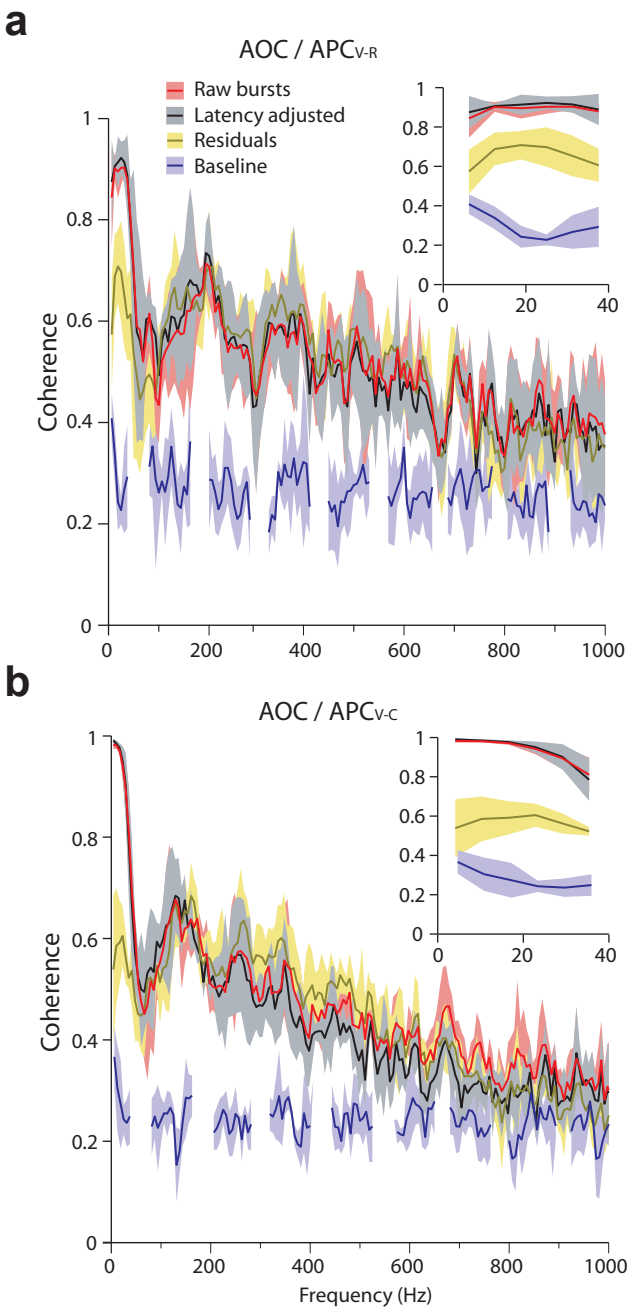
a
AOC / APCV-R
Raw bursts
Latency adjusted
Residuals
Baseline
Coherence
b
AOC / APCV-C
Coherence
Frequency (Hz)

Supplementary Figure 1

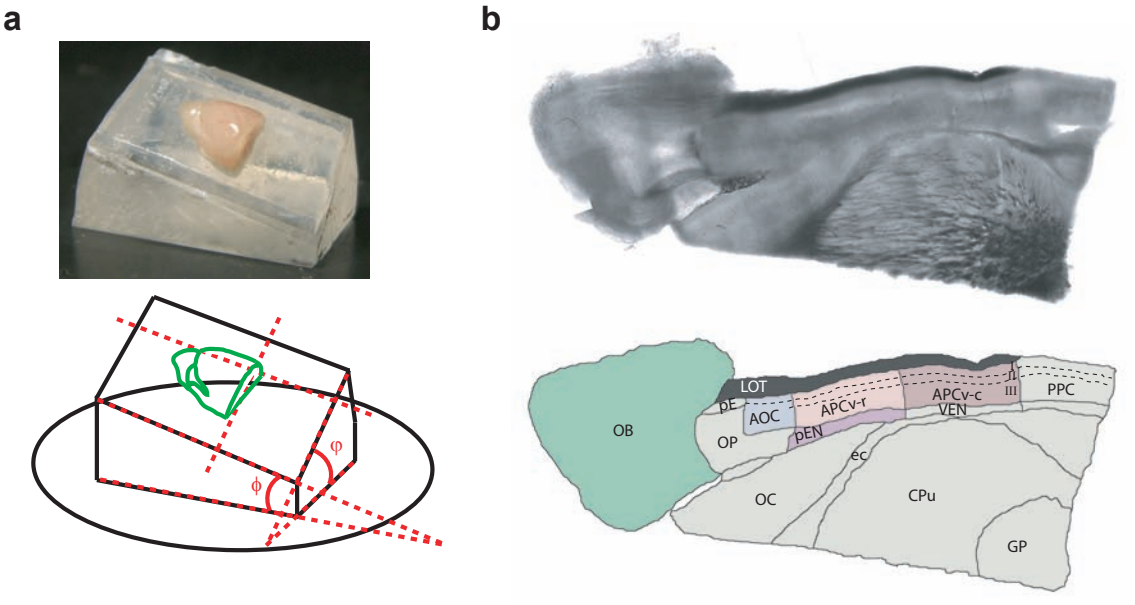

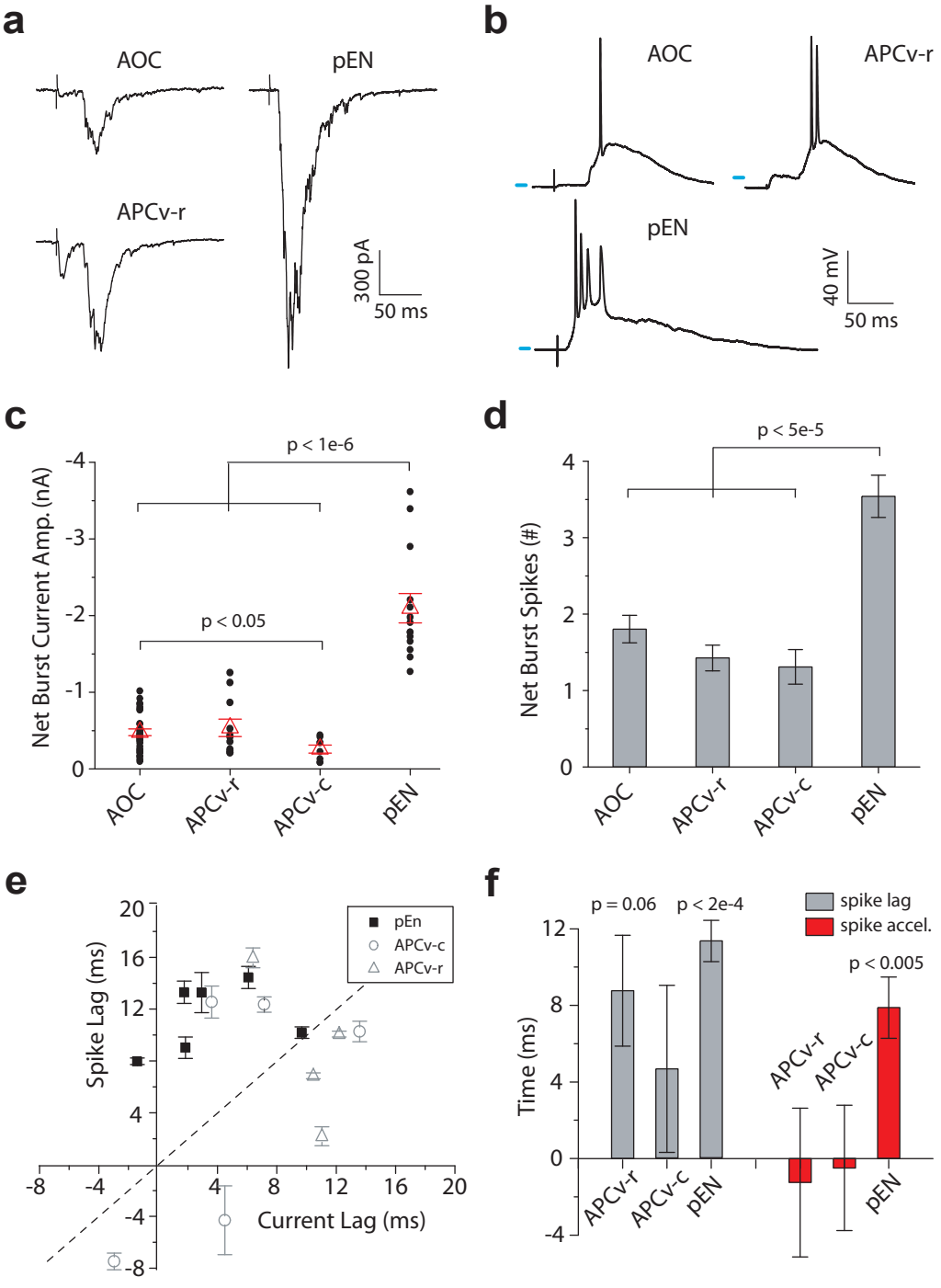
a
AOC
pEN
APCv-r
300 pA
50 ms
b
AOC
APCv-r
pEN
40 mV
50 ms
c
p < 1e-6
p < 0.05
Net Burst Current Amp. (nA)
AOC
APCv-r
APCv-c
pEN
d
p < 5e-5
Net Burst Spikes (#)
AOC
APCv-r
APCv-c
pEN
e
pEn
APCv-c
APCv-r
Spike Lag (ms)
Current Lag (ms)
f
p = 0.06
p < 2e-4
spike lag
spike accel.
p < 0.005
Time (ms)
APCv-r
APCv-c
pEN
APCv-r
APCv-c
pEN

Supplementary Figure 3

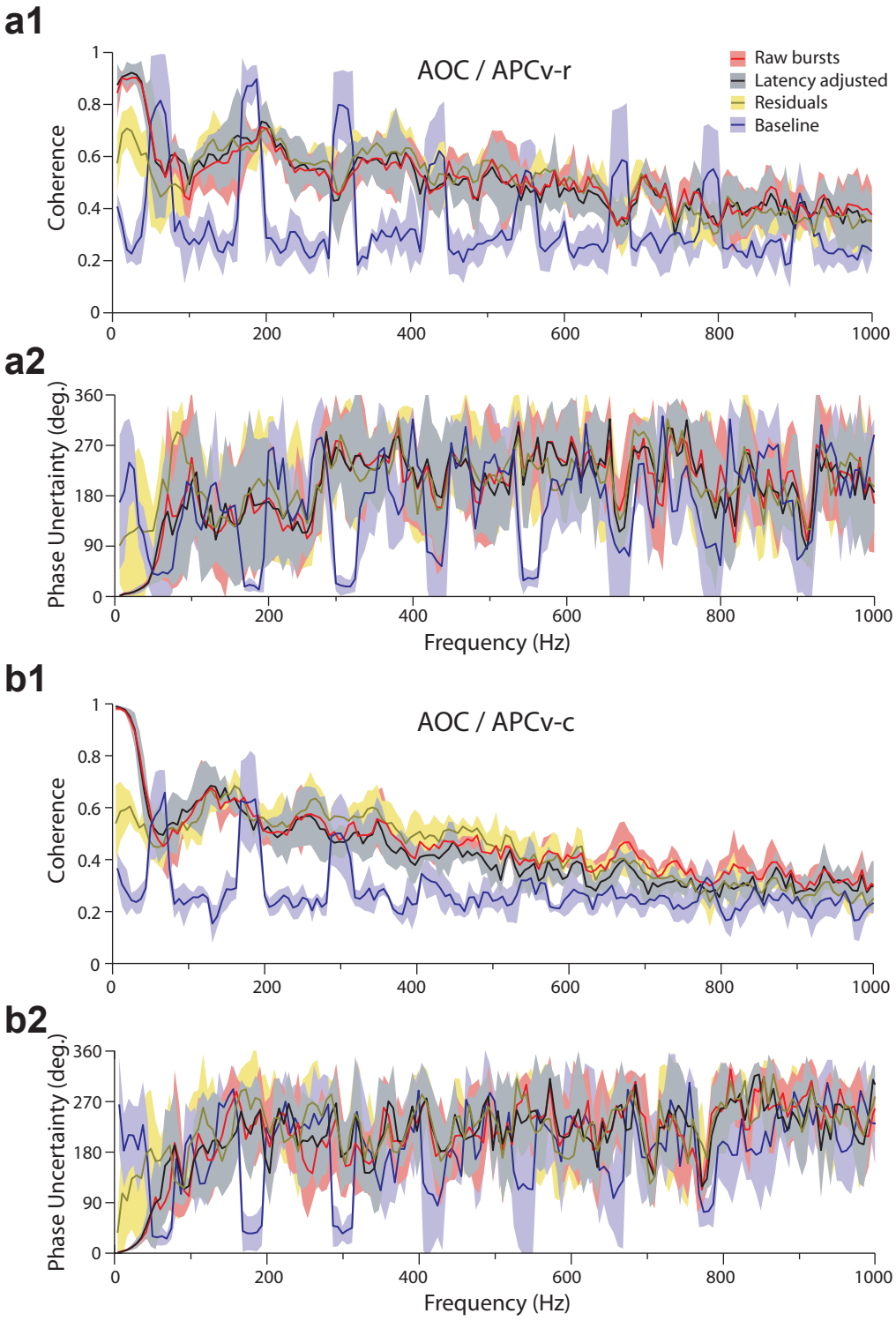

Membrane and synaptic properties of pyramidal neurons in the anterior olfactory nucleus

Matthew J. McGinley and Gary L. Westbrook

Vollum Institute

Portland, OR 97239

Running title: Pyramidal neurons in the anterior olfactory nucleus

Address correspondence to:

Matt McGinley

Vollum Institute, L474

3181 SW Sam Jackson Park Road

Portland, OR 97239

Email: matthew.j.mcginley@gmail.com

Keywords: AON, anterior olfactory cortex, piriform cortex, pre-endopiriform nucleus, area tempestas, AHP, inward rectifying potassium channels, cable properties

Acknowledgements

We thank Lew Haberly and Sherry Feig for help in developing the slice preparation and getting started in olfactory cortex. This work was supported by F31-NS058196 (MJM), a Max Planck Research Award (GLW) and NIH grant NS26494 (GLW).

Abstract

The anterior olfactory nucleus (AON) is positioned to coordinate activity between the piriform cortex and olfactory bulbs, yet the physiology of AON pyramidal neurons has been little explored. Here, we examined the membrane properties and excitatory synapses of AON pyramidal neurons in brain slices of PND22–28 mice, and compared their properties to principal cells in other olfactory cortical areas. AON principal neurons had firing rates, spike rate adaptation, spike shape, and I-V relationships that were generally similar to pyramidal neurons in piriform cortex, and typical of cerebral cortex, consistent with a role for AON in cortical processing. Principal neurons in AON had more hyperpolarized action potential thresholds, smaller afterhyperpolarizations, and tended to fire doublets of action potentials on depolarization compared to ventral anterior piriform cortex (APC_V) and the adjacent epileptogenic region pre-endopiriform nucleus (pEN). Thus, AON pyramidal neurons have enhanced membrane excitability compared to surrounding subregions. Interestingly, principal neurons in pEN were the least excitable, as measured by a larger input conductance, lower firing rates, and more inward rectification. Afferent and recurrent excitatory synapses onto AON pyramidal neurons had small amplitudes, paired pulse facilitation at afferent synapses and $GABA_B$ modulation at recurrent synapses, a pattern similar to piriform cortex. The enhanced membrane excitability and recurrent synaptic excitation within the AON, together with its widespread outputs, suggest that the AON can boost and distribute activity in feedforward and feedback circuits throughout the olfactory system.

Introduction

With its feedback connections to the ipsilateral and contralateral olfactory bulbs, and feedforward connections to the piriform cortex, the AON is poised to coordinate the flow of activity between olfactory areas (Alheid et al. 1984; Reyher et al., 1988; Haberly and Price, 1978; Yan et al., 2008). The entire AON receives input from the ipsilateral olfactory bulb, but it is divided into subregions by the topography of output projections (Haberly and Price, 1978; Brunjes et al., 2005). Three subregions (*pars lateralis*, *dorsalis*, and *ventroposterioralis)* have heavy reciprocal feedforward and feedback connections. Collectively termed *pars principalis*, or anterior olfactory cortex (AOC; Davis and Macrides, 1981; Luskin and Price, 1983a) these three subregions have primitive layering, and their principal neurons have pyramidal shapes, not unlike cortical structures elsewhere (Haberly and Price, 1978; Haberly, 2001; Meyer et al., 2008; Herrick, 1924; Brunjes et al., 2005; Brunjes et al., 2009).

Principal neurons in *pars principalis* of AON are particularly well positioned to influence activity in piriform cortex for several reasons. Tufted cells in the olfactory bulb project selectively to the AON as well as the neighboring ventrorostral anterior piriform cortex ($APC_{V\text{-}R}$; Matsutani et al., 1989). Tufted cells show enhanced excitation relative to mitral cells that project to the entire olfactory cortex (Schneider and Scott, 1983; Orona et al., 1984; Scott et al., 1985; Christie et al., 2001; Nagayama et al., 2004). AON projections to the APC terminate directly adjacent to the cell bodies of pyramidal neurons (Haberly and Price, 1978; Luskin and Price, 1983a). Furthermore, $APC_{V\text{-}R}$ is densely and reciprocally connected with the underlying pre-endopiriform nucleus (pEN), which has been implicated in hyperexcitability and seizure generation (Piredda and Gale, 1985;

Ekstrand et al., 2001a). These organizational features suggest that principal cells in AON, $APC_{V\text{-}R}$ and pEN serve distinct, important roles in olfactory processing, yet very little is know about the physiological properties of these cells and circuits. Here we examined the membrane and synaptic properties of principal cells in the *pars principalis* of AON using whole-cell recording in brain slices from juvenile mice. We also recorded from pyramidal neurons in the rostral and caudal subdivisions of ventral anterior piriform cortex ($APC_{V\text{-}R}$ and $APC_{V\text{-}C}$) and principal neurons in pEN, and compared their properties.

Methods

Slice Preparation

Brain slices were prepared from C57BL/6J mice at PND 22-28 (300 μm, Leica VT 1200S). Isoflurane anesthetized mice were euthanized by decapitation. The brain was cut coronally at the superior colliculus and sagitally at the midline. The right hemisphere was mounted on an acrylic block specially machined so that slices contained the AON, APC_V, and pEN, and layering within these regions, were easily discerned. Dissection and slicing were conducted in ice cold carbogenated saline (in mM): 83 NaCl, 26.2 $NaHCO_3$, 2.5 KCl, 1 mM NaH_2PO_4, 3.3 $MgSO_4$, 0.5 $CaCl_2$, 22 glucose, 72 sucrose. Slices were incubated in the same solution (33^oC for 35-45 minutes) and subsequently placed at room temperature for at least 30 minutes until recording. All animal handling and experimental procedures were approved by the institutional IACUC in accord with NIH guidelines for ethical treatment of animals.

Targeting principal neurons

Recordings of AON neurons were restricted to the broad cell body layer of the lateral part of the AON, deep to the axodendritic layer that borders the LOT and posterior from *pars exterior* of AON. This region, known as *pars principalis*, has three anatomical subdivisions. We largely recorded from *pars lateralis* with possibly a few recordings in *pars ventroposterialis* or *pars dorsalis*. For simplicity, we refer to the recorded area as 'AON.' Principal neurons in AON were targeted based on morphology, having a teardrop shaped cell body, and one or two tapering apical dendrites oriented toward the pial surface. Piriform pyramidal neurons were targeted in the deep half of layer II (*layer IIb*)

in order to avoid semilunar neurons (Suzuki and Bekkers, 2006). Principal neurons in pEN were targeted based on multipolar morphology (Tseng and Haberly, 1989). A few neurons that had membrane physiology consistent with GABAergic interneurons were excluded from analysis.

Electrophysiological Recording

Voltage and current clamp data were low-pass filtered online at 10 kHz and acquired at 25 kHz using a Multiclamp 700B amplifier (Molecular Devices). Recordings were further low-pass filtered offline (2 kHz), except for calculations of the series resistance and curve fits to charging transients. Neurons with high series resistance (>20 MΩ) or unstable recordings were excluded from further analysis. Series resistance in the bath was 11.8 ± 0.4 MΩ (n= 230). In most experiments, a potassium-based pipette solution was used. The pipette solution contained (in mM): 135 K-gluconate, 5 NaCl, 10 HEPES, 12 phosphocreatine, 3 MgATP, 0.3 NaGTP, 0.1 EGTA, 0.025 $CaCl_2$ (pH, 7.3; 285 mOsm). The bath solution contained (in mM): 119 NaCl, 26.2 $NaHCO_3$, 2.5 KCl, 1 NaH_2PO_4, 1.0 $MgSO_4$, 2.0 $CaCl_2$, and 22 glucose (300 mOsm). In some experiments, as indicated, R-CPP (5 μM), picrotoxin (100 μM), or CGP55845 (10 μM) were included in the bath in order to block NMDA, $GABA_A$ or $GABA_B$ receptors, respectively. The calculated potassium reversal potential was -105 mV. Voltage measurements were not corrected for the calculated liquid junction potential (16.3 mV). Series resistance was corrected in current clamp recordings. For whole cell voltage clamp of synaptic responses, the compensation circuit was not employed.

For analysis of membrane properties, neurons were recorded across regions in the same slices, often in pairs, to avoid variability or artificial differences resulting from slice condition. We applied a family of 21 evenly spaced current steps to each neuron (starting from rest, 800 ms duration, 5 second pause between steps, 2-3 repetitions per cell) with amplitudes ranging from -2.5 to +2.5 times the rheobase in each neuron. Rheobase was defined as the amplitude of the smallest depolarizing current step that elicited one or more action potentials on most trials. Single action potentials at rheobase were scored as 1.25 Hz in calculations of firing rates. Slope conductance was calculated as the slope of a linear fit to 3 points on the I-V curve spanning a 10 mV range centered at the specified voltage. I_h sag was fitted with a single exponential starting after the anti-peak, for the trace with anti-peak nearest to -105 mV. I_h modulation depth was calculated as: $(V_{SS} - V_{AP}) / (V_{REST} - V_{SS})$, where: SS, steady state; AP, anti-peak; rest, resting potential.

For specified synaptic experiments, K-gluconate was replaced by an equal concentration of Cs-methanesulfonate to block postsynaptic potassium channels, thus isolating presynaptic effects of $GABA_B$ receptors and or improving voltage clamp of synaptic currents. Electrical stimulation was performed using a bipolar steel electrode (100 μm spacing) placed in the LOT above the AON (Frederick Haer Co., Bowdoinham, ME).

Passive cable analysis

For cable analysis of dendritic structure, we used the ball-and-stick model of Rall (1969) with procedures outlined by Jackson (1992). An average of 20 to 50 charging

transients, from depolarizing and hyperpolarizing voltage pulses, were fit with sums of 3 exponentials.

$$I(t) = A_{fast} \cdot e^{t/\tau_{fast}} + A_{middle} \cdot e^{t/\tau_{middle}} + A_{slow} \cdot e^{t/\tau_{slow}} \quad (1)$$

The dendritic length, L, for each neuron was calculated as:

$$L = \frac{\pi}{2} \cdot \sqrt{\frac{9 - R_\tau}{R_\tau - 1}} \quad (2)$$

where $R_\tau = \tau_{slow} / \tau_{middle}$. The membrane time constant, τ_{mem}, was calculated as:

$$\tau_{mem} = \tau_{slow} \cdot [1 + (\pi / 2L)^2] \quad (3)$$

The somatic-to-dendritic resistance ratio, ρ, was calculated as:

$$\rho = \frac{(\tau_{mem} / \tau_{fast}) / [(V_0 / R_s) + A_{middle} + A_{slow}]}{2 \cdot [(\tau_{mem} / \tau_{slow}) - 1] / [A_{slow} \cdot (\tau_{mem} / \tau_{slow}) \cdot L \cdot \tanh(L)]} \quad (4)$$

where V_0 is the amplitude of the voltage step (10 mV) and R_s is the measured series resistance.

We used three consistency checks to validate the compatibility of the data with assumptions of the model. The assumption that the roots of the transcendental equation are well approximated by analytical expressions requires that:

$$V_0 \cdot (\tau_{mem} / \tau_{fast}) / [(V_0 / R_s) + A_{middle} + A_{slow}] < \frac{49 \cdot \pi^2}{4 \cdot L^2} \quad (5)$$

The validity of the ball-and-stick model requires, by equation (2), that:

$$R_\tau < 9 \quad (6)$$

The derivation of the Fourier coefficients from the orthogonality condition, used for equation (4), implies that the following inequality be obeyed:

$$A_{slow} < A_{middle} \quad (7)$$

All neurons in all regions satisfied equation 5 indicating that the assumptions underlying the remaining analytical expressions were valid (Jackson, 1992). Furthermore, all neurons except one in $APC_{V\text{-}R}$ also satisfied equation 6, thus supporting the appropriateness of the cable model (Figure 4B, left). However, 5 of 13 AON neurons violated equation 7 for voltage steps in both directions, and 2 AON neurons violated equation 7 in one direction (see Figure 4B, right). One neuron in each of the remaining regions also failed equation 7 for a voltage step in one direction ($APC_{V\text{-}R}$ (n=5); $APC_{V\text{-}C}$ (n=7); pEN (n=9); Figure 4B, right). Violation of equation 7 might indicate contamination by active conductances or the effect of the multiple apical dendrites that characterize AON neurons (Brunjes et al., 2009). Neurons were excluded from cable analysis if they violated any of the inequalities. Three additional AON neurons were included, in order to replace those that failed a consistency check on the model.

Statistics

Data are presented as mean ± S.E.M. Statistical comparisons were made with the two-tailed Student's t-test, or ANOVA (F statistic and p-value reported) followed by Tukey's post-hoc (p-value reported) for multiple comparisons; or Friedman ANOVA was used, and the χ^2 value is reported. Statistics were calculated using OriginPro 8 (OriginLab Corporation, Northampton, MA).

Results

Despite its large size and extensive interconnectivity across the mammalian olfactory system, the physiological properties of AON neurons have not been reported. Thus, we performed whole-cell recordings from 122 neurons in AON, to assess their membrane properties and compared them with pyramidal neurons in *layer IIb* in rostral and caudal ventral anterior piriform cortex ($APC_{V\text{-}R}$ and $APC_{V\text{-}C}$, respectively, n=52) and principal neurons in the pre-endopiriform nucleus (pEN, n=21). An example family of voltage responses to current steps, for a typical neuron from each region, is shown in Figure 1A. Principal cells in all regions responded to depolarizing currents with a pattern of accommodating action potentials. Hyperpolarizing currents produced modest voltage sags consistent with activation of I_h.

To quantitatively compare membrane properties, we randomly chose 9 neurons from AON, 6 neurons from *layer IIb* of $APC_{V\text{-}R}$, 7 neurons from *layer IIb* of $APC_{V\text{-}C}$, and 9 neurons in pEN for more detailed analysis. Current-voltage (I-V) relationships are shown in Figure 1B. I-V curves had similar slopes near rest, as reflected in the slope conductance at -85 mV (Figure 1C, left), although there was a small but significant difference between pEN and $APC_{V\text{-}C}$ ($F=4.7$; $p < 0.01$). I-V curves differed more substantially at -105 mV ($F=7.1$, $p < 0.001$), where pEN neurons showed more inward rectification (Figure 1C, middle). The larger conductance in pEN neurons at hyperpolarized voltages was reflected in the 2-fold larger 'difference' conductance than all other regions (subtraction of slope conductances at -85 and -105 mV; $F=5.8$; $p<0.005$; Figure 1C, right). The inward-rectification in pEN probably resulted from inward-rectifying potassium channels because the I_h voltage sag was small in all regions (Figure

1D; see Figure 2B, bottom right). Furthermore, the time constant of the I_h sag was not different between regions (F=0.56, p = 0.91; AON, 132 ± 6 ms; APC_{V-R}, 137 ± 19 ms; APC_{V-C}, 141 ± 26 ms; pEN, 125 ± 27 ms).

Action potentials in principal neurons across regions, measured at threshold (Figure 2A&B, blue traces), had similar amplitudes (peak - threshold; F=3.7; p=0.29; AON, 86.9 ± 2.0 mV; APC_{V-R}, 81.6 ± 1.4 mV; APC_{V-C}, 82.9 ± 1.4 mV; pEN, 82.3 ± 1.4 mV) and half widths (F=4.3; p=0.23; AON, 1.31 ± 0.07 ms; APC_{V-R}, 1.21 ± 0.07 ms; APC_{V-C}, 1.29 ± 0.06 ms; pEN, 1.35 ± 0.04 ms). These values are typical of pyramidal neurons in cerebral cortex (Larkman and Mason, 1990; Krahe and Gabbiani, 2004). The current necessary to trigger an action potential (rheobase) was similar in AON and piriform pyramidal neurons, but larger in pEN (Figure 2C; F=7.9; $p < 0.05$), consistent with the larger slope conductance in pEN. AOC pyramidal neurons had a lower threshold for action potential initiation (F=9.2; $p < 0.05$; Figure 2D) and a smaller afterhyperpolarization (F=11.2; $p < 0.01$; Figure 2E) than pyramidal neurons in piriform cortex, which would be expected to enhance firing.

To analyze intrinsic firing patterns, we calculated f-I curves for principal neurons across regions. F-I curves were shallower in pEN (Figure 3A), mirroring the differences in rheobase shown in Figure 2. Futhermore, average firing rates at threshold, and at 2.5X rheobase, were lower in pEN than in all other regions (F=5.7; $p<0.005$; F=10.3; $p < 0.02$; Figure 3C,D). The percent of neurons that fired bursts (2 or more APs) at threshold was also lowest in pEN (0%) and highest in AON (78%) compared to piriform cortex (APC_{V-R}, 50%; APC_{V-C}, 38%). Firing rates in all regions adapted to long current pulses, as shown for AON (Figure 3B). However, there was a rostral-to-caudal decrease in

adaptation across AON and APC (Figure 3E; $F=8.4$, $p < 0.05$) whereas pEN neurons had comparable adaptation to AON (Figure 3E). These results suggest enhanced excitability in the rostral corner of piriform cortex.

Passive properties of principal neurons

In order to understand how differences in passive properties contribute to the shaping of activity, we analyzed passive charging transients in responses to voltage steps in depolarizing and hyperpolarizing directions, starting from rest, in neurons from each region (Figure 4A, inset). Supporting the applicability of a passive model, and ability to make comparisons between regions, I-V curves were linear near the resting potential (see Figure 1B), and resting potentials were nearly identical (AON: -79.4 ± 0.8 mV; $APC_{V\text{-}R}$: -79.8 ± 2.3 mV: $APC_{V\text{-}C}$, -79.9 ± 0.9 mV; pEN: -79.9 ± 1.3 mV; $F = 0.114$, $p = 0.99$). Three time constants were necessary to fit the waveform of charging transients (Figure 4A), suggesting substantial dendritic charging (Rall, 1969). The fast and middle time constants were not different between regions ($F= 1.1$, $p=0.36$ and $F= 1.5$, $p=0.21$, respectively; Figure 4B, left). However, AON and $APC_{V\text{-}R}$ had faster slow time constants than pEN (Figure 4B, left; $F= 4.7$, $p<0.005$), reflecting differences in the rate of current spread into the dendrites. Furthermore, the fractional contribution of middle and slow time constants was different between all regions, except between $APC_{V\text{-}R}$ and $APC_{V\text{-}C}$ (Figure 4B, right; $F = 3.6$, $p < 0.02$ and $F = 9.2$, $p < 0.00005$, respectively). The differences between regions, in middle and slow time constants indicate a more extended electronic structure in AON.

To extract passive membrane parameters from the charging transients, we applied a uniform cable and lumped soma model (Rall, 1969; Jackson, 1992). The dendritic length (in units of length constants) was longest in AON, and decreased in the rostro-caudal direction (Figure 4C; $F= 6.0$, $p < 0.005$). The membrane time constant (τ_{mem}) also showed a rostro-caudal gradient ($F = 6.1$, $p < 0.002$; AON, 4.8 ± 0.5 ms; $APC_{V\text{-}R}$, 5.3 ± 0.7 ms; $APC_{V\text{-}C}$, 8.9 ± 1.4 ms; pEN, 8.8 ± 0.9 ms), such that the membrane time constant was slower in $APC_{V\text{-}C}$ than in AON ($p < 0.02$). pEN neurons had a membrane time constant comparable to $APC_{V\text{-}C}$ neurons ($p = 0.99998$) and slower than AON neurons ($p < 0.01$). The somatic-to-dendritic resistance ratio (ρ) was larger in AON, and intermediate in pEN (Figure 4D; $F = 17.2$, $p < 2E\text{-}7$). These results suggest a greater filtering of dendritic inputs in AON pyramidal neurons.

Weak single fiber LOT inputs to AON and APC_V

Afferent and associational synapses in piriform cortex show distinct features thought to be important for cortical function, in terms of plasticity, modulation, and synaptic strength (Bower and Haberly, 1986; Hasselmo and Bower, 1990, 1991, 1992; Tang and Hasselmo, 1994; Linster and Hasselmo, 2001; McNamara et al., 2004; Franks and Isaacson, 2006). To examine the synaptic properties of AON pyramidal neurons, we measured the strength of single afferent inputs from the LOT using minimal stimulation (Raastad et al., 1992). Single shocks (0.1 Hz) of low amplitude (3-10 V) evoked failures on some trials, and successes on other trials. In 14 of 18 neurons, we isolated a single shock strength at which similar amplitude successes occurred on some trials, and failures occurred on other trials, indicating that the successes resulted most likely from a single

fiber input (Figure 5A). The amplitude of the single fiber input for these neurons was 16.1 ± 2.4 pA (Figure 5B). For the remaining 4 neurons, a small increase in shock strength (≤ 1V) resulted in an abrupt transition from all failures to all successes, thus providing a least-upper-bound (LUB) estimate of the single fiber input strength. The LUB estimate of 28.4 ± 3.5 pA was larger then the well-isolated single fiber input estimates ($p < 0.02$), suggesting that LUB estimates represented the recruitment of multiple fibers. To address the possibility that our single fiber measurements were underestimates because of reduced voltage clamp control with a potassium-based pipette solution, we used a cesium-based internal solution in 6 additional neurons. In 5 of 6 neurons, threshold stimulation indicated a single fiber amplitude of 28.5 ± 7.0 pA. The remaining neuron had a LUB estimate of 57.3 pA. These values were larger than with a potassium-based solution ($p<0.02$) but not as large as the single fiber input strengths in piriform cortex (Franks and Isaacson, 2006).

To compare LOT input strengths between AON and piriform pyramidal neurons, we recorded pyramidal neurons in APC_V in response to minimal stimulation of the LOT. Successful threshold stimulation was achieved in 4 of 5 piriform pyramidal neurons. The single fiber input strength was 17.4 ± 4.8 pA, not different from the value obtained in AON ($p=0.82$; Figure 5B). The remaining piriform pyramidal neuron had a LUB estimate of 40.9 pA. Similarly, the single fiber amplitude, with a cesium-based solution was 33.4 ± 8.7 pA ($n=4$), larger than with intracellular potassium ($p < 0.05$), and not different from cesium-loaded AON neurons ($p=0.6$). To further evaluate the strength of single fiber inputs, we performed graded stimulation in 5 AON principal neurons and 5 piriform pyramidal neurons. The EPSC amplitude increased gradually with shock strength,

consistent with the results of minimal stimulation (Figure 5C&D). Our results indicate that LOT inputs to AON and APC_V are weak under the conditions of our experiments.

In addition to LOT inputs, we examined local excitatory interactions between AON neurons. Extensive recurrent excitatory connectivity is a hallmark of cortical regions including the piriform cortex (Tsodyks et al., 2000; Holmgren et al., 2003; Haberly and Price, 1978; Luskin and Price, 1983b; Johnson et al., 2000). In paired recordings of AON neurons using potassium electrodes, 3 of 18 pairs exhibited an excitatory monosynaptic connection in one direction (3 of 36 connections, or 8.3%), which is similar to layer 2/3 of neocortex (Nicoll and Blakemore, 1993; Holmgren et al., 2003). These recurrent connections had small EPSC amplitudes (26 ± 12 pA), which is also similar to piriform cortex (Shikorski and Stevens, 1990; Bower and Hasselmo, 1986) and neocortex (Tsodyks and Markram, 1997; Tsodyks et al., 2000; Holmgren et al., 2003; Bruno and Sakmann, 2006).

Short-term plasticity and pathway specific $GABA_B$ modulation in AON

LOT synaptic inputs to piriform pyramidal neurons show paired pulse facilitation (Bower and Haberly, 1986; Hasselmo and Bower, 1992). Furthermore, and unlike recurrent excitatory connections, LOT inputs to piriform pyramidal neurons lack presynaptic $GABA_B$ receptors (Tang and Hasselmo, 1994). We looked for these patterns in AON. For LOT inputs to AON principal neurons, paired pulse stimulation (ISI, 50–1000 ms) evoked paired pulse facilitation for short ISIs (Figure 6A) that was unaffected by $GABA_B$ receptors ($p=0.31$; Figure 6B). With a potassium-based internal solution, baclofen reversibly reduced LOT-evoked EPSCs (Figure 6C, left; see also Figure 7A).

However, with a cesium-based internal solution, the EPSC amplitude was only slightly reduced by baclofen (Figure 6C, right), indicating postsynaptic shunting by $GABA_B$ receptors. Consistent with this interpretation, baclofen shifted the holding current with a potassium-based (Figure 6D, left) but not cesium based (Figure 6D, right) solution and reduced the input resistance with a potassium-based (n=3; χ^2=6; p<0.05; control, 69.7 ± 14.6 MΩ; baclofen, 48.1 ± 6.0 MΩ; CGP55845, 78.4 ± 9.7 MΩ) but not with a cesium-based pipette solution (n=3; χ^2=4.7; p=0.10; control, 232 ± 53 MΩ; baclofen, 195 ± 42 MΩ; CGP55845, 261 ± 46 MΩ). The small effect of $GABA_B$ receptors in cesium may reflect post-synaptic cesium permeable GIRK channels (Hommers et al., 2003).

Recurrent excitatory synapses in piriform cortex are suppressed by $GABA_B$ receptors (Tang and Hasselmo, 1994). In AON, baclofen markedly reduced polysynaptic bursts of excitation evoked by LOT stimulation in the presence of $GABA_A$ and NMDA receptor antagonists (Figure 7A; McGinley and Westbrook, in preparation), and the bursts were restored in CGP55845 (Figure 7A, right). Paired pulse stimulation of the LOT (ISI, 0.2–5 seconds) resulted in paired pulse depression of bursts for short ISIs (Figure 7B, top and C) that was partially relieved by CGP55845 (Figure 7B, bottom, and C). These result indicate endogenous $GABA_B$ receptor suppression of associational excitation in AON.

Discussion

Intrinsic membrane and synaptic properties influence the circuit dynamics of cortical networks. Our results indicate that AON pyramidal neurons share many of the properties of principal neurons in the piriform cortex as well as other areas of cerebral

cortex. However, there were regional differences that may provide insight into region-specific functions in the olfactory system. In particular, AON neurons showed enhanced excitability whereas pEN showed diminished excitability compared to piriform cortex. Lateral olfactory tract inputs from olfactory bulb to AON and ventral anterior priform cortex were weak, suggesting that activation of these regions requires synchronous sensory input.

Regional differences in excitability

Only a few physiological studies have included the AON (Nakajima and Iwasaki, 1973; Boulet et al., 1978; McNamara et al., 2004; Lei et al., 2006) and none have explored their physiology with whole-cell recording. AON pyramidal neurons had enhanced membrane excitability at threshold and at 2.5x rheobase, compared to piriform pyramidal neurons. Pyramidal neurons in neocortex and hippocampus show a range of excitable properties, consistent with the differences we observed between AON and subregions of piriform cortex (Larkman and Mason, 1990; Krahe and Gabbiani, 2004). However, burst firing was not as pronounced as for thalamic relay neurons (Jahnsen and Llinas, 1984). AHP amplitudes in piriform pyramidal neurons are affected by learning (Cohen-Matsliah et al., 2010), thus the smaller AHP in AON may reflect different intrinsic plasticity (Liraz et al., 2009; Saar and Barkai, 2009; Cohen-Matsliah et al., 2010). The membrane properties were surprisingly uniform for *pars principalis* pyramidal neurons, which project to piriform. Other subregions (*pars externa* and *pars medialis*) that project exclusively to the olfactory bulb were not explored, and thus could

exhibit different membrane properties. It is also possible that there are differences between subregions of *pars principalis* (Meyer et al., 2006).

Perhaps surprisingly, pEN neurons were less excitable than the other regions we explored. The pEN is a known epileptogenic locus within the olfactory system (Gale and Piredda, 1985; Ekstrand et al., 2001a). pEN principal neurons had a pronounced inward rectification, probably because of a higher expression of IRK and/or GIRK channels. In olfactory cortex, neurons, rather than glia, may buffer extracellular potassium, during local increases in extracellular potassium such as seizures (Howe et al., 2008). Therefore, a high potassium buffering capacity of pEN neurons could be important in controlling excitation. Pyramidal neurons in the neocortex and hippocampus have a large I_h, particularly in dendrites where I_h is thought to normalize or scale synaptic inputs (Williams and Stuart, 2000; Spruston, 2008). Although it has been reported that piriform pyramidal neurons do not express I_h (e.g. Howe et al., 2008), we observed small, but consistent I_h sags on AON, piriform and pEN neurons. A small I_h, as well as the results of our passive cable analysis, is consistent with a more passive and compact dendritic tree in piriform pyramidal neurons compared to neocortex (Bathellier et al., 2009; Spruston, 2008).

The olfactory cortex is shaped like a long ribbon, extended in the rostro-caudal direction, with sensory input arriving at the rostral end. As a result, there has long been interest in rostral-caudal gradients in physiological properties in olfactory cortex. For example, there is a rostral-to-caudal gradient in the amount of afferent versus associational fibers in *layer I* (Luskin and Price, 1983b), as well as a rostral-to-caudal decrease in the contribution of tufted cell fibers to the LOT afferent pathway (Matsutani

et al., 1989). Tufted cells are more strongly excited by odorants (Schneider and Scott, 1983; Christie et al., 2001; Nagayama et al., 2004), so the gradient in tufted cell innervation should result in relatively less activity in caudal regions. Our results also indicate a rostral-caudal gradient, extending across AON and ventral anterior piriform cortex, in intrinsic membrane properties of pyramidal neurons, namely: firing rate adaptation, the percent of neurons that fired bursts at threshold, dendritic length, and membrane time constant. These patterns would be expected to create a gradient in temporal integration and input-output transformation, which may help spread and synchronize activity in response to sensory stimuli.

The strength of afferent inputs

Our results indicate single fiber inputs to pyramidal neurons in piriform cortex and AON are weak. However, it has previously been reported that these inputs to piriform pyramidal neurons are 'strong,' (Franks and Isaacson, 2006; Perez-Orive et al., 2002). As our experiments were performed in physiological levels of calcium and magnesium, this difference could result from the fact that small inputs are harder to resolve in high divalents, the conditions used in the prior experiments in piriform cortex (see Supplementary Figure 1). Ultrastructural evidence suggests LOT synapses are comparable to CA1, though somewhat larger on average (Schikorski and Stevens, 1999). Integration of many weak inputs is consistent with the broad and complex receptive fields of piriform pyramidal neurons (Wilson, 2001; Stettler and Axel, 2009) and sparse activity in the piriform cortex (Schoenbaum and Eichenbaum, 1995; Stettler and Axel, 2009). Weak afferent inputs are the norm in neocortex (Bruno and Sakmann, 2006) and at the

analogous olfactory synapse in the locust (Jortner et al., 2007). As our results were restricted to AON and APC_V, single fiber inputs to PPC and/or APC_D may be stronger, possibly to compensate for a reduction in the number of LOT inputs. Furthermore, a distinct class of principal neuron in piriform cortex, semilunar neurons, receive stronger LOT input than pyramidal neurons, perhaps because of stronger single fiber input (Suzuki and Bekkers, 2006).

The role of the AON in olfaction

The AON was originally considered a nuclear structure because it has only two distinct layers (Herrick, 1924). However, recent evidence is more consistent with a cortical architecture (Haberly, 2001; Brunjes et al., 2005). Individual neurons in AON respond to multiple distinct odor mixtures as well as several chemically unrelated components of individual mixtures (Lei et al., 2006). Commissural pathways connecting the AON allow contralateral recall of memories (Haberly and Price, 1978; Kucharski and Hall, 1987), suggesting a role for the AON in conveying information about the learning process. AON neurons can change their preferred side (Kikuta et al., 2008), and neurons in *pars externa* receive side-specific excitation and inhibition (Kikuta et al., 2010). On the basis of cortical organization, topographically-specific, reciprocal feedforward and feedback projections, and bilateral connectivity, the group of subregions of the anterior olfactory nucleus (AON) referred to AOC has been proposed to act as a primary cortex for the olfactory system (Haberly, 2001). Alternatively, it has been suggested that the bulb functions as the primary cortex, encoding chemical features, and that AOC has similarities to area V2 in the visual system (Cleland, 2010). The traditional view of the

AON as a ‘relay’ places it at the level of the thalamus, though the olfactory bulb may serve functions similar to the thalamus (Kay and Sherman, 2007). It has also been suggested that the thalamus evolved to allow other systems to create patterns of cortical activity that emerged in the piriform cortex, and so the olfactory system has no analogy to the thalamus (Fontanini and Bower, 2006).

Our results support the interpretation of the AON as a cortical structure. The AON is integrated into the excitatory circuit of piriform cortex (Luskin and Price, 1983a; see Chapter 1) and shares with piriform cortex and neocortex in exhibiting weak synaptic strengths as well as pathway-specific short term plasticity and modulation by $GABA_B$ receptors (Bruno and Sakmann, 2006; Tsodyks and Markram, 1997; Tsodyks et al., 2000; Bower and Haberly, 1986; Hasselmo and Bower, 1990, 1991, 1992; Tang and Hasselmo, 1994; Linster and Hasselmo, 2001; McNamara et al., 2004). *Pars principalis* of AON has less elaborate layering than piriform cortex (it lacks a layer III), but contains a large population of neurons with pyramidal morphology (Brunjes et al., 2005; Brunjes et al., 2009). The membrane properties of pyramidal neurons in AON were typical of cerebral cortex in their spike shape, firing rates, and adapting/bursting firing patterns (Larkman and Mason, 1990; Krahe and Gabbiani, 2004). However, common properties of AON and piriform cortex are not shared by all targets of the olfactory bulb, as neurons in the olfactory tubercle exhibit diverse intrinsic membrane properties, not resembling those of pyramidal neurons (Chiang and Strowbridge, 2007). A special class of principal neurons in piriform cortex, semilunar neurons, also has distinct intrinsic and synaptic properties (Suzuki and Bekkers, 2006).

Figure 1 Responses to long current steps in principal neurons across recording regions. **A)** Voltage responses (top) for a family of current steps (bottom) in a typical example neuron from each of: AON (left), $APC_{V\text{-}C}$ (middle) and pEN (right). Red lines indicate a trans-membrane voltage of -80 mV. Blue traces correspond to 2.5x the rheobase for an action potential. Voltage responses between 1x and 2.5x rheobase are not shown, for clarity. **B)** Current-voltage relationships for principal neurons. Inset indicates the recording region. Voltage values were calculated at the peak or anti-peak voltage reached during for depolarizing or hyperpolarizing current steps, respectively. **C)** Membrane conductance for principal neurons from recording regions indicated by the inset. Conductances were calculated as the slope of I-V curves at peak voltage, for three adjacent voltages near the voltage indicated on the x-axis. Conductance at -85 mV (left) reflects the resting input conductance. Conductance at -105 mV (middle) reflects the conductance activated in the range below the potassium reversal potential (xx mV). The subtraction of the conductances at -85 mV and -105 mV on a cell-by-cell basis (right) reflects the magnitude of hyperpolarization-activated conductances. Neurons in pEN had substantially larger hyperpolarization-activated conductance than principal neurons in the other recording regions. **D)** The extent of I_h sag for the same three traces used to determine the slope conductance at -105 mV in panel C. Small differences between regions in I_h sag do not account for the large conductance at hyperpolarized voltages in pEN. Asterisks indicate level of statistical significance: *, $p < 0.05$; **, $p < 0.01$; ***, $p < 0.001$.

Figure 2 Action potentials across regions have similar shapes expect for AP thresholds and after-hyperpolarization (AHP). **A)** Voltage response (top) for three current steps (bottom) in a typical example neuron from the AON. Red line indicates a trans-membrane voltage of -80 mV. Blue traces are at the rheobase for action potentials in this neuron (160 pA). **B)** At left is an example of the action potential waveform at rheobase (blown-up from panel A), illustrating the voltage threshold (red circle) and action potential half-width (red bar). At top right is a further blow-up of the threshold region for (same action potential), illustrating the definition of the after hyperpolarization (AHP, red bar). Bottom right, hyperpolarized step (blown up from panel A) indicating the parameters used to calculate I_h sag (b/a). A single exponential is fit to the I_h time course (red curve, labeled 'tau'). **C)** The amount of current necessary to trigger an action potential (rheobase) was similar for principal neurons across subregions (left three bars). pEN neurons had a higher rheobase (right bar). Recording region indicated below the x-axis. **D)** Neurons in AON had consistently hyperpolarized action potential thresholds compared to pyramidal neurons in piriform cortex. **E)** The after-hyperpolarization (AHP), measured relative to AP threshold. Pyramidal neurons in AON had consistently smaller AHPs compared to in piriform cortex. Asterisks indicate level of statistical significance: *, $p < 0.05$; **, $p < 0.01$; ***, $p < 0.001$.

Figure 3 Principal neurons differ between regions in firing rates and the extent of firing rate adaptation. **A)** The average firing rate versus current amplitude (f-I curve) reveals lower firing rates in pEN neurons. **B)** Examples (grey symbols) and average (black) of instantaneous firing rates ($1/\Delta t$) for 14 AON pyramidal neurons during current

application at 2.5x rheobase. Inset (top right) shows an example AON firing pattern (top) in response to a current step at 25x rheobase (400 pA, bottom). Red bar indicates the interspike interval (Δt) for the 7^{th} AP interval. Scale bars apply to inset. **C)** The average firing rate (at rheobase) is smallest in pEN, reflecting a tendency to fire only 1 action potential at threshold. **D)** The average firing rate at 2.5x rheobase (first 10 action potentials) was lower in pEN neurons. **E)** Principal neurons in all subregions showed firing rate adaptation. Neurons in AON and pEN showed more firing rate adaptation than neurons in $APC_{V\text{-}C}$. Neurons in $APC_{V\text{-}R}$ were intermediate. Asterisks indicate level of statistical significance: *, $p < 0.05$; **, $p < 0.02$; ***, $p < 0.01$; ****, $p < 0.005$.

Figure 4 Pyramidal neurons are less electrically compact in AON than in piriform cortex and pEN. **A)** At bottom left is the average response to voltage pulses (xx pulses, 10 ms duration, and 10 mV amplitude) in an example AON neuron. Data points are in black, curve fits with 1, 2, or 3 exponentials are superimposed. At middle is a blowup of the first 800 μs of the pulse (indicate by the black dashed box at left), showing that 3 exponentials were necessary to achieve a good fit (red curve). At top right is the same current trace, showing the depolarizing and hyperpolarizing component (top) in response to a 10 mV step (bottom). Red line indicates 0 pA of current. **B)** Time constants (left) and amplitude fractions (right) for the 3 exponential components indicated by the inset. The recording region is indicated on the x-axis. Middle and slow exponential components, reflecting dendritic charging, show differences between all brain areas, except between $AOPC_{V\text{-}R}$ and $APC_{V\text{-}C}$. **C)** Dendritic length estimates differed between brain areas. **D)** The somatic to dendritic resistance ratio (ρ) differed between brain regions. Asterisks indicate level of

statistical significance: *, $p < 0.05$; **, $p < 0.01$; ***, $p < 0.005$; ****, $p < 0.0001$; *****, $p < 5E\text{-}6$.

Figure 5 Weak single fiber inputs from the LOT onto pyramidal neurons in piriform cortex and the AON. **A)** Single fiber synaptic responses in an example AON pyramidal indicated by all-or-none behavior across three stimulus intensities straddling the single fiber threshold. Top, responses to a single LOT shock. Color of each trace indicates the intensity of stimulation (indicated at middle). Bottom, amplitude of the monosynaptic EPSC on each trial. The single fiber EPSC amplitude for this cell was 33.0 pA. **B)** Cumulative histogram of single fiber EPSC amplitudes for principal neurons in AON (dark blue) and pyramidal neurons in layer IIb of piriform cortex (red). **C)** EPSC amplitudes increased smoothly over a wide range of shock strength in an example piriform pyramidal neuron (top), with no apparent large jumps in amplitude. The series resistance on each trial is plotted below. **D)** Superimposed EPSCs corresponding to the plot in panel C.

Figure 6 Afferent synapses in AON are facilitating and unmodulated by $GABA_B$ receptors. **A)** The paired pulse ratio of voltage clamp responses to LOT stimulation is plotted as a function in the interstimulus interval (ISI). Black circles and gray lines show individual neurons, whereas open triangles and black lines show the average response. LOT synapses onto AON principal neurons were facilitating for ISIs ranging from 50-200 ms. Inset shows an example response to paired pulse stimulation. **B)** Bath application of baclofen, followed by CGP55845, did not change the paired pulse ratio of LOT

stimulation. **C)** Bath application of baclofen reversibly reduced the EPSC amplitude by almost 50% with a potassium based pipette solution (left), whereas it irreducibly reduced the EPSC amplitude by < 25% with a cesium based electrode (right). **D)** Bath application of baclofen caused a reversible shift in the holding current with a potassium based pipette solution (left) that was abolished with a cesium based solution (right), suggesting activation of $GABA_B$ receptors in the recorded (postsynaptic) neuron.

Figure 7 Suppression of intra-cortical feedback by endogenous $GABA_B$ receptor activation. **A)** $GABA_B$ pharmacology of responses to LOT stimulation in an AON neuron. Left, before drug application; middle, after wash-in of baclofen; and right, after washout of baclofen and wash-in of CGP55845. Light blue line in each panel indicate 0 pA of current. Insets show inward currents (indicated by dashed box, left panel) at higher temporal resolution. Obscured grey traces show 3 additional repetitions in each condition in the same cell. **B**, Paired pulse stimulation of LOT at several interstimulus intervals (ISIs) in control conditions (top) and in the presence of CGP55845 (bottom). CGP55845 application relieves $GABA_B$ receptor-mediated suppression of the second burst response. **C)** Summary data of the recovery time course of network burst currents in control conditions (black) and in CGP55845 (red). Fits are with a single exponential. For control conditions, $\tau_{recovery}$ = xx ms, and in CGP55845 $\tau_{recovery}$ = xx ms.

Figure 1

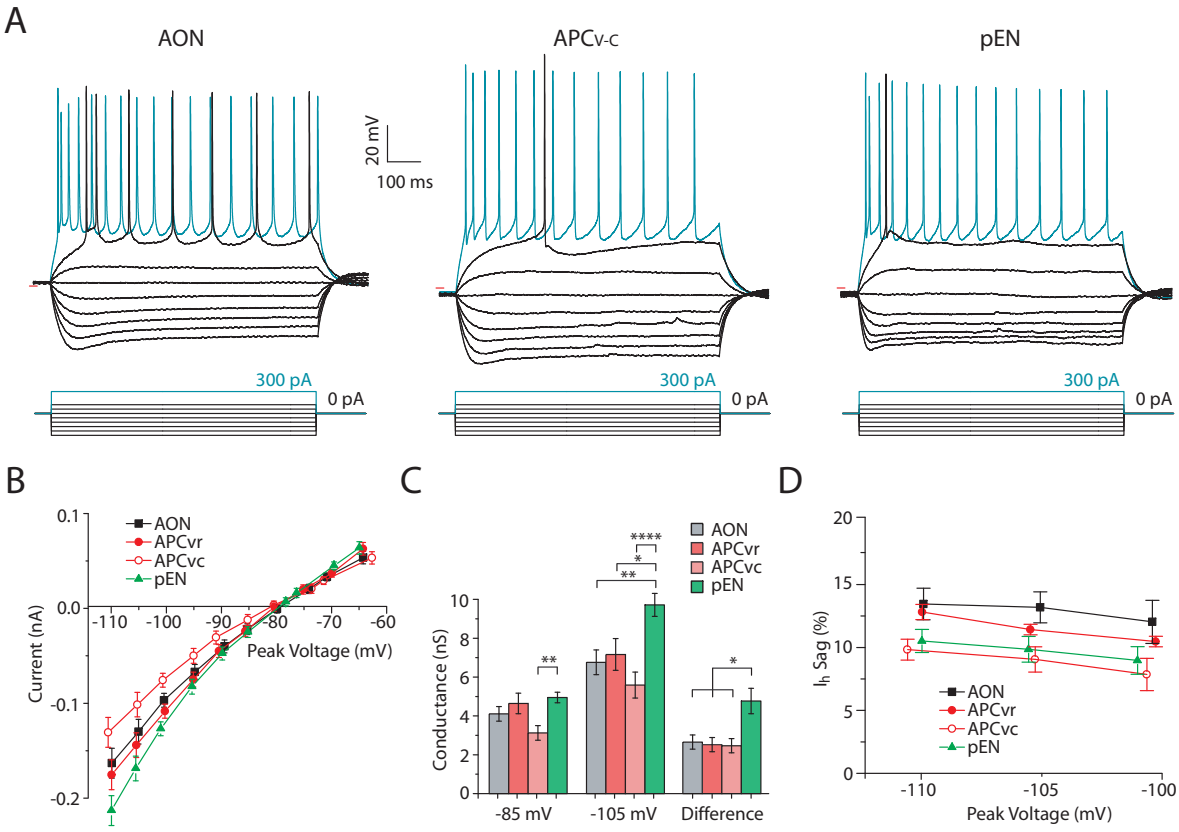
A
AON
APCV-C
pEN
20 mV
100 ms
300 pA
0 pA
B
AON
APCvr
APCvc
pEN
Current (nA)
Peak Voltage (mV)
C
Conductance (nS)
-85 mV
-105 mV
Difference
D
Ih Sag (%)
Peak Voltage (mV)

Figure 2

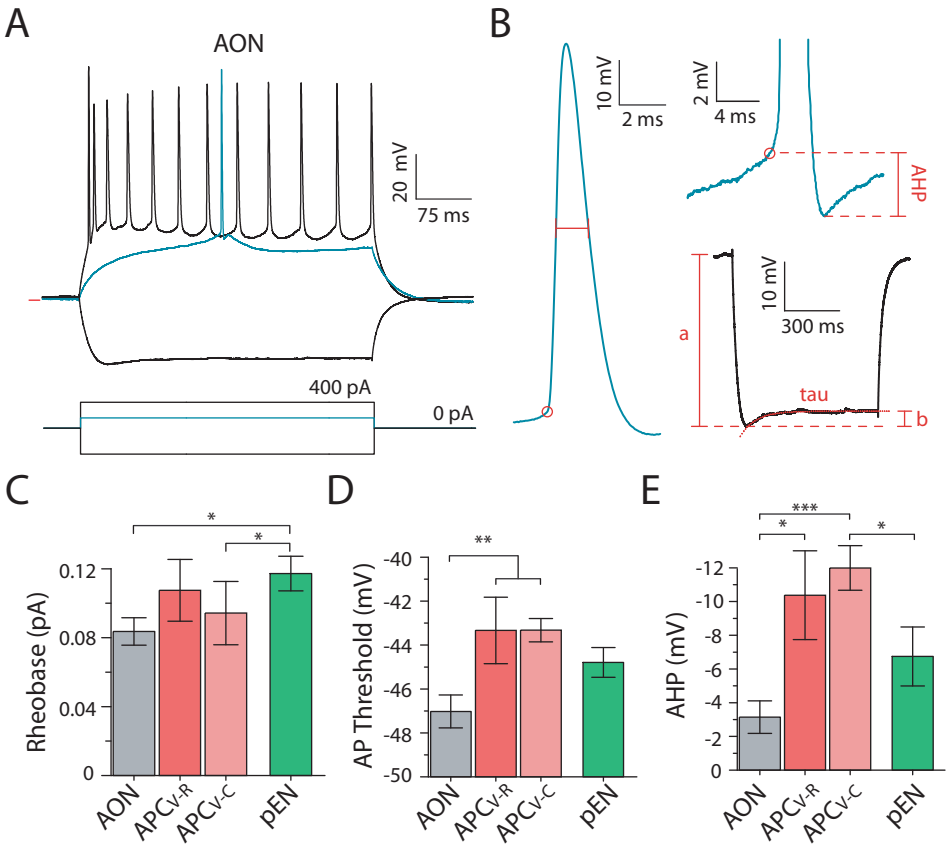
A
AON
20 mV
75 ms
400 pA
0 pA
B
10 mV
2 ms
2 mV
4 ms
AHP
10 mV
300 ms
a
tau
b
C
Rheobase (pA)
0.12
0.08
0.04
0
AON
APCV-R
APCV-C
pEN
D
AP Threshold (mV)
-40
-42
-44
-46
-48
-50
E
AHP (mV)
-12
-10
-8
-6
-4
-2
0

Figure 3

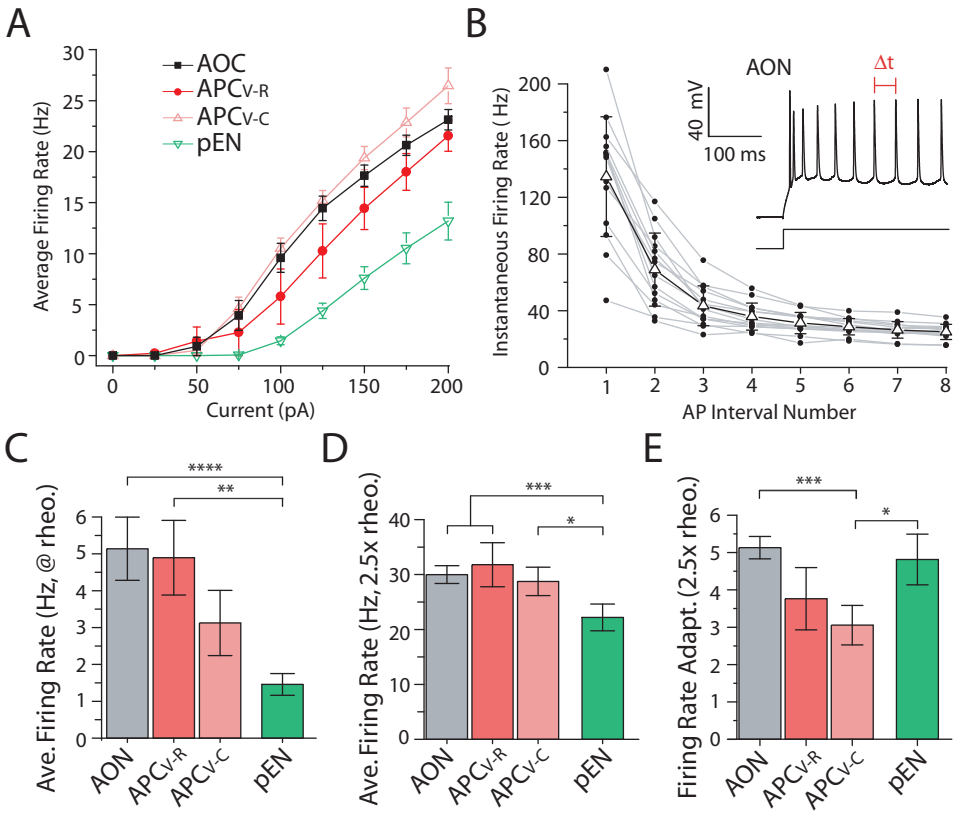
A
B
AOC
APCV-R
APCV-C
pEN
Average Firing Rate (Hz)
Current (pA)
Instantaneous Firing Rate (Hz)
AP Interval Number
AON
Δt
40 mV
100 ms
C
D
E
Ave. Firing Rate (Hz, @ rheo.)
Ave. Firing Rate (Hz, 2.5x rheo.)
Firing Rate Adapt. (2.5x rheo.)
AON
APCV-R
APCV-C
pEN

Figure 4

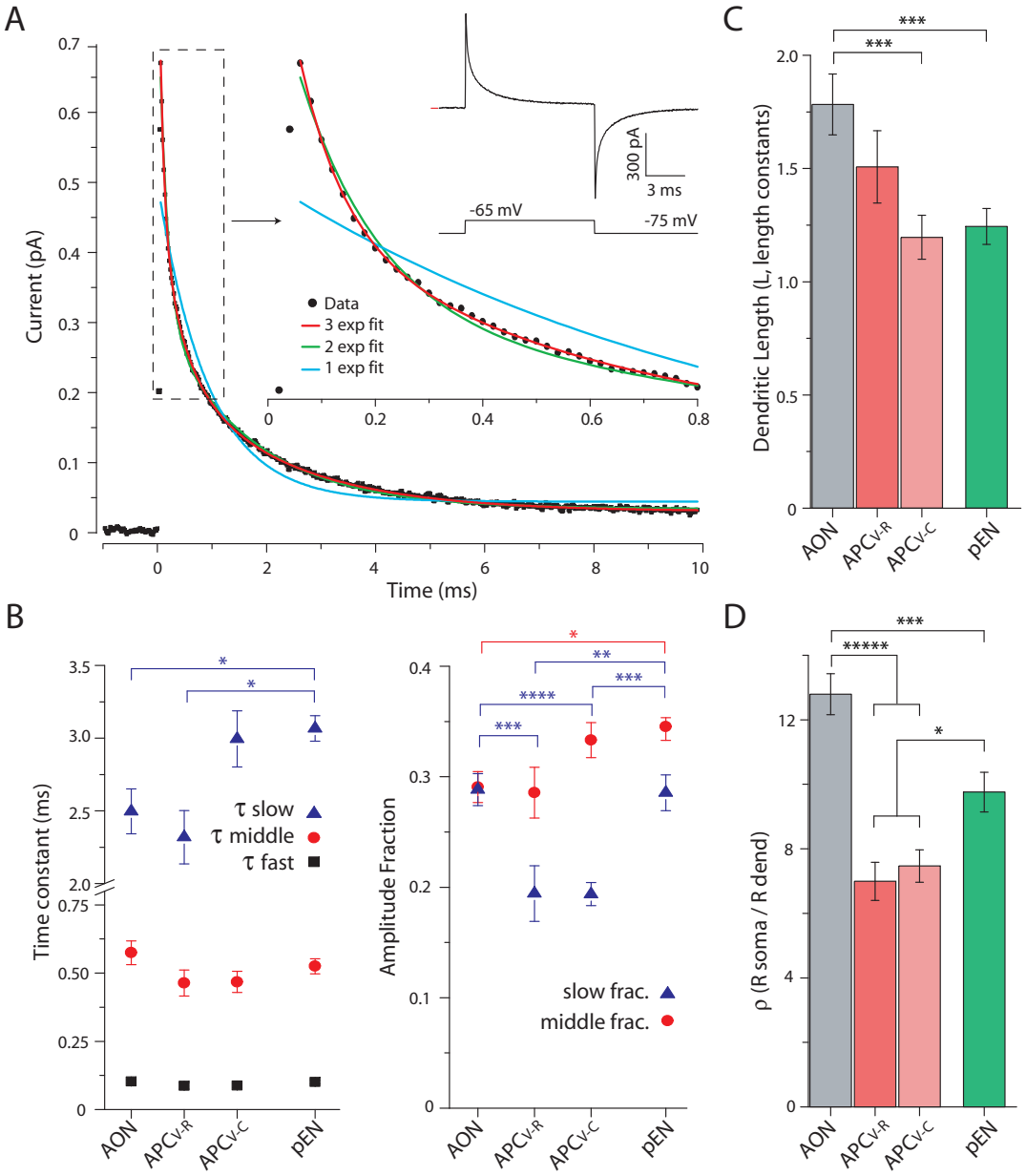
A
Current (pA)
Time (ms)
Data
3 exp fit
2 exp fit
1 exp fit
300 pA
3 ms
-65 mV
-75 mV
C
Dendritic Length (L, length constants)
AON
APCv-R
APCv-C
pEN
B
Time constant (ms)
τ slow
τ middle
τ fast
Amplitude Fraction
slow frac.
middle frac.
D
ρ (R soma / R dend)

Figure 5

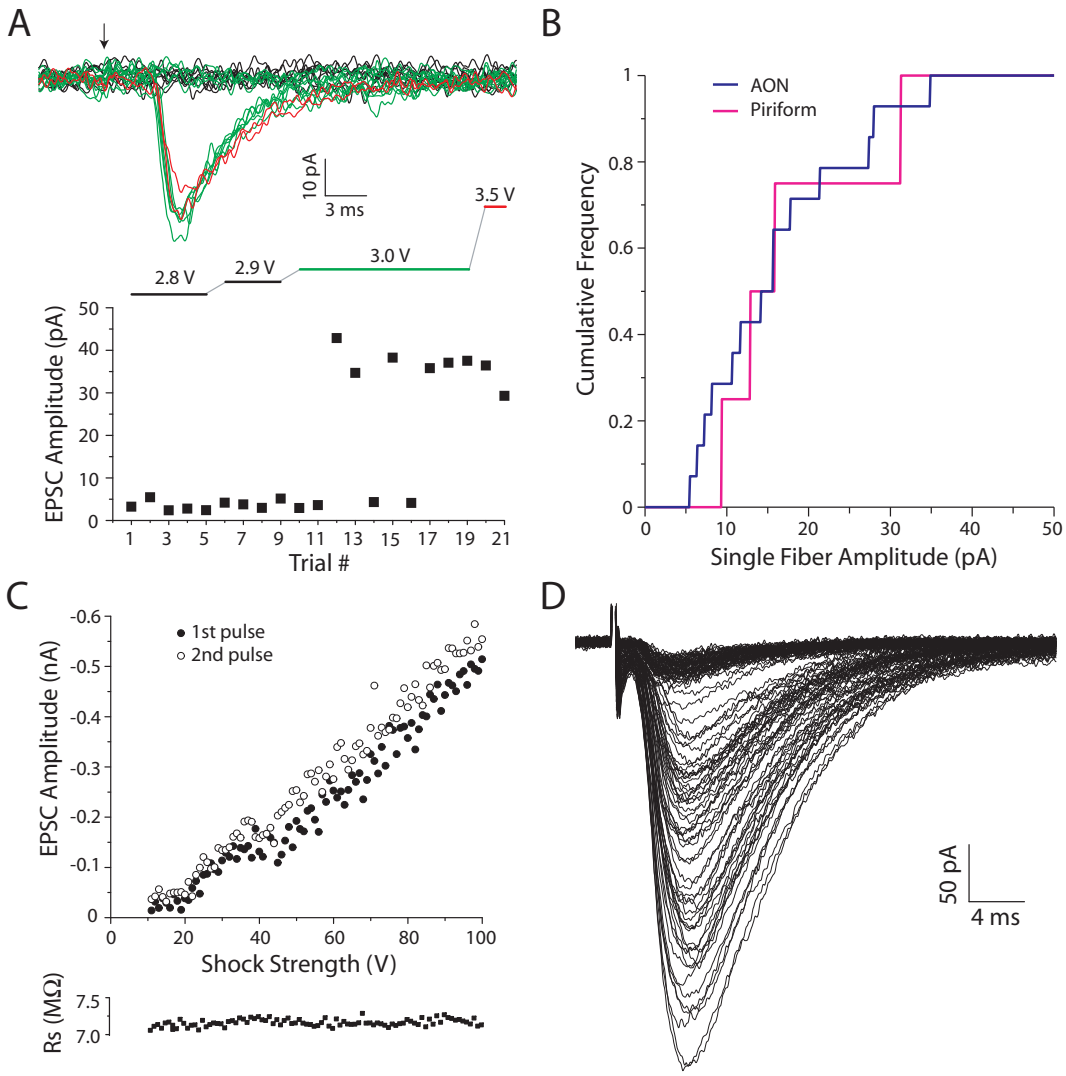
A
10 pA
3 ms
2.8 V
2.9 V
3.0 V
3.5 V
EPSC Amplitude (pA)
Trial #
B
AON
Piriform
Cumulative Frequency
Single Fiber Amplitude (pA)
C
1st pulse
2nd pulse
EPSC Amplitude (nA)
Shock Strength (V)
Rs (MΩ)
D
50 pA
4 ms

Figure 6

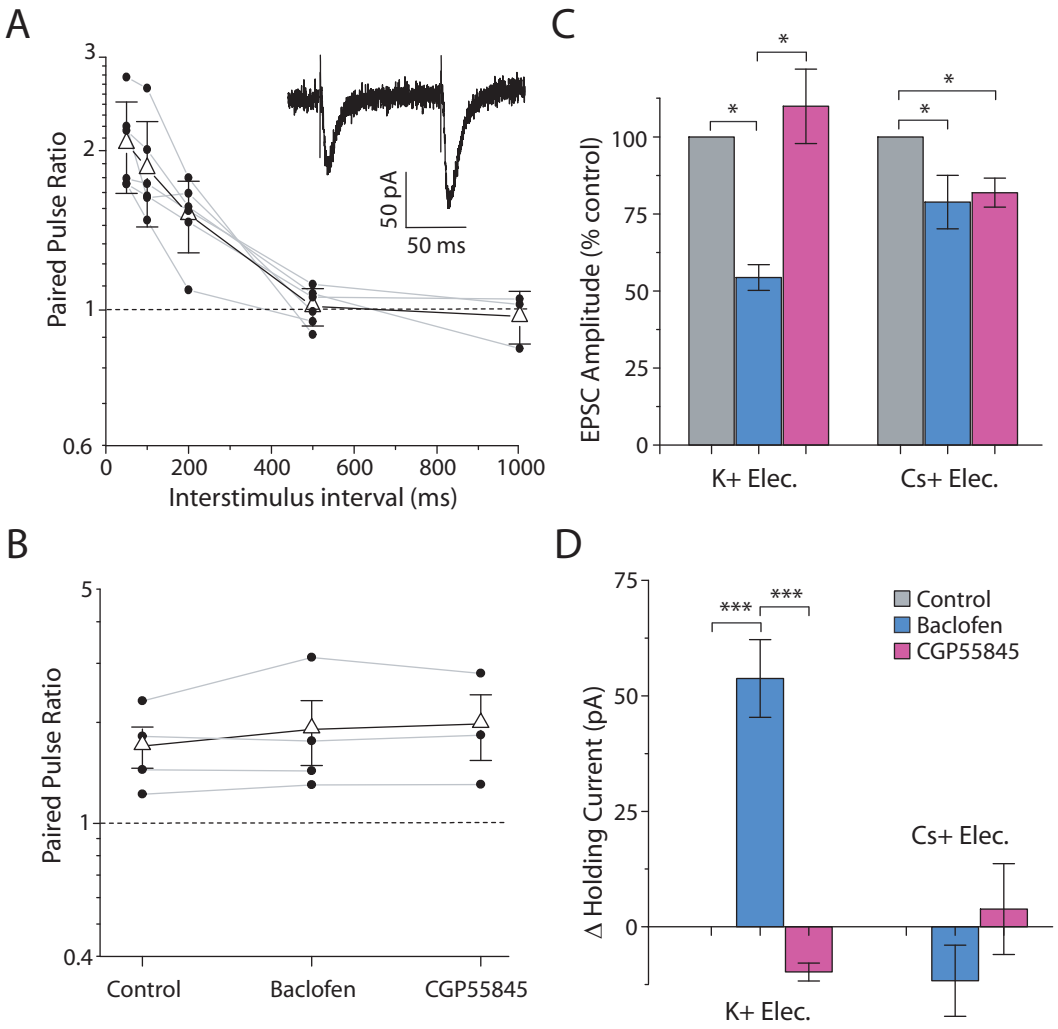
A
Paired Pulse Ratio
3
2
1
0.6
0
200
400
600
800
1000
Interstimulus interval (ms)
50 pA
50 ms
C
EPSC Amplitude (% control)
100
75
50
25
0
*
*
*
*
K+ Elec.
Cs+ Elec.
B
Paired Pulse Ratio
5
1
0.4
Control
Baclofen
CGP55845
D
Δ Holding Current (pA)
75
50
25
0
***
***
Control
Baclofen
CGP55845
Cs+ Elec.
K+ Elec.

Figure 7

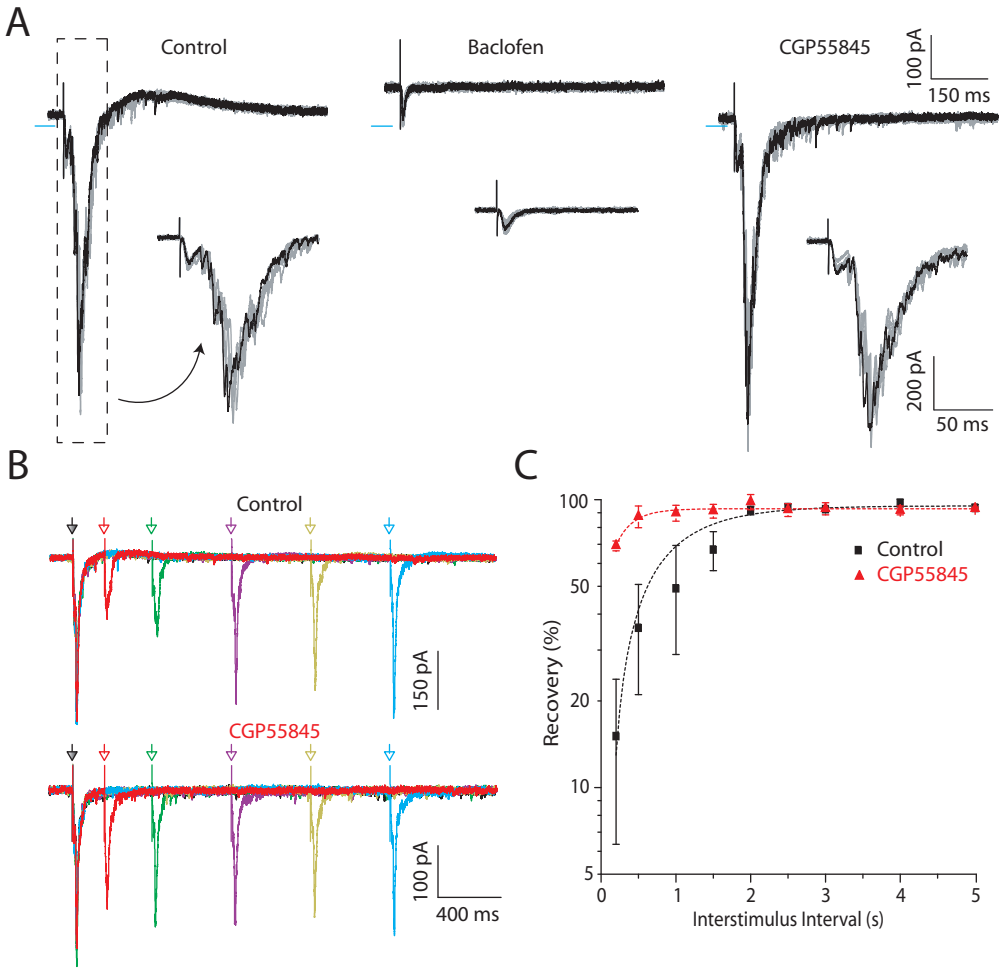
A
Control
Baclofen
CGP55845
100 pA
150 ms
200 pA
50 ms
B
Control
150 pA
CGP55845
100 pA
400 ms
C
Recovery (%)
100
50
20
10
5
0
1
2
3
4
5
Interstimulus Interval (s)
Control
CGP55845

Supplementary Figure 1

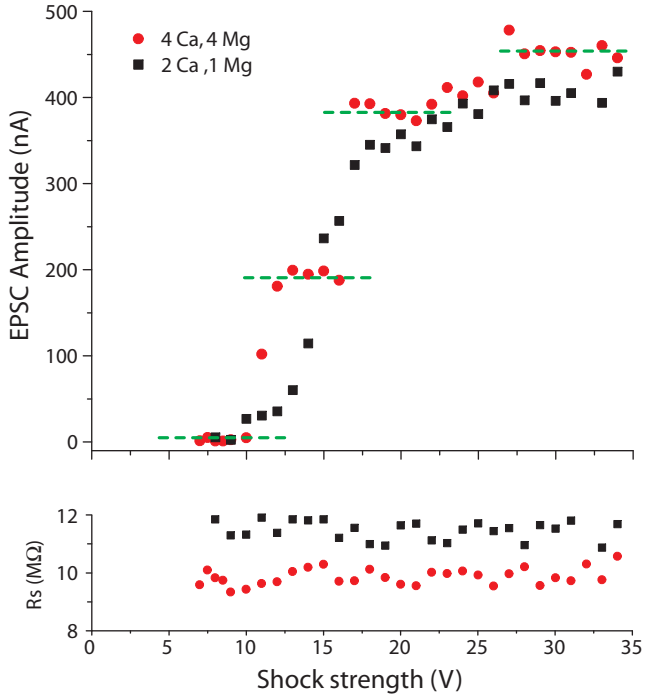

Supplementary Figure 1 Large jumps in EPSC amplitude in high divalents. Top, the EPSC amplitude in an $APC_{V\text{-}R}$ neuron in two different divalent concentrations, as a function of LOT stimulation intensity. Graded stimulation in 1V increments (0.1 Hz) was conduced in physiological divalents (2 mM Ca, 1 mM Mg, black squares) and high divalents (4 mM Ca, 4 mM Mg, red circles) in the same neuron, with a 10 minute wait period in between for solution exchange. Horizontal green dashed lines indicate large jumps in EPSC amplitude, which were seen in high divalents (n=4 cells). Large jumps were not observed in physiological divalents (n=8 cells). Bottom, the series resistance, measured 1 second before each shock, was stable throughout the recording periods.

Chapter 3

Abstract

The study of GABAergic neurons in cerebral cortex has been enhanced by the development of mutant mouse lines that label molecularly defined cell classes. Such mouse lines have been widely used in neocortex, hippocampus, and other brain areas, whereas paleocortex, the cortex of the olfactory system, has remained comparatively unexplored. Here, I evaluate the expression in two regions of paleocortex (piriform cortex and anterior olfactory cortex) in 7 transgenic or knockin mouse lines intended to label interneuron populations. Five of 7 showed severe misexpression, and one line had health problems with the animals. However, 2 lines – a PV-cre / YFP-reporter cross, and a NPY-GFP BAC – showed very accurate expression patterns as assessed by immunohistochemistry and recordings, and should be useful tools for the study of GABAergic interneurons in piriform cortex.

Introduction

GABAergic interneurons in cerebral cortex exhibit a baffling degree of diversity. For example, a collection of 39 scientists recently formed the 'Petilla Interneuron Nomenclature Group,' and created a system for classifying cortical interneurons based on 23 morphological, molecular, and physiological features (Ascoti et al., 2008). Efforts have been made to simplify interneuron classification with organizing principles such as: synaptic function (Gupta et al., 2000); wiring economy (Buzsaki et al., 2004);

developmental lineage (Wonders and Anderson, 2006); and expression of calcium-binding proteins or neuropeptides (Markram et al., 2004; Freund, 2003; Karagiannis et al., 2009).

Classification based on molecular expression is particularly attractive, because of the ability to genetically label, and even manipulate, a molecularly defined cell class (Heintz, 2001; Bernard et al., 2009). A molecularly defined cell class may in some cases exhibit consistent properties, such as parvalbumin expressing interneurons, which tend to have similar spiking characteristics ('fast-spiking') and synaptic characteristics (perisomatic targeting; Freund, 2003). A molecularly defined cell class may, however, exhibit extreme diversity, such as NPY-expressing interneurons (Karagiannis et al., 2009) and somatostatin-expressing interneurons (Halabisky et al., 2006; Ma et al., 2006). None the less, genetic targeting remains a powerful approach.

Genetic targeting strategies fall into two broad classes: transgenic and knockin. Transgenic mice have the advantage that they do not disrupt the relevant endogenous gene locus, whereas knockin mice have the advantage that they can be expected to precisely reproduce the endogenous expression pattern. Knockin mice may result in a fusion protein with a fluorophore (Tamamaki et al., 2003; Chiu et al., 2002), or express a fluorophore or cre after an internal ribosome entry site (ires) sequence (Madisen et al., 2010; Hippenmeyer et al., 2005). Transgenics come in many varieties. 'BAC' transgenics – transgenic lines derived by insertion of a bacterial artificial chromosome – have been suggested as a win-win strategy, because a large amount of DNA (up to several hundred kilobases) is inserted into the genome, preserving upstream, and sometimes downstream, regulatory sequences and therefore, in theory, also expression patterns (Giraldo and

Montoliu, 2001; Heintz, 2001; GENSAT, 2010). Whether BAC transgenics actually reproduce endogenous expression patterns is, however, an empirical matter, to be determined in each line and in each brain area.

In contrast to the neocortex, where interneurons have been studied extensively, very little is known about the diversity and functions of inhibitory interneuron classes in the paleocortex, the cortex of the olfactory system (Ketchum and Haberly, 1993; Kanter el al., 1996; Kapur et al., 1997; Ekstrand et al., 2001; Young and Sun, 2009; Suzuki and Bekkers, 2010a; Suzuki and Bekkers, 2010b). To begin such study, I evaluated the accuracy of expression in 7 interneuron-specific mouse lines. The accuracy of expression was poor in most lines (5 of 7) – particularly the transgenics (4 of 5) – and health issues were observed with one line. Two lines (1 BAC, 1 knockin) had healthy animals and accurate expression.

Results and Discussion

Targeting cell classes with transgenic mice

The first transgenic line I evaluated was the so-called GIN mouse (GFP in Interneurons; Oliva et al., 2000). The GIN mouse is a transgenic that uses a GAD67 promoter to drive expression of EGFP. Several lines were made, and 1 line was found to express, in the hippocampus, selectively in somatostatin-expressing (SOM) interneurons, for unknown reasons (Oliva et al., 2000). It was later found that this line also expresses in SOM neurons in neocortex (Halabisky et al., 2006). It has since been shown that the GIN mouse labels a non-random subset of SOM interneurons, sampling a subspace of the physiological properties of SOM interneurons (Ma et al., 2006).

In the olfactory cortex, immunohistochemsitry has shown that somatostatin is expressed in a rather large numbe of neurons with diverse morphologies in layer III and, to a lesser extent, in endopiriform nucleus (Cummings, 1997; Kowianski et al., 2004). In fixed sections of piriform cortex from GIN mice, a small number of neurons were labeled, mostly in layer III (**Figure 1A**, left, black arrow), probably sampling only a small percentage of SOM neurons (Cummings, 1997; Kowianski et al., 2004). Though small in number, the GFP+ piriform neurons were very strongly labeled, so that their dendritic profiles were apparent (**Figure 1A&B**). Lone labeled dendrites were also apparent, presumably from neurons whose cell bodies were located in adjacent sections (**Figure 1B, black arrows**). In contrast to the piriform cortex, an extremely high density of lightly labeled cell bodies was apparent in endopiriform (EN) and pre-endopiriform nucleus in fixed tissue (pEN; **Figure 1A**, green arrowheads) and live imaging of endogenous fluorescence (data not shown). This was not expected (Cummings, 1997; Kowianski et al., 2004), and most likely represents ectopic expression in excitatory neurons or glia. Supporting expression in pyramidal neurons, αCamKII immunolabling colocalized with GFP in most GIN neurons in endopiriform (data not shown).

A wide range of responses was observed in current clamp recordings from GIN neurons in layer III of piriform cortex, employing long hyperpolarizing and depolarizing steps (**Figure 2**). For example, some neurons exhibited deep, sharp, fast AHPs (**Figure 2**, top left and bottom left). Other neurons exhibited responses typical of pyramidal neurons (**Figure 2**, middle left). Some neurons exhibited accelerating followed by decelerating spiking (**Figure 2**, bottow left), delayed spiking (**Figure 2**, top right), or regular spiking (**Figure 2**, middle right). Some neurons exhibited strong rebound spiking (**Figure 2**,

middle right). This diversity was expected, based on the known diversity of intrinsic membrane properties in SOM neurons in other cortical areas (Halabisky et al., 2006; Ma et al., 2006). The GIN line was not pursued further, because the low cell density in piriform made achieving a reasonable throughput of recordings difficult, in addition to raising concerns about what subset this small sample represented. I was also discouraged by the apparent misexpression in EN/pEN.

The second transgenic line evaluated was a parvalbumin-GFP BAC (Meyer et al., 2002). Initial imaging in this line looked promising (data not shown), so immunohistochemistry for parvalbumin was performed to assess the accuracy of expression (**Figure 3**). Expression looked generally reasonable throughout piriform upon gross inspection (**Figure 3A**, white arrows). However, the AON had a high density of ectopically labeled cells (**Figure 3A**, green arrows; also **Figure 3B**, left). Furthermore, a plexus of ectopically labeled neurons and processes was also observed in piriform cortex in some sections (**Figure 3B**, right). Cell-by-cell comparison at higher magnification (**Figure 3C**) revealed that many cells colabeled (**Figure 3C**, white arrow) however many other cells showed ectopic EGFP expression by antibody (**Figure 3C**, red arrow).

Since modest colocalization indicated that the parvalbumin-GFP BAC (Meyer et al., 2002) showed some promise, I performed whole cell recordings from GFP+ neurons in this line (**Figure 4**). Like the GFP+ neurons in the GIN line, parvalbumin-GFP neurons showed a diversity of responses to long current steps (**Figure 4**). However, this diversity was unexpected for parvalbumin neurons, which in other cortical structures show consistent “fast-spiking” behavior (Freund, 2003). Only about half of recorded neuron showed “fast spiking” behavior (data not shown). Furthermore, despite a

conservative breeding strategy – breeding pairs of a heterozygous male with a WT female– GFP+ pups were smaller than their WT littermates (data not shown). As a result of the only modestly accurate expression pattern, unexpected intrinsic membrane properties, and ill health of the mice, I did not further pursue this BAC transgenic line.

A second BAC transgenic was evaluated which expressed EGFP driven by the CCK promoter (Meyer et al., 2010). Live imaging of expression in 300 μm live slices was performed to preliminarily assess expression (**Figure 5**). CCK protein is expressed in two distinct populations of neurons in the olfactory system: basket cells in piriform cortex, and middle tufted cells (but not mitral cells) in the olfactory bulb (Ekstrand et al., 2001; Seroogy et al., 1985; Wouterlood and Härtig, 1995). In the CCK-EGFP BAC, expression in the olfactory bulb appeared to be almost completely inaccurate (**Figure 5A**). EGFP was ectopically expressed in mitral cells (**Figure 5A**, green arrows), but no labeled cell bodies were observed in the external plexiform layer (EPL) where middle tufted cells are located and should have been labeled. Furthermore, extremely bright and dense labeling was unexpectedly observed in the glomerular layer (GL; **Figure 5A**). Consistent with the labeling in mitral but not tufted neurons, labeling was observed in the full extent of the lateral olfactory tract (LOT) and layer Ia, where mitral (but not tufted) cells project (**Figure 5B**). In piriform, labeling was sparse, and appeared to be distributed fairly evenly throughout layers II and III (**Figure 5B&C**). This was again unexpected, as immunostaining for CCK+ basket cells is predominantly in layer II of piriform cortex (Ekstrand et al., 2001). Due to gross misexpression, this line was not pursued further. A second CCK BAC transgenic from the GENSAT project (GENSAT, 2010) was also

evaluated, and appeared to express in neither mitral nor tufted cells, and had sparse labeling in piriform cortex (data not shown), so it was not pursued further.

Despite the discouraging results with several BAC transgenic mouse lines, an NPY-GFP BAC transgenic was developed that appeared to show nice expression in piriform cortex (van den Pol et al., 2009). This line was obtained, and immunostained for NPY (**Figure 6B**, top). The expression of GFP closely matched labeling for NPY in the piriform cortex and pre-endopiriform nucleus **Figure 6B**, top right). In recording from GFP+ neurons in this NPY line, intrinsic membrane properties were again diverse, as expected from the literature (Karagiannis et al., 2009). An example recording is shown in **Figure 7A**, middle. An analysis of the intrinsic membrane properties from a population of NPY neurons (**Figure 7B**) showed that NPY-GFP showed the diversity in the large standard deviations (**Figure 7B**). Therefore, this BAC transgenic line appears promising for study of NPY neurons in piriform cortex and endopiriform / pre-endopiriform nucleus.

Targeting cell classes with knockin mice

Because most of the transgenic lines evaluated showed inaccurate expression patterns in the olfactory system, I sought instead to label interneurons using the cre-lox system in knockin mouse lines. A line expressing cre at the endogenous parvalbumin locus, after an ires sequence, was obtained (Hippenmeyer et al., 2005), and crossed to a reporter line expressing YFP at the ROSA26 locus (Srinival et al., 2001). Immunostaining for parvalbumin revealed extremely accurate expression of YFP compared to parvalbumin antibody labeling (**Figure 6A**). Whole cell recordings from

YFP+ neurons also showed extremely consistent intrinsic membrane properties, typical of 'fast-spiking' neurons (**Figure 7A**, left; **Figure 7B**), consistent with expectations from prior results (Freund, 2003).

To quantitatively assess colocalization, expression was analyzed in 7 sections from each of 2 animals in each layer, in pEN, APC_{V-R}, APC_{V-C}, and AOC (also called AON). Results are tabulated in Figure 8. Overall, the cre-reporter cross was >90% accurate, particularly in piriform cortex (**Figure 8A**) and expressed in a large subset (~40%) of parvalbumin neurons (**Figure 8B**). Expression was less accurate in AOC (**Figure 8C**), but the number of neurons that express parvalbumin in AOC is small, so the overall accuracy of labeling was not substantially affected by this ectopic expression. Furthermore, all recorded YFP+ neurons in piriform cortex in this line were fast-spiking (n=40), so it is possible that some YFP+, but antibody-negative, cells were actually parvalbumin neurons not labeled by antibody, perhaps due to activity dependence of expression (Patz et al., 2004).

Conclusions

I assessed the accuracy of expression in the paleocortex of 7 knockin or transgenic mouse lines. Five of 7 lines showed misexpression, some dramatically, particularly the transgenics, including BAC transgenics. Furthermore, one BAC line had mice with ill health. Since all were published lines, this raised serious concerns about the validity of the BAC transgenic approach. One might trivialize the results by arguing that the issue was with the antibody used, not the transgenic. However, physiology results from the Parvalbumin BAC and the Parvalbumin-cre / YFP-reporter very closely

matched the antibody staining in terms of the fraction of neurons with “fast-spiking” phenotype. Therefore, the issue is very likely with the transgenics themselves. As such, despite the large chunk of DNA inserted with a BAC transgenic, the endogenous expression profile is not preserved.

The most obvious explanation is that being in the right location on the right chromosome actually matters for gene expression. Such ‘insertional effects’ are widely recognized (e.g. Wilson et al., 1990; Giraldo and Montoliu, 2001), and can occur even with yeast artificial chromosome (YAC) transgenics – which insert three times larger DNA fragments than BACs – due to distantly located regulatory sequences (Lakshmanan et al., 1999). As a result of insertional effects, transgenics in which gene insertion is directed to a locus known to express well, such as the ROSA26 locus, may be more effective (Giel-Moloney et al., 2007). A more conservative, and perhaps interesting, interpretation of my results would be that regulation of gene expression in the olfactory system more frequently involves distantly located regulatory sequences, perhaps due to the ancient phylogeny of the system. Whatever the cause, my results show the importance of carefully characterizing the accuracy of expression in the brain area(s) of interest, in any mutant mouse line, before relying on it as a tool.

Materials and Methods

Electrophysiological recordings were performed using methods described in Chapter 1. For immunohistochemistry, animals were transcardially perfused at age PND30-40, first with ice cold PBS (1-3 minutes) and then with filtered 4% paraformaldehyde (PFA; 8-10 minutes) at a rate of 1-2 ml/minute. Brains were then

removed from the skull and drop fixed in 4% PFA for an addition 16-24 hours. 50 μm sections, at the slice angle described in Chapter 1, Supplementary Figure 1, were made using a Leica vibratome dedicated to working with fixed material. Immunohistochemistry was then peformed with the following standard protocol (example is for parvalbumin):

First Day

Rinse fixed block of brain in PBS for 10 minutes

Slice at 50 μm in PBS

Rinse slices in PBS 3x (10 minutes)

0.2% Triton PBS for 30 minutes at room temp

Add 6% Normal Goat Serum, agitate for 30 minutes at room temp

1^0 Mouse anti-parvalbumin (1:2000), 3% Goat Serum, 0.1% Triton PBS at 4^0 C, 24 hrs.

Next Day

Quick rinse in PBS

Rinse in PBS 3x (10 minutes)

2^0 antibody (1:250, Goat anti-Mouse 555, mol. probes), 3% Goat Serum and 0.1% Triton PBS for 2.5 hours at room temp.

Quick rinse in PBS

Rinse in PBS 3x (10 minutes)

Mount in vector-shield w/dapi medium

For NPY staining, the following antibody was used: anti-NPY (1:800, Abcam, Cambridge, MA, ab10980).

Figure Legends

Figure 1 Expression of GFP in the GIN mouse in piriform cortex and endopiriform nucleus. **A.** Two images (10x objective) of unenhanced GFP expression. Black arrow points to a typical layer III GIN neuron, and green arrows point to dense ectopic cell body labeling in EN / pEN. Yellow text indicates layer of piriform or endopiriform / pre-endopiriform nucleus. Most of the labeling in EN/pEN is probably ectopic, and the labeling in layer III samples only a small number of SOM neurons. **B.** Two images from the same line (20x), indicating the labeling of dendritic profiles (black arrows), prominent in layer III.

Figure 2 Voltage responses to hyperpolarizing and depolarizing current steps in 5 GIN neurons from layer III of piriform cortex. Overlapping traces are shown in different colors for clarity. GIN neurons exhibited diverse intrinsic membrane properties.

Figure 3 Immunhistochemistry for parvalbumin in a PV-GFP BAC transgenic shows modest colocalization. **A.** A montage of confocal images of endogenous GFP (green, top) and parvalbumin antibody staining (red, bottom). There was modest colocalization throughout piriform (white arrows). Dense ectopic GFP labeling was observed in AON, probably pars externa (green arrows). Also note false negative expression in the striatum (yellow arrows), and ectopic expression in the hippocampus, particularly in dentate gyrus (aqua arrows). See Chapter 1, Supplementary Figure 1, for a detailed diagram of brain areas in the slice preparation. **B.** Left, higher magnification image of ectopic GFP expression in pars externa of AON. Right, ectopic GFP expression in a plexus of neurons

in piriform cortex, which was apparent in some sections. Red streaks are large diameter blood vessels **C.** Higher magnification images of modest colocalization in piriform cortex: GFP (left), parvalbumin antibody labeling (middle), and overlay (right). Green arrow indicates an area with many ectopic GFP expressing cells. White arrow indicates an area with many co-labeled cells.

Figure 4 A. Recordings from a PV-GFP BAC transgenic show diverse intrinsic membrane properties. Left column, low resolution images showing the position of the recording electrode Rows 3 and 6 image GFP fluorescence, rows 4 and 5 are DIC images. All recordings were in layer III of anterior piriform cortex. Middle column, higher resolution image of the recorded GFP+ neuron. Right column, voltage responses to a family of current steps in each neuron.

Figure 5 Highly ectopic expression in a CCK-GFP BAC transgenic in the olfactory system. **A.** Left, low resolution image of GFP expression in the olfactory bulb. GL, glomerular cell layer; EPL, external plexiform layer. The bright, dense labeling in the GL is probably mostly ectopic. Green arrow indicates ectopic expression in mitral cells. Right, higher resolution image of the olfactory bulb, from a different section. **B.** Montage of low resolution images of expression in the olfactory system. PPC, posterior piriform cortex; APC, anterior piriform cortex; AON, anterior olfactory nucleus; LOT, lateral olfactory tract; I,II,III, layer of piriform; En, endopiriform nucleus. Note bright expression in the full rostro-caudal extent of the LOT. This is consistent with the ectopic labeling in mitral cells in the bulb. **C.** DIC image (left) and image of GFP (right) at the

same location. Note low density of GFP labeled cells throughout the layers of piriform and En. This is unexpected, as CCK is mostly expressed in layer II of piriform.

Figure 6 Maximal intensity projections of line scan confocal images of 50 μm sections with the indicated transgenics and antibodies. **A.** Endogenous YFP expression (left), parvalbumin antibody staining (middle) and merge (right) from a PV-cre / YFP reporter cross. YFP is accurately expressed in a large subpopulation of parvalbumin expressing interneurons in piriform cortex. **B**. Endogenous GFP transgenic (left), immunostain for NPY (middle), and merge (right), in a NPY BAC transgenic. The NPY-GFP transgenic accurately labeled NPY expressing neurons in the piriform cortex. **C**. Immunostain for parvalbumin (left), immunostain for NPY (middle, repeated from above), and merge (right). Parvalbumin and NPY neurons in piriform cortex form largely non-overlapping populations.

Figure 7 Distinct intrinsic excitability of parvalbumin neurons, NPY neurons, and principal neurons in several cortical subregions. **A.** Example current clamp recording from a GFP neuron in a PV-cre / YFP-reporter line (left), a GFP neuron from a NPY-GFP BAC (middle), and a pyramidal neuron in APC_{V-C} (right). Blue line indicates a potential of -80 mV. **B.** Comparison of 6 parameters of intrinsic membrane properties across cell types.

Figure 8 Highly accurate expression in the PV-cre / YFP-reporter cross. **A.** Total parvalbumin antibody labeled red cells (top), fraction of YFP cells that were antibody

positive (accuracy, middle), and fraction of antibody labeled cells that expressed YFP (fraction labeled, bottom) in $APC_{V\text{-}R}$, from 7 sections in one animal. Layer or region indicated below the x-axis. **B.** Summary data from two animals of the fraction labeled and accuracy, taking into account all cells from pEN, VEN, AON, $APC_{V\text{-}R}$, $APC_{V\text{-}C}$). Animal labeled labeled below the x-axis. **C.** Total parvalbumin antibody labeled red cells (top), and fraction of YFP cells that were antibody positive (accuracy, middle), in AOC, from 7 sections in one animal.

A

Figure 1

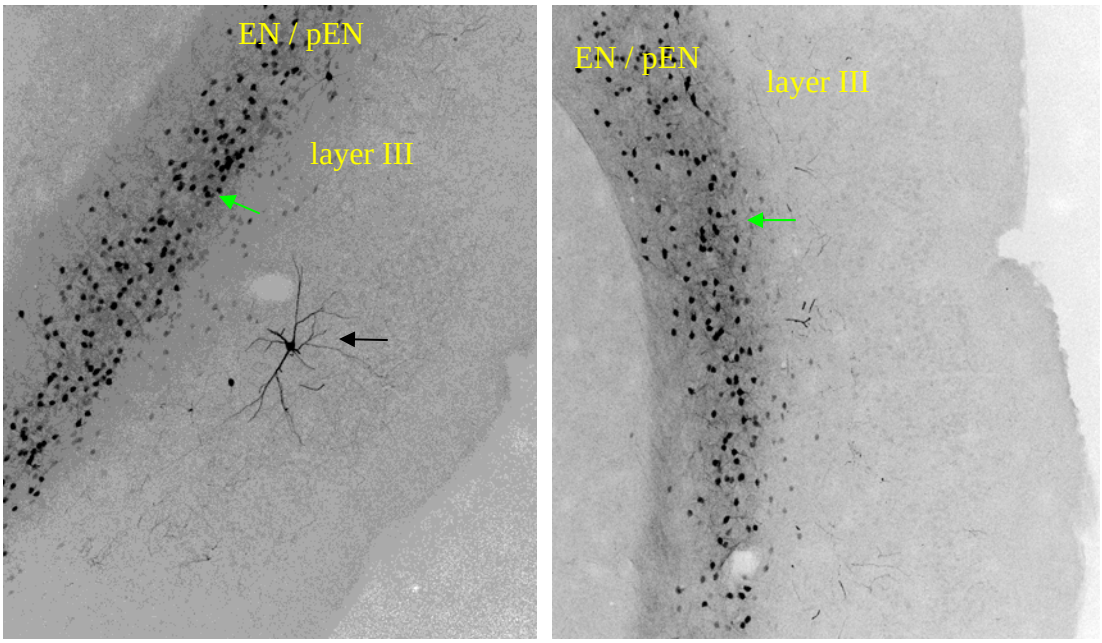
EN / pEN
layer III
EN / pEN
layer III

B

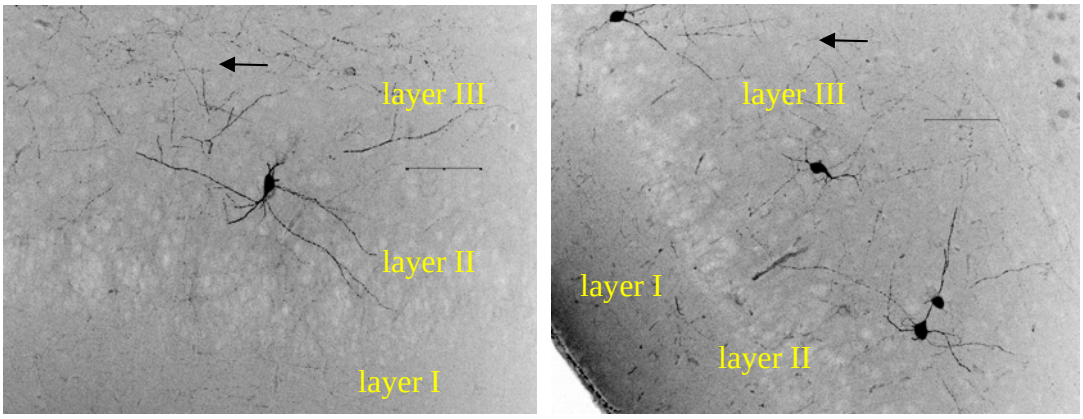
layer III
layer II
layer I
layer III
layer I
layer II

Figure 2

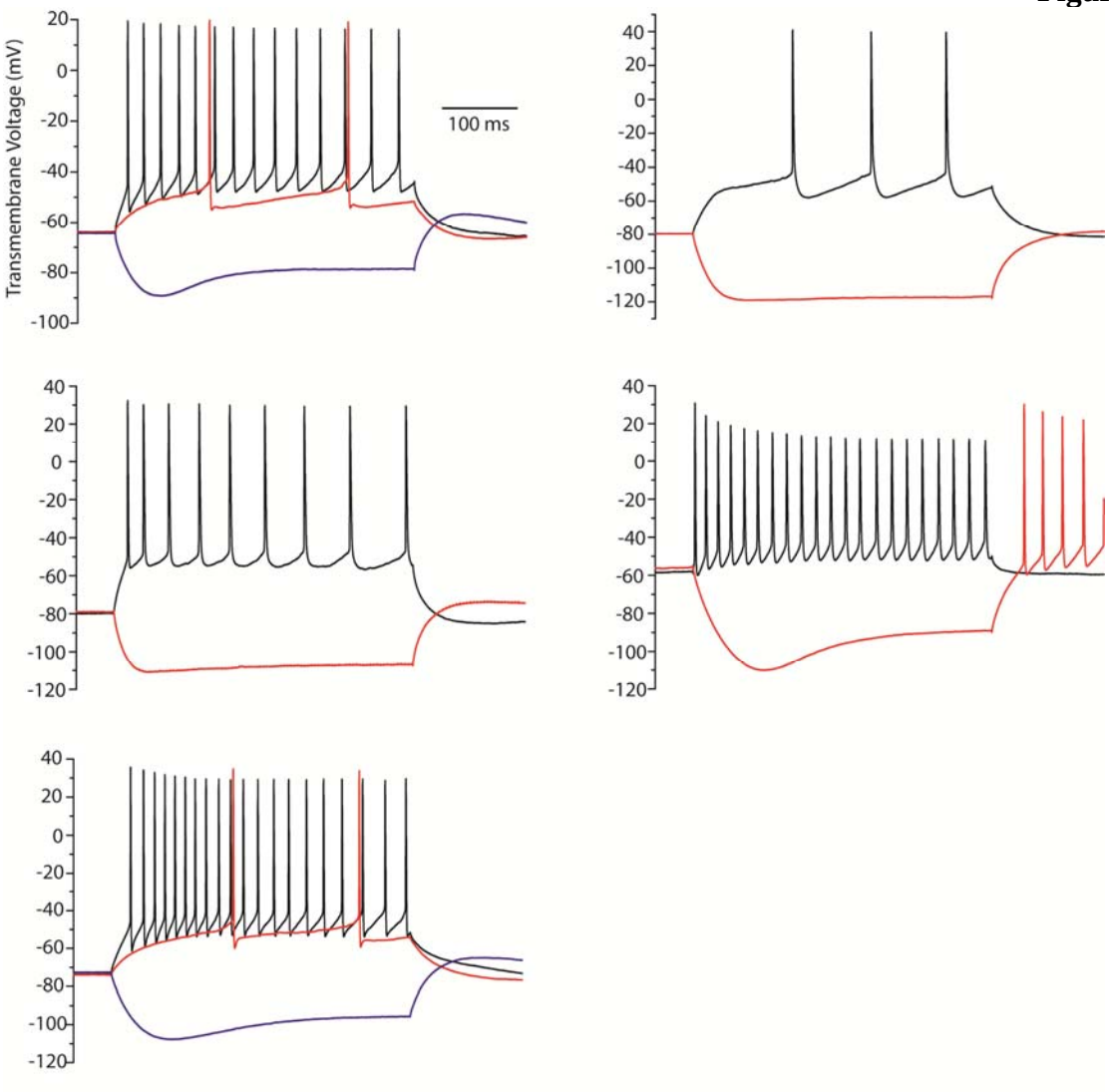
Transmembrane Voltage (mV)
100 ms
20
0
-20
-40
-60
-80
-100
40
20
0
-20
-40
-60
-80
-100
-120

Figure 3

A

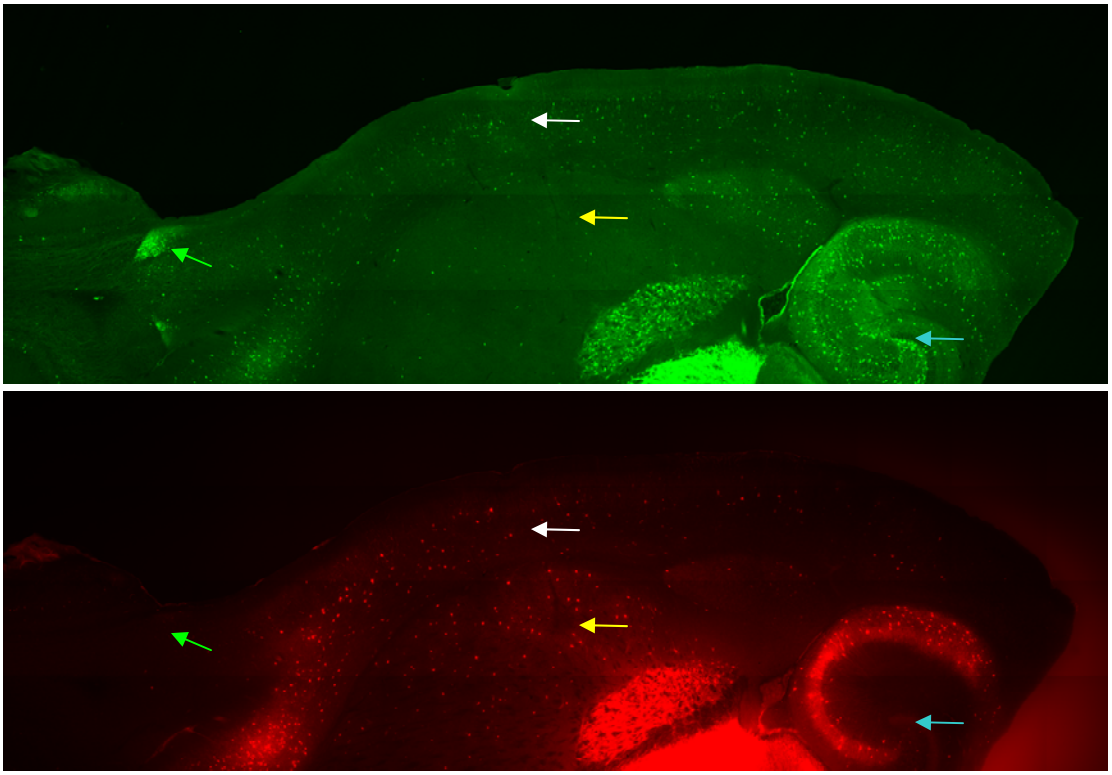

B

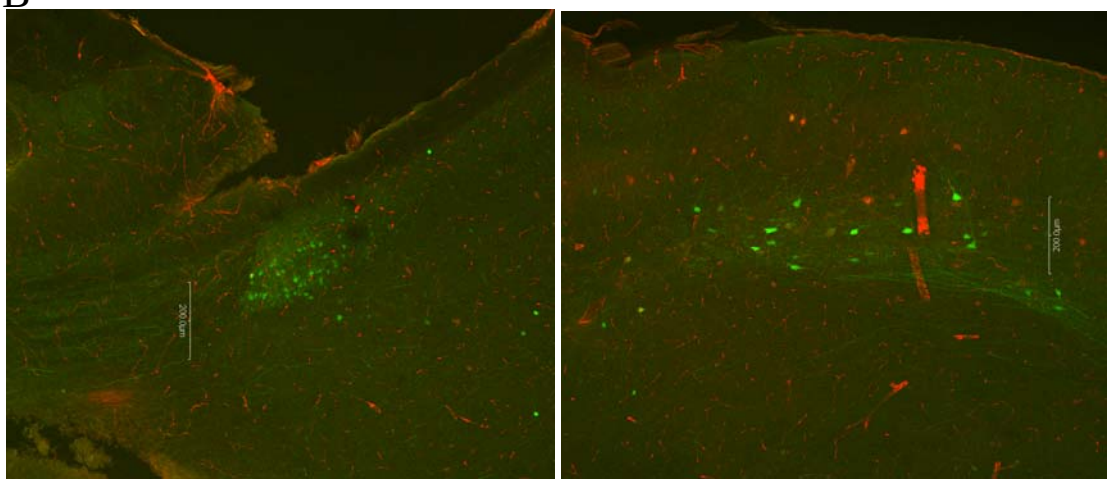

C

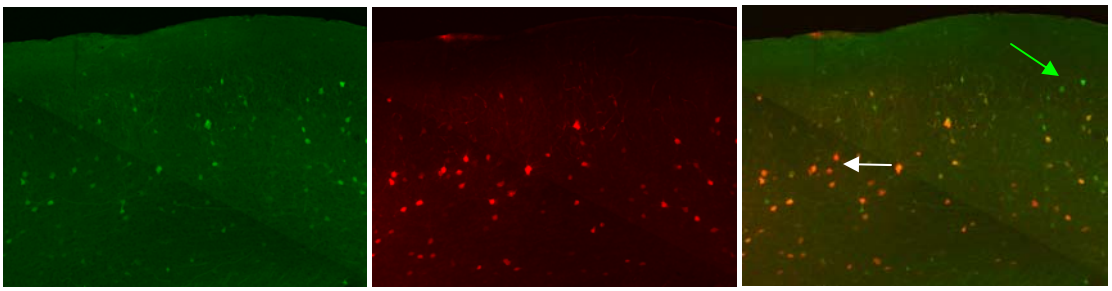

Figure 4

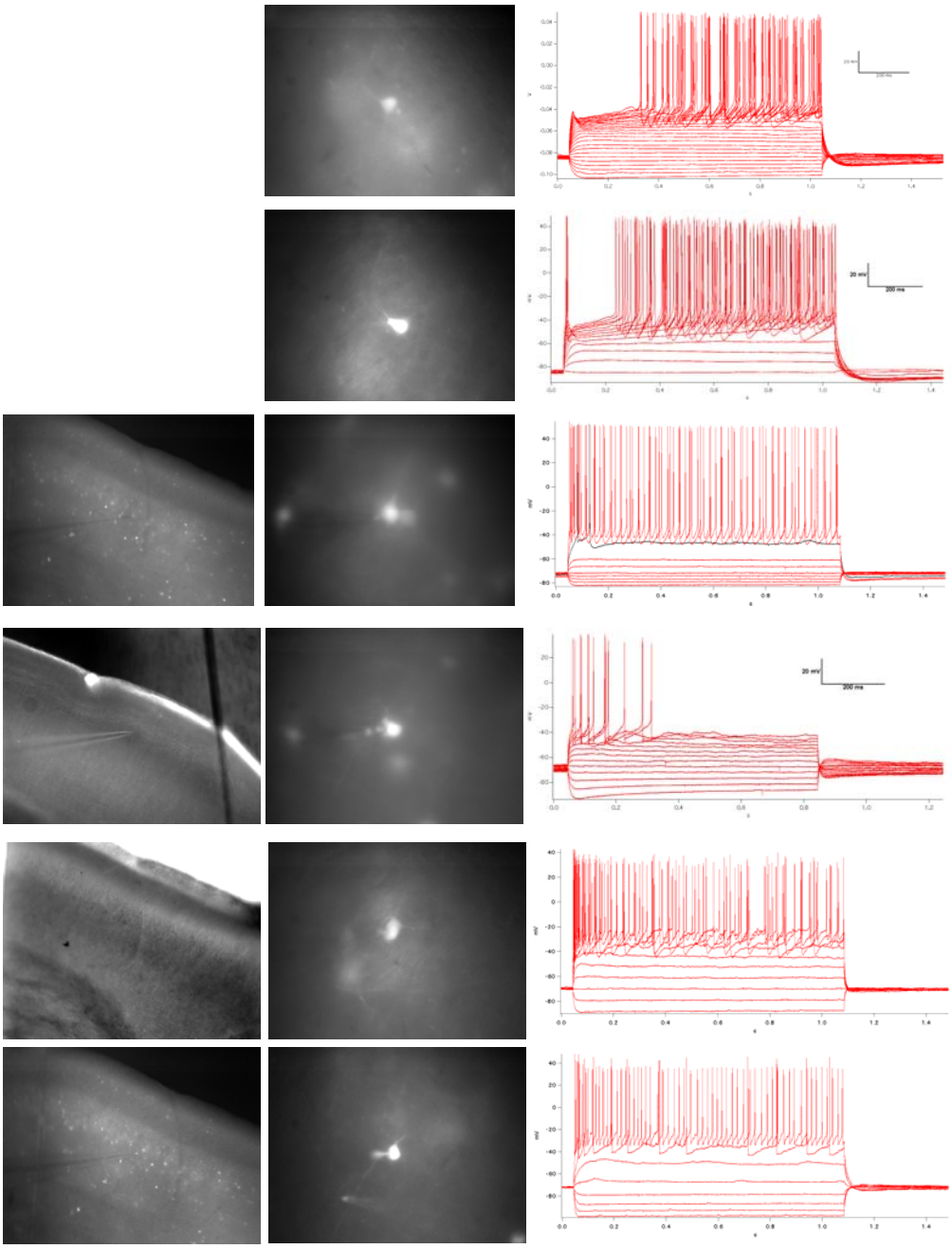

Figure 5

A

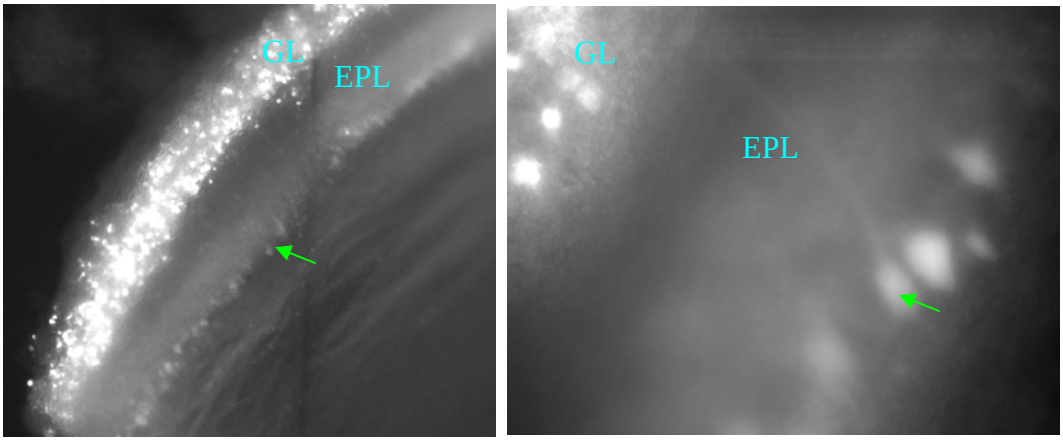

B

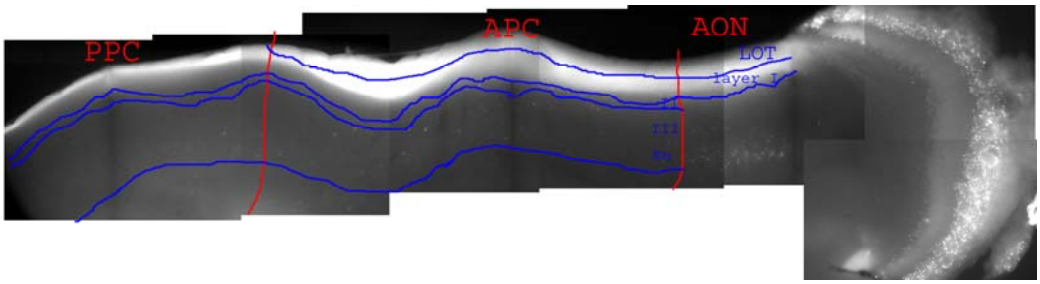

C

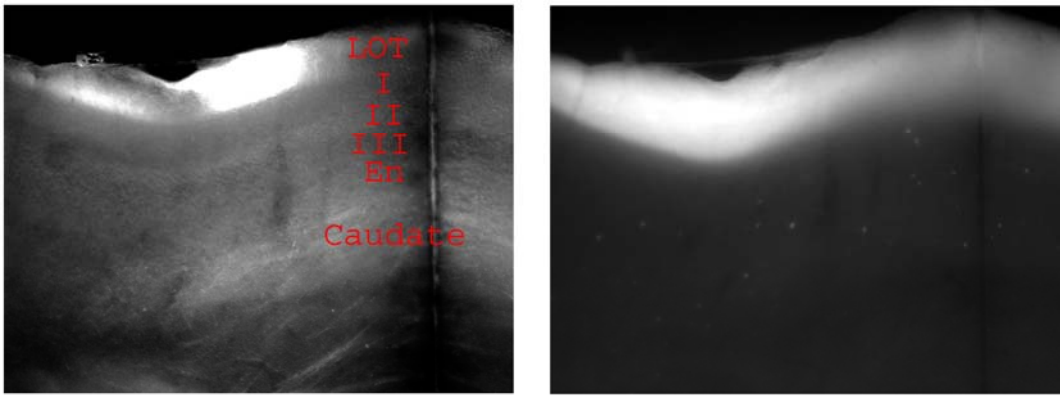

Figure 6

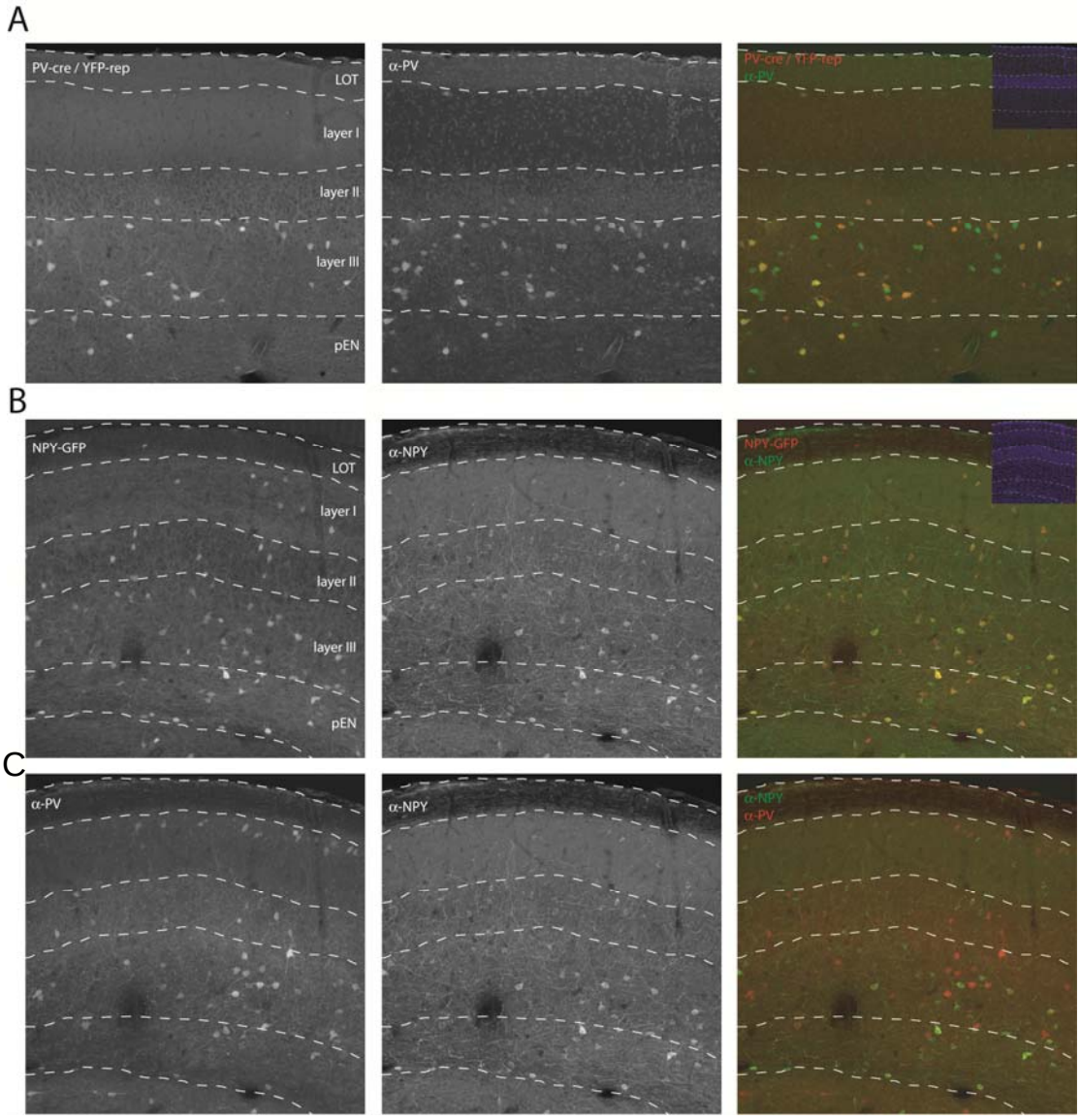
A
PV-cre / YFP-rep
LOT
layer I
layer II
layer III
pEN
α-PV
PV-cre / YFP-rep
α-PV
B
NPY-GFP
LOT
layer I
layer II
layer III
pEN
α-NPY
NPY-GFP
α-NPY
C
α-PV
α-NPY
α-NPY
α-PV

Figure 7

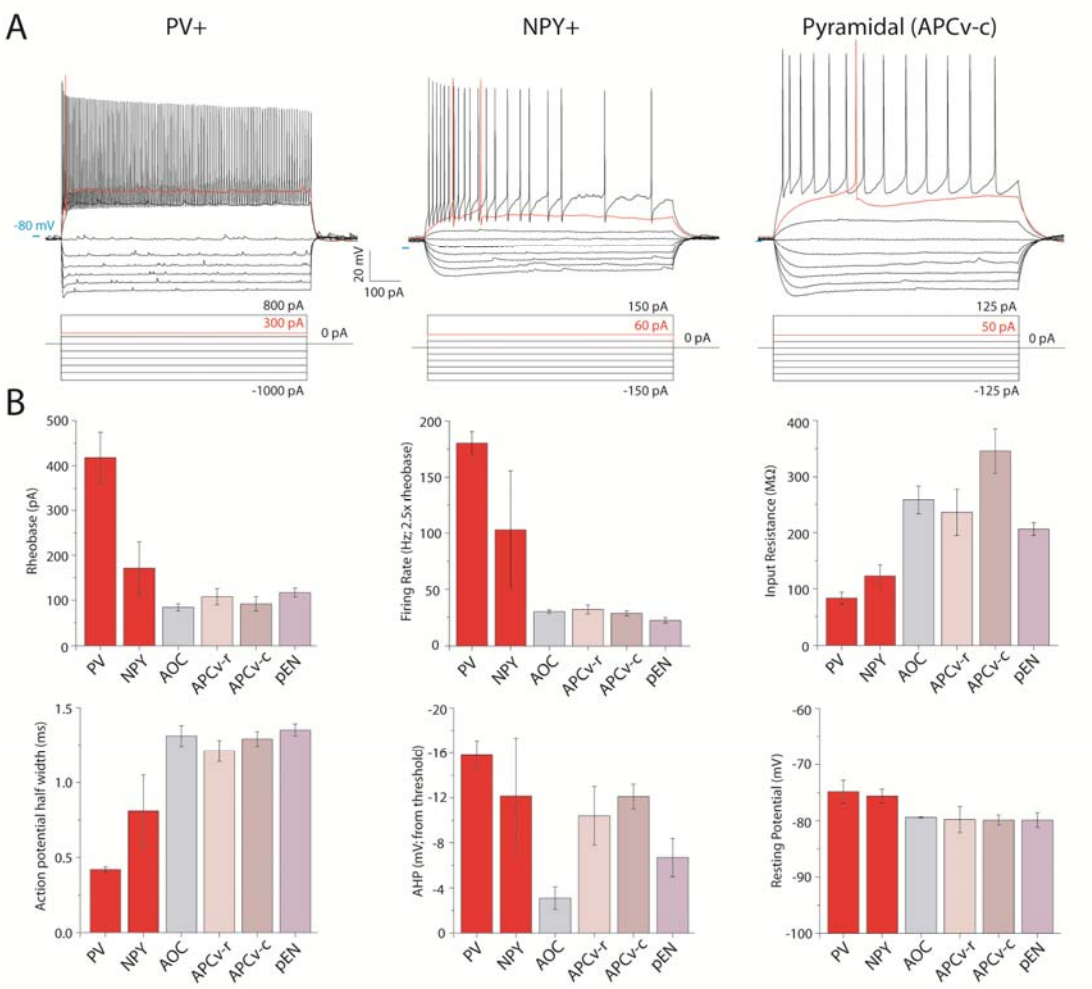
A
PV+
NPY+
Pyramidal (APCv-c)
-80 mV
20 mV
100 pA
800 pA
300 pA
0 pA
-1000 pA
150 pA
60 pA
0 pA
-150 pA
125 pA
50 pA
0 pA
-125 pA
B
Rheobase (pA)
Firing Rate (Hz; 2.5x rheobase)
Input Resistance (MΩ)
Action potential half width (ms)
AHP (mV; from threshold)
Resting Potential (mV)
PV
NPY
AOC
APCv-r
APCv-c
pEN

Figure 8

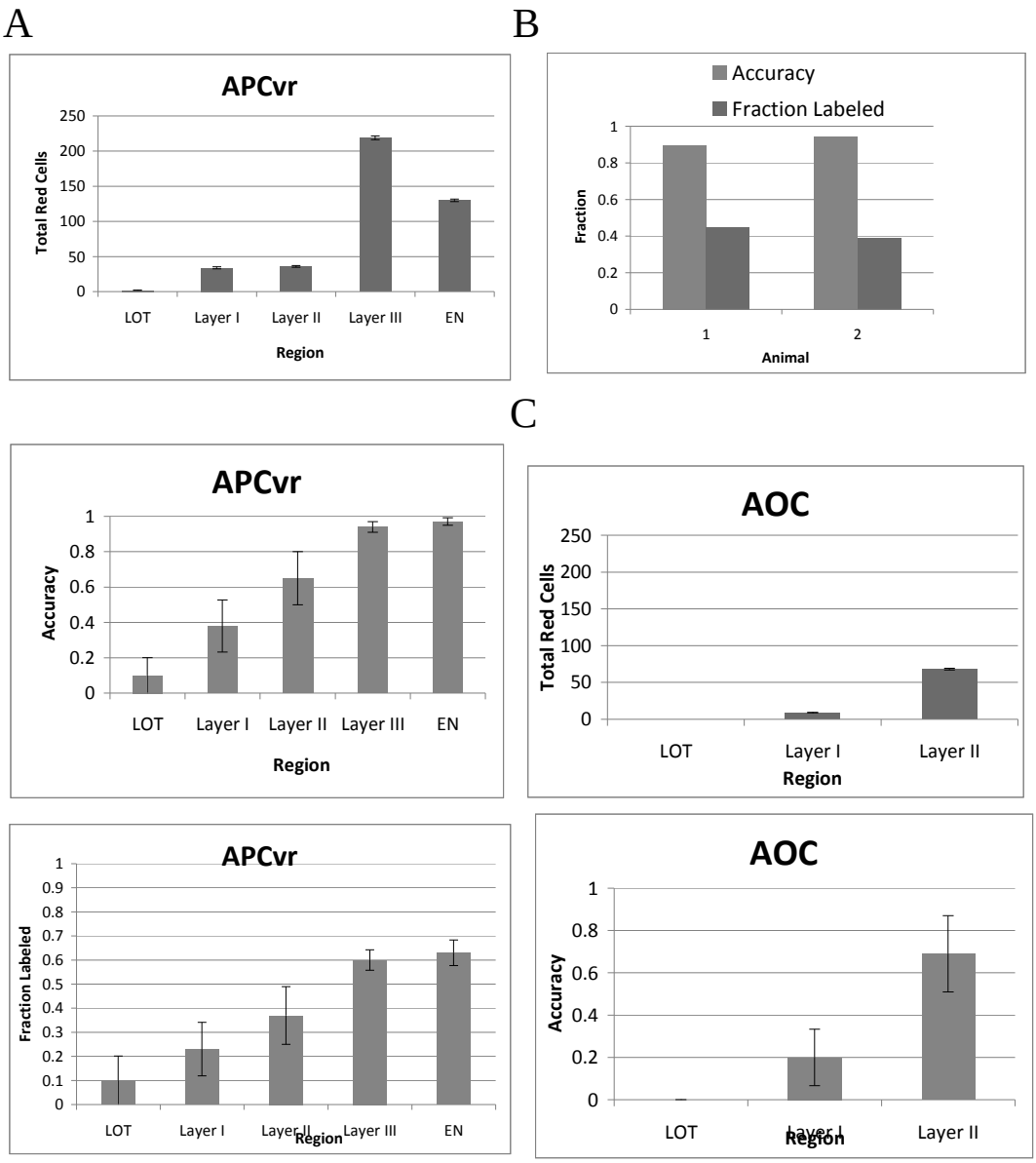
A
APCvr
Total Red Cells
250
200
150
100
50
0
LOT
Layer I
Layer II
Layer III
EN
Region
B
Accuracy
Fraction Labeled
Fraction
1
0.8
0.6
0.4
0.2
0
1
2
Animal
C
APCvr
Accuracy
1
0.8
0.6
0.4
0.2
0
LOT
Layer I
Layer II
Layer III
EN
Region
AOC
Total Red Cells
250
200
150
100
50
0
LOT
Layer I
Layer II
Region
APCvr
Fraction Labeled
1
0.9
0.8
0.7
0.6
0.5
0.4
0.3
0.2
0.1
0
LOT
Layer I
Layer II
Layer III
EN
Region
AOC
Accuracy
1
0.8
0.6
0.4
0.2
0
LOT
Layer I
Layer II
Region

SUMMARY AND CONCLUSIONS

In this thesis I sought to examine the network dynamics within and across subregions of the olfactory cortex. I developed a slice preparation containing the anterior olfactory nucleus (AON), ventral anterior piriform cortex (APC_V), pre-endopiriform nucleus (pEN) – and connections between them – and performed paired whole-cell recordings. I also performed immunohistochemistry to evaluate several mutant mouse lines, and developed analysis methods to help interpret data. My main findings were the following: excitatory interactions across subregions of olfactory cortex can support coherence at high frequencies; basic physiological properties of the AON are more excitable than piriform cortex, but typical of pyramidal neurons in cerebral cortex; expression patterns in several BAC transgenic lines are highly inaccurate in the olfactory system, whereas a knockin strategy gave better results.

Broadband coherence across olfactory cortex

In paired voltage-clamp recordings across subregions of the olfactory cortex, I found that the waveforms of bursts of excitatory synaptic current were extraordinarily similar across subregions, on a trial-to-trial basis. This was striking, because neurons in pairs were separated by several millimeters, in many cases, and were selected randomly. These results suggested that the excitatory network in olfactory cortex is highly distributed, and overlapping. That is, if subnetworks in the excitatory architecture exist at all, they extend broadly, and overlap, so that even randomly selected pairs receive very

similar temporal profiles of input, during bursts of excitatory activity. To quantitatively evaluate this interpretation, I performed several analyses on paired burst waveforms. First, I observed that the latency to bursts varied from trial-to-trial by as much as 80 ms, though bursts lasted around 25 ms, and occurred at very similar times (~10 ms lag, at most). Therefore, it was necessary to correct for trial-to-trial variability in latency. To accomplish this, I wrote a simplex algorithm to minimize the covariation – trial-specific cross-correlation – of bursts, while eliminating the latent period before bursts. Having eliminated latency effects, the trial-specific component of burst waveforms was determined by calculating the 'residuals,' or waveform on each trial after subtraction of the average burst waveform for each cell. To compare residuals, latency-corrected waveforms, and raw waveforms, I developed a coherence analysis method with good spectral performance and robust statistics. The results of the analysis clearly supported the initial interpretation that burst waveforms were similar, trial-to-trial, because coherence was reliably observed for freqencies up to 500 Hz.

These results pose the puzzling question: "how are memories formed and recalled in piriform cortex?" One would think there must be subnetworks in piriform cortex, hardwired together or developed, so that olfactory information is encoded as activity in these subnetworks. The enigma of an apparently 'random' distributed network in olfactory cortex illustrates that, in my opinion, the nature of the manifestation of memories as real brain activity is very poorly understood. For example, the notions of 'attractor states' and 'synfire chains' – popular models for encoding in networks that have been leveraged on theoretical grounds – are supported by scant, and often controversial, experimental evidence (Barbieri and Brunel, 2008; Schrader et al., 2008;

Ikegaya et al., 2004; Mokeichev et al., 2007). One intriguing possibility is that the piriform cortical network of a 3 week old mouse raised in an animal facility is relatively 'untrained.' That is, rich subnetwork structure is lacking because of the meager demands of the animal in terms of making olfactory associations. Experiments on older mice may be fruitful. Moreover, it would be interesting to perform experiments on field mice, or mice raised in enriched environments, with more realistic demands of their olfactory learning.

Future directions:

The principal criticism I received of these results was, 'You've blocked inhibition, so of course your bursts are coherent!' Implicit to this criticism is the claim that similar coherence would be seen in all cortical circuits. Therefore, I believe it will be important to perform similar experiments and analysis in other brain areas – such as barrel cortex, which has marked columnar structure – to better understand how sensitive my approach is to the architecture of excitatory connectivity. If my conclusions are correct, bursts would not exhibit the same degree of coherence in, i.e., barrel cortex, or other highly columnar cortical cortical areas, due to a relative lack of distributed connectivity.

In addition, the coherence analysis method developed, here, should be useful beyond this project, because it was developed to be a good coherence analysis method with good statistics, period, and only tailored to the current project in terms of the general experimental paradigm: paired measurements on repeated trials. Finally, it will be valuable to look at the distributed vs. local character of processing in other ways, such as

in other pharmacological conditions in the slice. Some such experiments are ongoing. The future of study of network dynamics in piriform cortex, in general, clearly will be very rich. The compact nature of the olfactory system, early evolutionary genesis, and progenesis of neocortex of piriform cortex, make it the perfect system to study the relationship between network dynamics and behavioral function, such as learning, memory, and epilepsy.

Basic physiology of the AON

Because one of the subregions under investigation (the AON) had not been studied, previously, in terms of single cell or network physiology, I performed a study characterizing basic physiology of the AON. I believe this study was important, because I found the idea of performing recordings in AON, without understanding its basic properties, to be prone to potential pitfalls of confusion and misinterpretation. In characterizing the AON, I performed recordings in APC_V and pEN, as well, for comparison. I thought this would be valuable, because comparisons across studies are always difficult, due to numerous possible confounding factors in experiments: i.e., slice quality, temperature, pH, extracellular ion concentration, cell-selection bias, and recording quality. This strategy proved fruitful, because AON principal neuron single cell physiology was quite consistent across cells, and numerous similarities and differences were observed between AON, APC_V and pEN principal neurons and synapses.

The results of this study can be summarized as follows: AON is quite similar to the piriform cortex, except more excitable, and pEN has several specializations that appear to dampen excitability. These results should place AON firmly ‘on the map’ as a

module of olfactory cortex, and will hopefully facilitate future study of the AON. The specializations of pEN to dampen excitability are interesting in light of the epileptogenicity of pEN. The fact that pEN principal neurons apparently express more (G)IRK channels than AON and APC_V supports the prediction that these channels may help buffer extracellular potassium accumulation during seizures (Howe et al., 2008). Furthermore, I observed that single fiber inputs to AON and APC_V were 'weak,' in contrast to a recent study reporting strong single fiber input to the piriform cortex (Franks and Isaacson, 2006). In experimental conditions similar to the Franks and Isaacson study, I observed a narrowed dynamic range in the shock strengths that elicited synaptic responses, and a sigmoidal relationship between shock strength and EPSC amplitude. These results point to at least two reasons for the discrepancy between studies. First, the narrowed dynamic range in Franks and Isaacson's experiments would make it harder to resolve the small inputs. Supporting this idea, many of the experiments in the Franks and Isaacson study did not meet strict criteria for resolving single inputs, that is, jumps in amplitude with a small change in shock strength that are stoichastic across trials. Second, the sigmoidal relationship between shock strength and response amplitude suggests that there may be some form of cooperativity going on in high divalents, such as gap junctions between axons in the LOT, or some calcium-dependent positive feedback process in the post-synaptic cell.

Future directions:

The primary goal of this study was to characterize the basic physiology of AON principal neurons. As such, this study will hopefully serve as a foundation for future work

on the AON. The highly consistent intrinsic membrane properties of AON principal neurons, and similarity therein to piriform pyramidal neurons, suggest that AON is a 'cortical' structure, and future work should focus on cortical function of the AON. Several results motivate specific future studies. The smaller fast AHP in AON compared to APC_V is interesting in light of studies indicating that the AHP amplitude changes with learning (Cohen-Matsliah et al., 2010). It would be interesting to know if the AHP in AON changes with learning, and if there are differences between AON and piriform in the properties of learning induced changes (Liraz et al., 2009; Saar and Barkai, 2009; Cohen-Matsliah et al., 2010). The higher expression of (G)IRK channels in pEN lend support to the recent extremely interesting study suggesting that neurons, rather than glia, buffer extracellular potassium in the olfactory cortex (Howe et al., 2008). As such it would be interesting to monitor the potassium reversal in pEN versus piriform neurons during seizures, and to do so in the presence versus absence of blockers of (G)IRK channels. Clearly, buffering of extracellular potassium is an important basic issue in neurobiology. It would also be interesting to determine which specific potassium channels have enhanced expression in pEN (using pharmacological or molecular methods) and, for example, examine the effect of knocking out this channel on seizure activity.

Targeting classes of interneurons with mutant mice

Several of the initial goals of this dissertation were critically dependent upon the use of mutant mouse lines to label certain cell types, including: 1) the selective labeling of tufted cell axons in the LOT by CCK; 2) labeling of chandelier and basket neurons by

parvalbumin; and 3) labeling of CCK+ basket neurons. Several lines were available at the time the projects were started, so I was optimistic about the likelihood of getting results. However, when these lines were evaluated for accuracy of expression, none were accurate enough to prove useful (Meyer et al., 2002; Meyer et al., 2010; GENSAT, 2010), as described in Chapter 3. Recently, a paralbumin-cre mouse became available from Jackson Labs (jax.org) that does have accurate expression (Hippenmeyer et al., 2005; see Chapter 3). This line should prove useful for future study of parvalbumin expressing interneurons in piriform cortex, including chandelier and basket neurons.

Future directions:

The future of research on interneurons in piriform cortex is undoubtedly extremely rich, as evidenced by several very recent studies delving into the topic (Young and Sun, 2009; Suzuki and Bekkers, 2010a; Suzuki and Bekkers, 2010b). It is my opinion that the best strategy, in the near future, will be to use cre-expressing knockin mice (i.e. Hippenmeyer et al., 2005) in conjunction with bright ROSA26 reporters (i.e. Madisen et al., 2010). This approach has the dual advantages of accurate expression (see Chapter 3), and the flexibility provided by the cre-lox system, such as the incorporation of optogenetic tools (Chow et al., 2010; Gradinaru et al., 2010). Perhaps using these tools, the logic underlying the baffling diversity of cortical interneurons will be elucidated.

REFERENCES

Introduction: References

Alheid, G.F., Carlsen, J., De Olmos, J., Heimer, L. (1984). Quantitative determination of collateral anterior olfactory nucleus projections using a fluorescent tracer with an algebraic solution to the problem of double retrograde labeling. *Brain Res.* **292**:17–22.

Belluscio, L., Lodovichi, C., Feinstein, P., Mombaerts, P., Katz, C. L. (2004). Odorant receptors instruct functional circuitry in the mouse olfactory bulb. *Nature* **419**:296–300.

Biella, G., Forti, M., de Curtis, M. (1996) Propagation of epileptiform potentials in the guinea-pig piriform cortex is sustained by associative fibres. *Epilepsy Res.* **24**:137–46.

Boulet, M., Daval, G. and Leveteau, J. (1978). Qualitative and quantitative odour discrimination by mitral cells as compared to anterior olfactory nucleus cells. *Brain Res.* **142**:123–34.

Brunjes, C.B., Illig, K.R., and Meyer, E.A. (2005). A field guide to the anterior olfactory nucleus (cortex). *Brain Res. Rev.* **50**(2)305–35.

Buck, L.B. (1996). Information coding in the vertebrate olfactory system. *Annu. Rev. Neurosci.* **19**:517–44.

Cajal, S. Ramón y (1911). *Histologie du Système Nerveaux de l' Homme et des Vertébrès*. Vol. II, Maloine, Paris.

Christie, J.M., Schoppa, N.E., and Westbrook, G.L. (2001). Tufted cell dendrodendritic inhibition in the olfactory bulb is dependent on NMDA receptor activity. *J. Neurophys.* **85**:169–73.

Collins, G.G.S. (1994). The characteristics and pharmacology of olfactory cortical LTP induced by theta-burst high frequency stimulation and 1S, 3R-ACPD. *Neuropharmacology* **33**:87**–**95.

de Curtis, M., Biella, G., Forti, M., and Panzica, F. (1994). Multifocal spontaneous epileptic activity induced by restricted bicuculline ejection in the piriform cortex of the isolated guinea pig brain. *J. Neurophys.* **71**(6):2463–76.

Davis, B.J. and Macrides, F. (1981). The organization of centrifugal projections from the anterior olfactory nucleus, ventral hippocampal rudiment, and piriform cortex to the main olfactory bulb in the hamster: an autoradiographic study. *J. Comp. Neurol.* **203**:475–93.

Demir, R., Haberly, L.B., Jackson, M.B. (2001). Epileptiform discharges with in-vivo-like features in slices of rat piriform cortex with longitudinal association fibers. J. Neurophys. **86**:2445–60.

Ekstrand, J.J., Domroese, M.E., Johnson, D.M.G., Feig, S.L., Knodel, S.M., Behan, M., and Haberly, L.B. (2001a). A new subdivision of anterior piriform cortex and associated deep nucleus with novel features of interest for olfaction and epilepsy. *J. Comp. Neurol.* **434**:289–307.

Ekstrand, J.J., Domroese, M.E., Feig, S.L., Illig, K.R. and Haberly, L.B. (2001b). Immunocytochemical analysis of basket cells in rat piriform cortex. *J. Comp. Neurol.* **434**:308–28.

Franks, M.K. and Isaacson, J.S. (2005). Synapse-specific downregulation of NMDA receptors by early experience: a critical period for plasticity of sensory input to olfactory cortex. *Neuron* **47**:101–14.

Franks, M.K. and Isaacson, J.S. (2006). Strong single-fiber sensory inputs to olfactory cortex: implications for olfactory coding. *Neuron* **49**:357–63.

Freund, T.F., and Buzsaki, G. (1996). Interneurons of the hippocampus. *Hippocampus* **6**:347–470.

Gnatkovsky, V. and de Curtis, M. (2006). Hippocampus-mediated activation of superficial and deep layer neurons in the medial entorhinal cortex of the isolated guinea pig brain. *J. Neurosci.* **26**(3):873–81.

Haberly, L.B. (1990) Comparative aspects of olfactory cortex. In: Comparative structure and evolution of cerebral cortex (Vol. 8B) (Jones, E.G. and Peters, A., eds), 137–166, *Plenum Publishing*.

Haberly, L.B. (2001) Parallel-distributed processing in olfactory cortex: new insights from morphological and physiological analysis of neuronal circuitry. *Chem. Senses* **26**:551–76.

Haberly, L.B. and Bower, J.M. (1989). Olfactory cortex: model circuit for study of associative memory? *Trends Neurosci.* **12**(7):258–64.

Hasselmo, M.E., and Bower, J.M. (1991). Selective suppression of afferent but not intrinsic fiber synaptic transmission by 2-amino-4-phosphonobutyric acid (AP4) in piriform cortex. *Brain Res.* **548**:248–55.

Hasselmo, M.E., and Bower, J.M. (1992). Cholinergic suppression specific to intrinsic not afferent fiber synapses in rat piriform (olfactory) cortex. *J. Neurophys.* **67**(5):1222-9.

Haberly, L.B. and Price, J.L. (1977). The axonal projection patterns of the mitral and tufted cells of the olfactory bulb in the rat. *Brain Res.* **129**:152–7.

Haberly, L.B. and Price, J.L. (1978). Association and commissural fiber systems of the olfactory cortex of the rat. *J. Comp. Neurol.* **181**:781–808.

Hayar, A., Karnup, S., Ennis, M., Shipley, M.T. (2004). External tufted cells: a major excitatory element that coordinates glomerular activity. *J. Neurosci.* **24**(30):6676–85.

Illig, K.R. and Haberly, L.B. (2003). Odor-evoked activity is spatially distributed in piriform cortex. *J. Comp. Neurol.* **457**:361–73.

Jerison, H.J. (1990) Fossil evidence on the evolution of the neocortex. In Comparative Structure and Evolution of Cerebral Cortex. Cerebral Cortex (Vol. 8A) (Jones, E.G. and Peters, A., eds), pp. 285–310, *Plenum Publishing*.

Johnson, D.M., Illig, K.R., Behan, M., Haberly, L.B. (2000). New Features of connectivity in piriform cortex visualized by intracellular injection of pyramidal cells suggest that “primary” olfactory cortex functions like “association” cortex in other sensory systems. *J. Neurosci.* **20**(18):6974–982.

Jung, M.W., and Larson, J. (1994). Further characteristics of long-term potentiation in piriform cortex. *Synapse* **18**(4):298–306.

Kadohisa, M. and Wilson, D.A. (2006). Olfactory cortical adaptation facilitates detection of odors against background. *J. Neurophys.* **95**:1888–96.

Kanter, E.D., and Haberly, L.B. (1990). NMDA-dependent induction of long-term potentiation in afferent and association fiber systems of piriform cortex in vitro. *Brain Res.* **525**(1):175-9.

Ketchum, K.L., and Haberly, L.B. (1993). Membrane currents evoked by afferent fiber stimulation in rat piriform cortex. I. Current source-density analysis. *J. Neurophys.* **69**(1):248–60.

Kucharski, D., and Hall, W.G. (1987). New routes to early memories. *Science* **238**(4828):786–8.

Lei, H., Mooney, R., and Katz, L.C. (2006). Synaptic integration of olfactory information in mouse anterior olfactory nucleus. *J. Neurosci.* **26**(46):12023-32.

Lodovichi, C., Belluscio, L., and Katz, L.C. (2003). Functional topography of connections linking mirror-symmetric maps in the mouse olfactory bulb. *Neuron* **38**(2):265–76.

Luskin, M.B. and Price, J.L. (1983a). The topographic organization of associational fibers of the olfactory system in the rat, including centrifugal fibers to the olfactory bulb. *J. Comp. Neurol.* **216**:264–91.

Luskin, M.B. and Price, J.L. (1983b). The laminar distribution of intracortical fibers originating in the olfactory cortex of the rat. *J. Comp. Neurol.* **216**:292–302.

McNamara, A.M., Cleland, T.A., and Linster, C. (2004). Characterization of the synaptic properties of olfactory bulb projections. *Chem. Senses* **29**:225–33.

Nagayama, S., Takahashi, Y.K., Yoshihara, Y., and Mori, K. (2004). Mitral and tufted cells differ in the decoding manner of odor maps in the rat olfactory bulb. *J. Neurophys.* **91**(6):2532–40.

Nakajima, S. and Iwaski, T. (1973). Dependence of the anterior olfactory area self-stimulation upon the lateral hypothalamic area. *Physiology and Behavior* **11**:827–31.

Neville, K.R., and Haberly, L.B. (2004). Olfactory cortex. In: The synaptic organization of the brain, Ed 5 (Shepherd, G.M., ed), 415–54. New York: Oxford, UP.

Orona, E., Rainer, E.C., and Scott, J.W. (1984). Dendritic and axonal organization of mitral and tufted cells in the rat olfactory bulb. *J. Comp. Neurol.* **226**:346–56.

Pinching, A.J. and Powell, T.P.S. (1972). The termination of centrifubal fibres in the glomerular layer of the olfactory bulb. J. Cell. Sci. **10**:621–35.

Piredda, S. and Gale, K. (1985). A crucial epileptogenic site in the deep prepiriform cortex. *Nature* **317**:623–5.

Price, J.L. and Sprich, W.W. (1975). Observations on the lateral olfactory tract of the rat. *J Comp. Neurol.* **162**(3):321–36.

Reyher, C.K., Schwerdtfeger, W.K., and Baumgarten, H.G. (1988). Interbulbar axonal collateralization and morphology of anterior olfactory nucleus neurons in the rat. *Brain Res. Bull.* **20**:549–66.

Rolls, E.T., and Baylis, L.L. (1994). Gustatory, olfactory, and visual convergence within the primate orbitofrontal cortex. *J. Neurosci.* **14**:5437–52.

Schneider, S. P. and Scott, J. W. (1983). Orthodromic response properties of rat olfactory bulb mitral and tufted cells correlate with their projection patterns. *J. Neurophys.* **50**(2):358–78.

Scott, J.W., Ranier, E.C., Pemberton, J.L., Orona, E., and Mouradian, L.E. (1985). Pattern of rat olfactory bulb mitral and tufted cell connections to the anterior olfactory nucleus pars externa. *J. Comp. Neurol.* **242**:415–24.

Stettler, D. and Axel, R. (2009). Representations of Odor in the Piriform Cortex. *Neuron* **63**(6):854–64.

Suzuki, N., and Bekkers, J.M. (2006). Neural coding by two classes of principal cells in the mouse piriform cortex. *J. Neurosci.* **26**(46):11938–47.

Szabadics, J., Varga, C., Molnár, G., Oláh, S., Barzó, P., Tamás, G. (2006). Excitatory effect of GABAergic axo-axonic cells in cortical microcircuits. *Science* **311**(5758):233–5.

Tang, A.C. and Hasselmo, M.E. (1994). Selective suppression of intrinsic but not afferent fiber synaptic transmission by baclofen in the piriform (olfactory) cortex. *Brain Res.* **659**(1-2):75–81.

Trevelyan, A.J., Sussillo, D., and Yuste, R. (2007). Feedforward inhibition contributes to the control of epileptiform propagation speed. *J. Neurosci.* **27**(13):3383–7.

Wilson, D.A. (2001). Receptive fields in the rat piriform cortex. *Chem. Senses* **26**:557–84.

Wilson, D.A. and Stevenson, R.J. (2006). Learning to smell: olfactory perception from neurobiology to behavior. *The Johns Hopkins University Press*, 1 edition.

Woodruff, A.R., Monyer, H., Sah, P. (2006). GABAergic excitation in the basolateral amygdala. *J. Neurosci*. **26**(46):11881–7.

Yan, Z., Tan, J., Qin, C., Lu, Y., Ding, Y., Luo, M. (2008). Precise circuitry links bilaterally symmetric olfactory maps. *Neuron* **58**(4):613–24.

Chapter 1: References

Averbeck, B.B., Latham, P.E., and Pouget, A. (2006). Neural correlations, population coding and computation. *Nat. Rev. Neurosci.* **7**(5):358–66.

Barabasi, A.L. and Albert, R. (1999). Emergence of scaling in random networks. *Science* **286**:509–12.

Behan, M. and Haberly, L.B. (1999). Intrinsic and efferent connections of the endopiriform nucleus in rat. *J. Comp. Neurol.* **408**:532–48.

Brody, C.D. (1999a). Correlations without synchrony. *Neural Comput.* **11**(7):1537–51.

Brody, C.D. (1999b). Disambiguating different covariation types. *Neural Comput.* **11**(7):1527–35.

Brunjes, C.B., Illig, K.R., and Meyer, E.A. (2005). A field guide to the anterior olfactory nucleus (cortex). *Brain Res. Rev.* **50**(2):305–35.

Cattarelli, M., Astic, L., and Kauer, J.S. (1988). Metabolic mapping of 2-deoxyglucose uptake in the rat piriform cortex using computerized image processing. *Brain Res.* **442**(1):180–4.

Connors, B.W. (1984). Initiation of synchronized neuronal bursting in neocortex. *Nature* **310**(5979):685–7.

Davis, B.J. and Macrides, F. (1981). The organization of centrifugal projections from the anterior olfactory nucleus, ventral hippocampal rudiment, and piriform cortex to the main olfactory bulb in the hamster: an autoradiographic study. *J. Comp. Neurol.* **203**:475–93.

Demir, R., Haberly, L.B., and Jackson, M.B. (2000). Characteristics of plateau activity during the latent period prior to epileptiform discharges in slices from rat piriform cortex. *J. Neurophysiol.* **83**:1088–98.

Demir, R., Haberly, L.B., and Jackson, M.B. (2001). Epileptiform discharges with in-vivo-like features in slices of rat piriform cortex with longitudinal association fibers. *J. Neurophysiol.* **86**(5):2445–60.

Dravnieks, A. (1985). Atlas of odor character profiles. *American Society for Testing and Materials, Data Series 61*, Philadelphia, PA, U.S.A.

Ekstrand, J.J., Domroese, M.E., Johnson, D.M.G., Feig, S.L., Knodel, S.M., Behan, M., and Haberly, L.B. (2001). A new subdivision of anterior piriform cortex and associated deep nucleus with novel features of interest for olfaction and epilepsy. *J. Comp. Neurol.* **434**:289–307.

Franks, K.M., and Isaacson, J.S. (2005). Synapse-specific downregulation of NMDA receptors by early experience: a critical period for plasticity of sensory input to olfactory cortex. *Neuron* **47**(1):101–14.

Golomb, D. (1998). Models of neuronal transient synchrony during propagation of activity through neocortical circuitry. *J. Neurophysiol.* **79**:1–12.

Golomb, D. and Hansel, D. (2000). The number of synaptic inputs and the synchrony of large, sparse neuronal networks. *Neural Comput.* **12**:1095–139.

Haberly, L.B. (1969). Single-unit responses to odors in the prepyriform cortex of the rat. *Brain Res.* **12**:481–4.

Haberly, L.B. (2001). Parallel-distributed processing in olfactory cortex: new insights from morphological and physiological analysis of neuronal circuitry. *Chem. Senses* **26**:551–76.

Hasenstaub, A., Shu, Y., Haider, B., Kraushaar, U., Duque, A., and McCormick, D.A. (2005). Inhibitory postsynaptic potentials carry synchronized frequency information in active cortical networks. *Neuron* **47**:423–35.

Hoffman, W.H. and Haberly L.B. (1991). Bursting-induced epileptiform EPSPs in slices of piriform cortex are generated by deep cells. *J. Neurosci.* **11**(7):2021–31.

Hoffman, W.H. and Haberly, L.B. (1996). Kindling-induced epileptiform potentials in piriform cortex slices originate in the underlying endopiriform nucleus. *J. Neurophysiol.* **76**(3):1430–8.

Huang, X., Troy, W.C., Yang, Q., Ma, H., Laing, C.R., Schiff, S.J., and Wu, J.Y. (2004). Spiral waves in disinhibited neocortex. *J. Neurosci.* **24**(44):9897–902.

Huybers, P. (2004). Comments on 'Coupling of the hemispheres in observations and simulations of glacial climate change' by A. Schmittner, O.A. Saenko, and A. J. Weaver. *Quat. Sci. Rev.* **23**:207–12.

Illig, K.R. and Haberly, L.B. (2003). Odor-evoked activity is spatially distributed in piriform cortex. *J. Comp. Neurol.* **457**:361–73.

Johnson, D.M., Illig, K.R., Behan, M., and Haberly, L.B. (2000). New Features of connectivity in piriform cortex visualized by intracellular injection of pyramidal cells suggest that "primary" olfactory cortex functions like "association" cortex in other sensory systems. *J. Neurosci.* **20**(18)6974–82.

Kadohisa, M. and Wilson, D.A. (2006). Separate encoding of identity and similarity of complex familiar odors in piriform cortex. *Proc. Natl. Acad. Sci. U.S.A.* **103**(41):15206–11.

Kumar, A., Rotter, S., and Aertsen, A. (2008). Condition for propagating synchronous spiking and asynchronous firing rates in a cortical network model. *J. Neurosci.* **28**(20):5268–80.

Ketchum, K.L. and Haberly, L.B. (1993). Synaptic events that generate fast oscillations in piriform cortex. *J. Neurosci.* **13**(9):3980–5.

Lei, H., Mooney, R., and Katz, L.C. (2006). Synaptic integration of olfactory information in mouse anterior olfactory nucleus. *J. Neurosci.* **26**(46):12023–32.

Lind, P.G., Gallas, J.A., and Herrmann, H.J. (2004). Coherence in scale-free networks of chaotic maps. *Phys. Rev. E Stat. Nonlin. Soft Matter Phys.* **70**(056207):1–8.

Luna, V.M. and Schoppa, N.E. (2008). GABAergic circuits control input-spike coupling in the piriform cortex. *J. Neurosci.* **28**(35):8851–9.

McGraw, P.N. and Menzinger, M. (2003). Topology and computational performance of attractor neural networks. *Phys. Rev. E Stat. Nonlin. Soft Matter Phys.* **68**(047102):1–4.

Mountcastle., V.B. (1997). The columnar organization of the neocortex. *Brain* **120**(4):701–22.

Neville, K.R. and Haberly, L.B. (2003). Beta and gamma oscillations in the olfactory system of the urethane-anesthetized rat. *J. Neurophysiol.* **90**(6):3921–30.

Percival, D.P. and Walden, A.T. (1993). *Spectral analysis for physical applications: Multitaper and conventional univariate techniques.* Cambridge University Press, UK.

Piredda, S. and Gale, K. (1985). A crucial epileptogenic site in the deep prepiriform cortex. *Nature* **317**(6038):623–5.

de la Prida, L.M., Huberfeld, G., Cohen, I., and Miles, R. (2006). Threshold behavior in the initiation of hippocampal population bursts. *Neuron* 49(1):131-42.

Rennaker, R.L., Chen, C.F., Ruyle, A.M., Sloan, A.M., and Wilson, D.A. (2007). Spatial and temporal distribution of odorant-evoked activity in the piriform cortex. *J. Neurosci.* **27**(7):1534–42.

Schwob, J.E., Haberly, L.B., and Price, J.L. (1984). The development of physiological responses of the piriform cortex in rats to stimulation of the lateral olfactory tract. *J. Comp. Neurol.* **223**(2):223–37.

Senkowski, D., Schneider, T.R., Foxe, J.J., and Andreas, A.K. (2008). Crossmodal binding through neural coherence: implications for multisensory processing. *Trends Neurosci.* **31**(8):401–9.

Stettler, D. and Axel, R. (2009). Representations of Odor in the Piriform Cortex. *Neuron* **63**(6):854 –64.

Suzuki, N. and Bekkers, J.M. (2006). Neural coding by two classes of principal cells in the mouse piriform cortex. *J. Neurosci.* **26**(46):11938–47.

Thomson, D.J. (1982). Spectral estimation and harmonic analysis. *Proc. IEEE* **70**:1055–96.

Tseng, G.F. and Haberly, L.B. (1989). Deep neurons in piriform cortex. I. Morphology and synaptically evoked responses including a unique high amplitude paired shock facilitation. *J. Neurophysiol.* **62**:369–85.

Voges, N., Guijarro, C., Aertsen, A., and Rotter, S. (2009). Models of cortical networks with long-range patchy projections. *J. Comput. Neurosci.*, Oct 29 [Epub ahead of print].

Wehr, M. and Laurent, G. (1999). Relationship between afferent and central temporal patterns in the locust olfactory system. *J. Neurosci.* **19**(1):381–90.

Weiler, N., Wood, L., Yu, J., Solla, S.A., and Shepherd, G.M. (2008). Top-down laminar organization of the excitatory network in motor cortex. *Nat. Neurosci.* **11**(3):360–6.

Wong, R.K.S. and Traub, R.D. (1983). Synchronized burst discharge in disinhibited hippocampal slice. I. Initiation in CA3-CA3 region. *J. Neurophysiol.* **29**(2):442–58.

Yoshida, I. and Mori, K. (2007). Odorant category profile selectivity of olfactory cortex neurons. *J. Neurosci.* **27**(34):9105–14.

Zoubir, A.M. (2009). Bootstrapping spectra: Methods, comparisons and application to knock data. *Signal Processing* **90**(5):1424-35.

Chapter 2: References

Alheid, G.F., Carlsen, J., De Olmos, J., Heimer, L. (1984). Quantitative determination of collateral anterior olfactory nucleus projections using a fluorescent tracer with an algebraic solution to the problem of double retrograde labeling. *Brain Res.* **292**:17–22.

Bacci, A., Huguenard, J.R., and Prince, D.A. (2005). Modulation of neocortical interneurons: extrinsic influences and exercises in self-control. *Trends Neurosci.* **28**(11):602–10.

Bathellier, J.B., Margrie, T.W., Larkum, M.E. (2009). Properties of piriform cortex pyramidal cell dendrites: implications for olfactory circuit design. *J. Neurosci.* **29**(40):12641–52.

Boulet, M., Daval, G. and Leveteau, J. (1978). Qualitative and quantitative odour discrimination by mitral cells as compared to anterior olfactory nucleus cells. *Brain Res.* **142**:123–34.

Bower, J.M., Haberly, L.B. (1986). Facilitating and nonfacilitating synapses on pyramidal cells: a correlation between physiology and morphology. *PNAS* **83**:1115–9.

Brunjes, C.B., Illig, K.R., and Meyer, E.A. (2005). A field guide to the anterior olfactory nucleus (cortex). *Brain Res. Rev.* **50**(2):305–35.

Brunjes, P.C., and Kenerson, M.C. (2009). The anterior olfactory nucleus: Quantitative study of dendritic morphology. *J. Comp. Neurol.* 518(9):1603–16.

Bruno, R.M., and Sakmann, B. (2006). Cortex is driven by weak but synchronously active thalamocortical synapses. *Science* **312**:1622–7.

Chiang, E., and Strowbridge, B.W. (2007). Diversity of neural signals mediated by multiple, burst-firing mechanisms in rat olfactory tubercle neurons. *J Neurophysiol* **98**:2716–28.

Christie, J.M., Schoppa, N.E., and Westbrook, G.L. (2001). Tufted cell dendrodendritic inhibition in the olfactory bulb is dependent on NMDA receptor activity. *J. Neurophys.* **85**:169–73.

Cleland, T.A. (2010). Early transformations in odor representation. *Trends in Neurosci.* **33**(3):130–9.

Cohen-Matsliah, S.I., Rosenblum, K., and Barkai, E. (2010). Olfactory-learning abilities are correlated with the rate by which intrinsic neuronal excitability is modulated in the piriform cortex. *European J. Neurosci.* **30(7)1339–48.**

Davis, B.J. and Macrides, F. (1981). The organization of centrifugal projections from the anterior olfactory nucleus, ventral hippocampal rudiment, and piriform cortex to the main olfactory bulb in the hamster: an autoradiographic study. *J. Comp. Neurol.* **203**:475–93.

de la Prida, L.M., Huberfeld, G., Cohen, I., and Miles, R. (2006). Threshold behavior in the initiation of hippocampal population bursts. *Neuron* **49**(1):131–42.

Demir, R., Haberly, L.B., Jackson, M.B. (2001). Epileptiform discharges with in-vivo-like features in slices of rat piriform cortex with longitudinal association fibers. *J. Neurophys.* **86**:2445–60.

Ekstrand, J.J., Domroese, M.E., Johnson, D.M.G., Feig, S.L., Knodel, S.M., Behan, M., and Haberly, L.B. (2001a). A new subdivision of anterior piriform cortex and associated deep nucleus with novel features of interest for olfaction and epilepsy. *J. Comp. Neurol.* **434**:289–307.

Fontanini, A., and Bower, J.M. (2006). Slow-waves in the olfactory system: an olfactory perspective on cortical rhythms. *Trends Neurosci.* **29**(8):429–37.

Franks, M.K., and Isaacson, J.S. (2006). Strong single-fiber sensory inputs to olfactory cortex: implications for olfactory coding. *Neuron* **49**:357–63.

Freund, T.F., and Buzsaki, G. (1996). Interneurons of the hippocampus. *Hippocampus* **6**:347–470.

Giocomo, L,M., and Hasselmo, M.E. (2007). Neuromodulation by glutamate and acetylcholine can change circuit dynamics by regulating the relative influence of afferent input and excitatory feedback. *Mol. Neurobiol.* **36**:184–200.

Haberly, L.B. (1990). Comparative aspects of olfactory cortex. In: Comparative structure and evolution of cerebral cortex (Vol. 8B) (Jones, E.G. and Peters, A., eds)137–66, *Plenum Publishing*.

Haberly, L.B. (2001). Parallel-distributed processing in olfactory cortex: new insights from morphological and physiological analysis of neuronal circuitry. *Chem. Senses* **26**:551–76.

Haberly, L.B. and Price, J.L. (1978). Association and commissural fiber systems of the olfactory cortex of the rat. II. Systems originating in the olfactory peduncle. *J. Comp. Neurol.* **181**:781–808.

Hasselmo, M. E. and Bower, J. M. (1990). Afferent and association fiber differences in short-term potentiation in piriform (olfactory) cortex of the rat. *J. Neurophysiol.* **64**(1):179–90.

Hasselmo, M.E., and Bower, J.M. (1991). Selective suppression of afferent but not intrinsic fiber synaptic transmission by 2-amino-4-phosphonobutyric acid (AP4) in piriform cortex. *Brain Res.* **548**:248–55.

Hasselmo, M.E., and Bower, J.M. (1992). Cholinergic suppression specific to intrinsic not afferent fiber synapses in rat piriform (olfactory) cortex. *J Neurophysiol.* **67**(5):1222–9.

Herrick, C.J. (1924). The nucleus olfactorius anterior of the opossum, *J. Comp. Neurol.* **37**:317–59.

Holmgren, C., Harkany, T., Svennenfors, B., and Zilberter, Y. (2003). Pyramidal cell communication within local networks in layer 2/3 of rat neocortex. *J. Physiol.* **551**:139–53.

Hommers, L.G., Lohse, M.J., and Bunemann, M. (2003). Regulation of the inward rectifying properties of G-protein-activated inwardly rectifying K+ (GIRK) channels by G(beta)(gamma) subunits. *J. Biol. Chem.* **278**(2):1037–43.

Howe, M.W., Feig, S.L., Osting, S.M.K., and Haberly, L.B. (2008). Cellular and subcellular localization of Kir2.1 subunits in neurons and glia in piriform cortex with implications for K+ spatial buffering. *J. Comp. Neurol.* **506**(5):**877–93.**

Jackson, M.B. (1992). Cable analysis with the whole-cell patch clamp. Theory and experiment. *Biophys. J.* **61**:756–66.

Jahnsen, H., Llinas, R. (1984). Ionic basis for the electroresponsiveness and oscillatory properties of guinea-pig thalamic neurones in vitro. *J. Physiol.* **349**:227–48.

Jerison, H.J. (1990). Fossil evidence on the evolution of the neocortex. In Comparative Structure and Evolution of Cerebral Cortex. Cerebral Cortex (Vol. 8A) (Jones, E.G. and Peters, A., eds), 285–310, *Plenum Publishing.*

Johnson, D.M., Illig, K.R., Behan, M., Haberly, L.B. (2000). New Features of connectivity in piriform cortex visualized by intracellular injection of pyramidal cells suggest that "primary" olfactory cortex functions like "association" cortex in other sensory systems. *J. Neurosci.* **20**(18):6974–82.

Jortner, RA, Farivar, SS, and Laurent, G (2007). A simple connectivity scheme for sparse coding in an olfactory system. *J Neurosci* **27**:1659–69.

Kay, L.M. and Sherman, S.M. (2007). An argument for an olfactory thalamus. *Trends Neurosci.* **30**(2):47–53.

Kikuta, S., Kashiwadani, H.., and Kensaku Mori, K. (2008). Compensatory rapid switching of binasal inputs in the olfactory cortex. *J. Neurosci.* **28**(46):11989–97.

Kikuta, S., Sato, K., Kashiwadani, H., Tsunoda, K., Yamasoba, T., and Mori, K. (2010). Neurons in the anterior olfactory nucleus pars externa detect right or left localization of odor sources. *PNAS* **107**(27):12363–68.

Kim, D., Song, I., Keum, S., Lee, T., Jeong, M.J., Kim, S.S., McEnery, M.W., Shin, H.S. (2001). Lack of the burst firing of thalamocortical relay neurons and resistance to absence seizures in mice lacking alpha(1G) T-type Ca(2+) channels. *Neuron* **31**(1):35**–**45.

Krahe, R., and Gabbian, F. (2004). Burst firing in sensory systems. Nat. Rev. Neurosci. **5**:13-23.

Kucharski, D., and Hall, W.G. (1987). New routes to early memories. *Science* **238**:786**–**8.

Larkman, A., and Mason, A. (1990). Correlations between morphology and electrophysiology of pyramidal neurons in slices of rat visual cortex. II Electrophysiology. *J. Neurosci.* **10***:*1415–28.

Lei, H., Mooney, R., and Katz, L.C. (2006). Synaptic integration of olfactory information in mouse anterior olfactory nucleus. *J. Neurosci.* **26**(46):12023**–**32.

Linster, C., and Hasselmo, M.E. (2001). Neuromodulation and the functional dynamics of piriform cortex. *Chem. Senses* **26**:585–94.

Liraz, O., Rosenblum, K., and Barkai, E. (2009). CAMKII activation is not required for maintenance of learning-induced enhancement of neuronal excitability. *PLoS ONE* doi: 10.1371/journal.pone.0004289.

Luskin, M.B. and Price, J.L. (1983a). The topographic organization of associational fibers of the olfactory system in the rat, including centrifugal fibers to the olfactory bulb. *J. Comp. Neurol.* **216**:264–91.

Luskin, M. B. and Price, J. L. (1983b). The laminar distribution of intracortical fibers originating in the olfactory cortex of the rat. *J. Comp. Neurol.* **216**:292–302.

Martinez-Marcos, A. (2009). On the organization of olfactory and vomeronasal cortices. *Prog Neurobiol.* **87**(1):21–30.

Matsutani, S., Senba, E., and Tohyama, M. (1989). Terminal field of cholecystokinin-8-like immunoreactive projection neurons of the rat main olfactory bulb. *J. Comp. Neurol.* **285**:73–82.

McNamara, A.M., Cleland, T.A., and Linster, C. (2004). Characterization of the synaptic properties of olfactory bulb projections. *Chem. Senses* **29**:225–33.

Meyer, E.A., Illig, K.R., and Brunjes, P.C. (2006). Differences in chemo- and cytoarchitectural features within pars principalis of the rat anterior olfactory nucleus suggest functional specialization. *J Comp Neurol.* **498**(6):786–95.

Nagayama, S., Takahashi, Y.K., Yoshihara, Y., and Mori, K. (2004). Mitral and tufted cells differ in the decoding manner of odor maps in the rat olfactory bulb. *J. Neurophys.* **91**(6):2532–40.

Nicoll, A, and Blakemore, C. (1993). Patterns of local connectivity in the neocortex. *Neural Comput.* **5**(5):665–80.

Orona, E., Rainer, E.C., and Scott, J.W. (1984). Dendritic and axonal organization of mitral and tufted cells in the rat olfactory bulb. *J. Comp. Neurol.* **226**:346–56.

Perez-Orive, J., Mazor, O., Turner, G.C., Cassenaer, S., Wilson, R.I., and Laurent, G. (2002). Oscillations and sparsening of odor representations in the mushroom body. *Science* **297**:359–65.

Piredda, S. and Gale, K. (1985). A crucial epileptogenic site in the deep prepiriform cortex. *Nature* **317**:623–5.

Raastad, M., Storm, J.F., and Andersen, P. (1992). Putative single quantum and single fibre excitatory postsynaptic currents show similar range and variability in rat hippocampal slices. *Eur. J. Neurosci.* **4**:113–7.

Rall, W. (1969). Time constants and electrotonic length of membrane cylinders and neurons. *Biophys. J.* **9**:1483–508.

Reyher, C.K., Schwerdtfeger, W.K., and Baumgarten, H.G. (1988). Interbulbar axonal collateralization and morphology of anterior olfactory nucleus neurons in the rat. *Brain Res. Bull.* **20**:549–66.

Saar, D., and Barkai, E. (2009). Long-lasting maintenance of learning-induced enhanced neuronal excitability: mechanisms and functional significance. *Mol. Neurobio.* **39**(3):171–7.

Scanziani, M., Debanne, D., Muller, M., Gahwiler, B.H. and Thompson, S.M. (1994). Role of excitatory amino acid and $GABA_B$ receptors in the generation of epileptiform activity in disinhibited hippocampal slice cultures. *Neuroscience* **61**(4):823–32.

Schikorski, T., and Stevens, C.F. (1999). Quantitative fine-structural analysis of olfactory cortical synapses. *PNAS* **96**(7):4107–12.

Schneider, S.P., and Scott, J.W. (1983). Orthodromic response properties of rat olfactory bulb mitral and tufted cells correlate with their projection patterns. *J. Neurophys.* **50**(2):358–78.

Schoenbaum, G., and Eichenbaum, H. (1995). Information coding in the rodent prefrontal cortex. I. Single-neuron activity in orbitofrontal cortex compared with that in pyriform cortex. *J. Neurophys.* **74**(2):733–50.

Scott, J.W., Ranier, E.C., Pemberton, J.L., Orona, E., and Mouradian, L.E. (1985). Pattern of rat olfactory bulb mitral and tufted cell connections to the anterior olfactory nucleus pars externa. *J. Comp. Neurol.* **242**:415–24.

Spruston, N. (2008). Pyramidal neurons: dendritic structure and synaptic integration. *Nat. Rev. Neurosci.* **9**:206–21.

Staley, K.J., Longacher, M., Bains, J.S., and Yee, A. (1998). Presynaptic modulation of CA3 network activity. Nat. Neurosci. **1**:201–9.

Suzuki, N., and Bekkers, J. M. (2006). Neural coding by two classes of principal cells in the mouse piriform cortex. *J. Neurosci.* **26**(46):11938–47.

Tang, A.C. and Hasselmo, M.E. (1994). Selective suppression of intrinsic but not afferent fiber synaptic transmission by baclofen in the piriform (olfactory) cortex. *Brain Res.* **659**(1-2):75–81.

Tseng, G.F., and Haberly, L.B. (1989). Deep neurons in piriform cortex. I. Morphology and synaptically evoked responses including a unique high-amplitude paired shock facilitation. J. Neurophysiol. **62**:369–85.

Tsodyks, M.V., and Markram, H. (1997). The neural code between neocortical pyramidal neurons depends on neurotransmitter release probability. *PNAS* **94**:719–23.

Tsodyks, M.V., Uziel, A., and Markram, H. (2000). Synchrony generation in recurrent networks with frequency-dependent synapses. *J. Neurosci.* **20**:RC50:1–5.

Williams, S.R., Stuart, G.J. (2000). Site independence of EPSP time course is mediated by dendritic I_h in neocortical pyramidal neurons. J. Neurophys. **83**(5)3177–82.

Wilson, D.A. (2001). Receptive fields in the rat piriform cortex. *Chem. Senses* **26**:557–84.

Yan, Z., Tan, J., Qin, C., Lu, Y., Ding, Y., Luo, M. (2008). Precise circuitry links bilaterally symmetric olfactory maps. *Neuron* **58**(4):613–24.

Chapter 3: References

Ascoti et al., The Petilla Interneuron Nomenclature Group (2008). Petilla terminology: nomenclature of features of GABAergic interneurons of the cerebral cortex. *Nat. Rev. Neurosci.* **9**:557–68.

Bernard, A., Sorensen, S.A., Lein, E.S. (2009). Shifting the paradigm: new approaches for characterizing and classifying neurons. *Curr. Opin. Neurobiol.* **19**(5):530–6.

Buzsaki, G., Geisler, C., Henze, D.A., and Wang, X.-J. (2004). Interneuron diversity series: circuit complexity and axon wiring economy of cortical interneurons. *Trends Neurosci.* **27**(4):186–193.

Chiu, C.S., Jensen, K., Sokolova, I., Wang, D., Li, M., Deshpande, P., Davidson, N., Mody, I., Quick, M.W., Quake, S.R., Lester, H.A. (2002). Number, density, and surface/cytoplasmic distribution of GABA transporters at presynaptic structures of knock-in mice carrying GABA transporter subtype 1-green fluorescent protein fusions. *J Neurosci.* **22**:10251–10266.

Cummings, S.L. (1997). Neuropeptide Y, somatostatin, and cholecystokinin of the anterior piriform cortex. *Cell Tissue Res.* **289**:39–51.

Ekstrand, J.J., Domroese, M.E., Feig, S.L., Illig, K.R., and Haberly, L.B. (2001). Immunocytochemical analysis of basket cells in rat piriform cortex. *J. Comp. Neurol.* **434**:308–328.

Freund, T.F. (2003). Interneuron diversity series: rhythm and mood in perisomatic inhibition. *Trends Neurosci.* **26**(9):489–495.

The Gene Expression Nervous System Atlas (GENSAT) Project, NINDS Contracts N01NS02331 & HHSN271200723701C to: The Rockefeller University (New York, NY, 2010).

Giel-Moloney, M., Krause, D.S., Chen, G., Van Etten, R.A., and Leiter, A.B. (2007). Ubiquitous and uniform In Vivo fluorescence in ROSA26-EGFP BAC transgenic mice. *Genesis* **45**(2): 83–89.

Giraldo, P., and Montoliu, L. (2001). Size matters: use of YACs, BACs and PACs in transgenic animals. *Transgenic research* **10**(2):83–103.

Gupta, A., Wang, Y., and Markram, H. (2000). Organizing principles for a diversity of GABAergic interneurons and synapses in the neocortex. *Science* **287**:273–8.

Halabisky, B., Shen, F., Huguenard, J.R., and Prince, D.A. (2006). Electrophysiological classification of somatostatin-positive interneurons in mouse sensorimotor cortex. *J. Neurophysiol.* **96**:834–845.

Heintz, N. (2001). Bac to the future: The use of bac transgenic mice for neuroscience research. *Nat. Rev. Neurosci.* **2**:861–70.

Hippenmeyer, S., Vrieseling, E., Sigrist, M., Portmann, T., Laengle, C., Ladle, D.R., Arber, S. (2005). A developmental switch in the response of DRG neurons to ETS transcription factor signaling. *PLoS Biol.* **3**(5):e159.

Kanter, E.D., Kapur,A., and Haberly, L.B. (1996). A dendritic $GABA_A$-mediated IPSP regulates facilitation of NMDA-mediated responses to burst stimulation of afferent fibers in piriform cortex. *J. Neurosci.* **16**:307–12.

Kapur, A., Pearce, R.A., Lytton, W.W., and Haberly, L.B. (1997). $GABA_A$-mediated IPSCs in piriform cortex have fast and slow components with different properties and locations on pyramidal cells. *J. Neurophysiol.* **78**(5):2531–2545.

Karagiannis, A., Gallopin, T., aDavid, C., Battaglia, D., Geoffroy, H., Rossier, J., Hillman, E.M.C., Staiger, J.F., and Cauli, B. (2009). Classification of NPY-expressing neocortical interneurons. *J. Neurosci.* **29**(11):3642–59.

Ketchum, K.L., and Haberly, L.B. (1993). Synaptic events that generate fast oscillations in piriform cortex. J. Neurosci. **13**:3980–3985.

Kowianski, P., Morys, J.M., Wojcika, Dziewiatkowski, S.J., Luczynsk, A., Spodnik, E., Timmerman, J.-P., Morys, J. (2004). Neuropeptide-containing neurons in the endopiriform region of the rat: morphology and colocalization with calcium-binding proteins and nitric oxide synthase. *Brain Res.* **996**:97–110.

Lakshmanan, G., Lieuw, K.H., Lim, K.C., Gu, Y., Grosveld, F., Engel, J.D. et al. (1999). Localization of distant urogenital system-, central nervous system-, and endocardium-specific transcriptional regulatory elements in the GATA-3 locus. *Mol Cell Biol* **19**:1558–1568.

Ma,Y., Hu, H., Berrebi, A.S., Mathers, P.H., and Agmon, A. (2006). Distinct subtypes of somatostatin-containing neocortical interneurons revealed in transgenic mice. *J. Neurosci.* **26**(19):5069–5082.

Madisen L, Zwingman TA, Sunkin SM, Oh SW, Zariwala HA, Gu H, Ng LL, Palmiter RD, Hawrylycz MJ, Jones AR, Lein ES, Zeng H. (2010). A robust and high-throughput Cre reporting and characterization system for the whole mouse brain. *Nat Neurosci*. **13**(1):133–40.

Markram, H., Toledo-Rodriguez, M., Wang, Y., Gupta, A., Silberberg, G., and Wu, C. (2004). Interneurons of the neocortical inhibitory system. *Nat. Rev. Neurosci.* **5**:793–807.

Meyer, A.H., Katona, I., Blatow, M., Rozov, A., and Monyer, H. (2002). *In vivo* labeling of parvalbumin-positive interneurons and analysis of electrical coupling in identified neurons. *J. Neurosci.* **22**(16):7055–7064.

Meyer, A.H., van Hooft, J.A., and Monyer, H. (2010). Serotonergic and cholinergic control of an electrically coupled network of cholecystokinin-containing interneurons in the hippocampus. In preparation.

Oliva Jr., A.A., Jiang, M., Lam, T., Smith, K.L., and Swann, J.W. (2000). Novel hippocampal interneuronal subtypes identified using transgenic mice that express green fluorescent protein in GABAergic interneurons. *J Neurosci.* **20**: 3354–3368.

Patz, S., Grabert, J., Gorba, T., Wirth, M.J., and Wahle, P. (2004). Parvalbumin expression in visual cortical interneurons depends on neuronal activity and TrkB ligands during an early period of postnatal development. *Cereb. Cortex* **14**:342–51.

Seroogy, K.B., Brecha, N., Gall, C. (1985). Distribution of cholecystokinin-like immunoreactivity in the rat main olfactory bulb. *J. Comp. Neurol.* **239**(4):373–383.

Srinivas, S., Watanabe, T., Lin, C.S., William, C.M., Tanabe, Y., Jessell, T.M., Costantini, F. (2001). Cre reporter strains produced by targeted insertion of EYFP and ECFP into the ROSA26 locus. *BMC Dev. Biol.* **1**(1):4.

Suzuki, N., and Bekkers, J.M. (2010a). Inhibitory neurons in the anterior piriform cortex of the mouse: classification using molecular markers *J. Comp. Neurol.* **518**(1):1670–87.

Suzuki, N., and Bekkers, J.M. (2010b). Distinctive classes of GABAergic interneurons provide layer-specific phasic inhibition in the anterior piriform cortex. *Cereb. Cortex* May 10, 2010 [Epub ahead of print].

Tamamaki, N., Yanagawa, Y., Tomioka, R., Miyazaki, J.-I., Obata, K., and Kaneko, T. (2003). Green fluorescent protein expression and colocalization with calretinin, parvalbumin, and somatostatin in the GAD67-GFP knock-in mouse. *J. Comp. Neurol.* **467**:60–79.

van den Pol, A.N., Yao, Y., Fu, L.-Y., Foo, K., Huang, H., Coppari, R., Lowell, B.B., and Broberger, C. (2009). Neuromedin B and gastrin-releasing peptide excite arcuate nucleus neuropeptide Y neurons in a novel transgenic nouse expressing strong *Renilla* green fluorescent protein in NPY neurons. *J. Neurosci.* **29**(14):4622–4639.

Wilson, C., Bellen, H.J., and Gehring, W.J. (1990). Position effects on eukaryotic gene expression. *Annu Rev Cell Biol* **6**: 679–714.

Wondors, C.P and Anderson, S.A. (2006). The origin and specificiation of cortical interneurons. *Nat. Rev. Neurosci.* **7**:687–696.

Wouterlood, F.G. and Härtig, W. (1995). Calretinin-immunoreactivity in mitral cells of the rat olfactory bulb. *Brain Res.* **682**:93–100.

Young, A., and Sun, Q.Q. (2009). GABAergic inhibitory interneurons in the posterior piriform cortex of the GAD67-GFP Mouse. *Cereb. Cortex* **19**(12):3011–29.

Summary and Conclusions: References

Barbieri, F., and Brunel, N. (2008). Can attractor network models account for the statistics of firing during persistent activity in prefrontal cortex? *Front. Neurosci.* **2**(1):114–122.

Chow, B.Y., Han, X., Dobry, A.S., Qian, X., Chuong, A.S., Li, M., Henninger, M.A., Belfort, G.M., Lin, Y., Monahan, P.E., and Boyden, E.S. (2010). High-performance genetically targetable optical neural silencing by light-driven proton pumps. *Nature* **463**, 98-102.

Cohen-Matsliah, S.I., Rosenblum, K., and Barkai, E. (2010). Olfactory-learning abilities are correlated with the rate by which intrinsic neuronal excitability is modulated in the piriform cortex. *European J. Neurosci.* **30**(7)1339–48.

Franks, M.K., and Isaacson, J.S. (2006). Strong single-fiber sensory inputs to olfactory cortex: implications for olfactory coding. *Neuron* **49**:357–363.

The Gene Expression Nervous System Atlas (GENSAT) Project, NINDS Contracts N01NS02331 & HHSN271200723701C to: The Rockefeller University (New York, NY, 2010).

Gradinaru, V., Zhang, F., Ramakrishnan, C., Mattis, J., Prakash, R., Diester, I., Goshen, I., Thompson, K.R., Deisseroth, K. (2010). Molecular and cellular approaches for diversifying and extending optogenetics. Cell, 141(1):154–165,

Hippenmeyer, S., Vrieseling, E., Sigrist, M., Portmann, T., Laengle, C., Ladle, D.R., Arber, S. (2005). A developmental switch in the response of DRG neurons to ETS transcription factor signaling. *PLoS Biol.* **3**(5):e159.

Howe, M.W., Feig, S.L., Osting, S.M.K., and Haberly, L.B. (2008). Cellular and subcellular localization of Kir2. 1 subunits in neurons and glia in piriform cortex with implications for K+ spatial buffering. J. Comp. Neurol. 506(5):877–93.

Ikegaya, Y., Aaron, G., Cossart, R., Aronov, D., Lampl, I., Ferster, D., Yuste, R. (2004). Synfire chains and cortical songs: temporal modules of cortical activity. *Science* **23**(304):559–64.

Liraz, O., Rosenblum, K., and Barkai, E. (2009). CAMKII activation is not required for maintenance of learning-induced enhancement of neuronal excitability. *PLoS ONE* doi: 10.1371/journal.pone.0004289.

Madisen, L., Zwingman, T.A., Sunkin, S.M., Oh, S.W., Zariwala, H.A., Gu, H., Ng, L.L., Palmiter, R.D., et al. (2010). A robust and high-throughput Cre reporting and characterization system for the whole mouse brain. *Nat. Neurosci.* **13**:133–140.

Meyer, A.H., Katona, I., Blatow, M., Rozov, A., and Monyer, H. (2002). *In vivo* labeling of parvalbumin-positive interneurons and analysis of electrical coupling in identified neurons. *J. Neurosci.* **22**(16):7055–7064.

Meyer, A.H., van Hooft, J.A., and Monyer, H. (2010). Serotonergic and cholinergic control of an electrically coupled network of cholecystokinin-containing interneurons in the hippocampus. In preparation.

Mokeichev, A., Okun, M., Barak, O., Katz, Y., Ben-Shahar, O., Lampl, I. (2007). Stochastic emergence of repeating cortical motifs in spontaneous membrane potential fluctuations In Vivo, *Neuron* **53**:413–25.

Saar, D., and Barkai, E. (2009). Long-lasting maintenance of learning-induced enhanced neuronal excitability: mechanisms and functional significance. *Mol. Neurobio.* **39**(3):171–7.

Schrader, S., Grün, S., Diesmann, M., Gerstein, G.L. (2008). Detecting synfire chain activity using massively parallel spike train recording. *J Neurophysiol.* **100**:2165–76.

Suzuki, N., and Bekkers, J.M. (2010a). Inhibitory neurons in the anterior piriform cortex of the mouse: classification using molecular markers *J. Comp. Neurol.* **518**(1):1670–87.

Suzuki, N., and Bekkers, J.M. (2010b). Distinctive classes of GABAergic interneurons provide layer-specific phasic inhibition in the anterior piriform cortex. *Cereb. Cortex* May 10, 2010 [Epub ahead of print].

Young, A., and Sun, Q.Q. (2009). GABAergic inhibitory interneurons in the posterior piriform cortex of the GAD67-GFP Mouse. *Cereb. Cortex* **19**(12):3011–29.

APPENDIX

Matlab Code for Chapter 1

General Comments

These instructions are intended to assist someone to implement or modify any of the Matlab code developed for the manuscript presented in Chapter 1. I used the Matlab Parallel Processing Toolbox, throughout, so many 'for loops' have been implemented using 'parfor' instead of the typical 'for.' If you do not have the Parallel Processing Toolbox, and 'parfor' loops cause a problem, change all instances of 'parfor' to 'for.' (consider that parallel processing may be integrated into future versions of Matlab). Without a 'fast' computer with sufficient memory and implementing parallel processing, some of this code may take a very long time to run. For each m-file, the file name is in bold at the top of the page, followed by the code. NOTE: Additional Matlab Toolboxes are necessary for some code, as described below and in the manuscript.

If you incorporate any of our code into a publication or presentation, please reference the relevant manuscript and this thesis. If you incorporate any of Peter Huybers' code that was used for this manuscript, please also reference: Huybers, P. (2004). Comments on 'Coupling of the hemispheres in observations and simulations of glacial climate change' by A. Schmittner, O.A. Saenko, and A. J. Weaver. Quaternary Science Reviews 23:207–12. If you have any questions, comments, or criticisms: matthew.j.mcginley@gmail.com

Cross-correlation calculations

To calculate and plot cross-correlations, as well as peak lags for multiple trials and their average and standard deviation, load the signals as matrices, and load a time vector, into the workspace. Include all relevant Matlab files from this manuscript in Matlab's path. Then run 'XcorrAve.m'.

Latency-adjustment

To adjust the latency at the beginning of paired signals to minimize covariation due to latency, while keeping the relative timing on each trial between signals unchanged, first load the signals as matrices, and a time vector, into the workspace. Include all relevant Matlab files from this manuscript in Matlab's path. Then, run: 'Simplex_latency_adjust.m'. NOTE: requires the Optimization Toolbox.

Coherence calculations

To calculate multitaper coherences and bootstrap statistics between signals 'A' and 'B' that were simultaneously measured on multiple repetitions (i.e. of stimulation), load the currents into the workspace as matrices: 'currentsA.mat' and 'currentsB.mat'. Include all relevant Matlab files from this manuscript in Matlab's path (including, preferably, cohbias.mat from Peter Huybers!). Then, run 'Bootstrap_coherences.m.' NOTE: Multitaper coherence calculations require the Signal Processing Toolbox, and bootstrap statistical calculations require the Statistics Toolbox.

File List

File name	Comments
XcorrAve.m	Calculates cross-correlations, peak values, peak lags, and average and standard deviation, and plots/outputs the results.
Simplex_latency_adjust.m	Calculates 'latency adjusted' signals by minimizing the maximum cross-covariation between signals while truncating arbitrary time segments from the beginning of traces for all-but-one pair.
x_init.m	Calculates the initial guess of the truncations corresponding to minimum cross-covariation. It is calculated as the time from the stimulus to the maximum on each repetition of signal 'A,' minus the shortest time from stimulus to maximum across repetitions.
slide_cov_simplex.m	Calculates the maximum cross-covariation for a given set of latency-adjusted signals. Called repeatedly by 'Simplex_latency_adjust.m' during mini-max optimization.

slide_cov_ts.m	Calculates the maximum cross-covariation and 2*S.D. confidence intervals for latency-adjusted signals. Also, outputs adjusted signals and plots. Called at the end of 'Simplex_latency_adjust.m'. Note: Should also be called separately, using full signal data matrices, to generate 'adjusted' signals of desired length. Unadjusted signals should be windowed to the same length.
Bootstrap_coherences.m	Runs the full coherence, phase, and bootstrap statistical calculations. Parameters of slepian tapers and statistical calculations are specified in the first 5 lines. WARNING: This may take a long time to run, depending on the size of your dataset and computing resources. Consider running cmtmMM.m and statistical calculations separately, first. Also consider running on small data sets and with a small number of bootstrap repetitions before building up to larger calculations.
cohbiasQ.m	A 'quick' version of Peter Huybers' 'cohbias.m' file. It uses preallocation and 'interp1q.m' instead of 'interp1.m' for faster interpolation of bias curves. Will create 'cohbias.mat' if it is not in the matlab path, but this takes a

	long time. Preferably, download cohbias.mat from Peter Huybers' website or the Matlab Central File Exchange.
cmtmMM.m	Coherence-MultiTaper-Method-by-Matt-McGinley. Calculates the coherence between two signals using a multitaper method based on trial-averaged coherences. Substantially adapted, with permission, from Peter Huybers' cmtm.m. Adaptations are commented in the file.
c_mean_boot.m	Calculates a bootstrap estimate of the coherence based on trial-averaged coherences. Called repeatedly during bootstrap calculations.
ph_trial_boot.m	Calculates a phase-corrected bootstrap estimate of the phase based on trial-averaged coherences and the respective mean phase. Called repeatedly during bootstrap calculations.
phase_smooth.m	Adjusts the phase value at each frequency by +/- 360 degrees so that the phase function 'jumps' less often in phase plots as a result of wraparound.

phase_correct.m	Adjusts the phase value at each frequency by +/ 360 or +/-720 degrees so that the phase stays in the same range as a reference phase function. For use in bootstrap statistical calculations on phase calculations.

Peter Huybers' m-files

File name	Comments
cohbias.mat	IMPORTANT: This file should be used with 'cohbiasQ.m.' Otherwise it is generated by 'cohbiasQ.m,' taking a long time.
pmtmPH.m	Power-spectra-MultiTaper-Method-by-Peter-Huybers. Can be used to calculate multitaper power spectra estimates.

Where to find Peter Huybers' Matlab files:

Peter Huybers' code is currently available at his website:

http://www.people.fas.harvard.edu/~phuybers/Mfiles/index.html

Or on the Matlab Central File Exchange:

http://www.mathworks.com/matlabcentral/fileexchange/2927

http://www.mathworks.com/matlabcentral/fileexchange/22551

Bootstrap_coherences.m

```
matlabpool open;
tic;
tstep = .04; % acquisition sampling time step
NW = 7; % frequency bandwidth product
boot_reps = 1000; % number of bootstrap repetitions
boot_length = 500; %Number of frequencies to which bootstrapping is applied (starting with the
lowest)
adj = 1; % If 'adj' is set to '1,' phase estimates are shifted by 360 degrees for continuity.
[f, c_ave, ph_ave, c, ph, fkx, fky] = cmtmMM(currentsA,currentsB,tstep,NW,adj);
%[f, c_trial, ph_trial, c_mean, ph_mean, c, ph, fkx, fky] = cmtmMM(fullA,fullB,tstep,tapers,adj);
disp('Started bootstrapping on:');
disp(' coherences');
c_trial_ci = zeros(boot_length,2);
parfor i = 1:boot_length
c_trial_ci(i,:) = bootci(boot_reps,@mean,c(i,:));
end
disp(' phases');
ph_trial_ci = zeros(boot_length,2);
parfor i = 1:boot_length
fkx_i = squeeze(fkx(i,:,:))';
fky_i = squeeze(fky(i,:,:))';
ph_trial_ci(i,:) = bootci(boot_reps,@(x,y)ph_trial_boot(x,y,ph_ave(i)),fkx_i,fky_i);
end
disp('Finished');
```

```
CI_ave = ph_trial_ci(:,2)-ph_trial_ci(:,1);

subplot(3,1,1); plot(f(1:boot_length),[c_trial_ci,c_ave(1:boot_length)]);

subplot(3,1,2); plot(f(1:boot_length),[ph_trial_ci,ph_ave(1:boot_length)]);

subplot(3,1,3); plot(f(1:boot_length),CI_ave);

toc

matlabpool close
```

c_mean_boot.m

```
function [c_boot] = c_mean_boot(fkx_i,fky_i);

fkx_i = fkx_i';

fky_i = fky_i';

Sxy=squeeze(sum(conj(fky_i).*fkx_i,1));

Sx=squeeze(sum(conj(fkx_i).*fkx_i,1));

Sy=squeeze(sum(conj(fky_i).*fky_i,1));

Sxy=squeeze(mean(Sxy));

Sx=squeeze(mean(Sx));

Sy=squeeze(mean(Sy));

c_boot=abs(Sxy)./sqrt(Sx.*Sy);

%c_boot = cohbias(v*m,c_boot);

c_boot = cohbias(50,c_boot);
```

cmtmMM.m

```
%function [f, c_ave, ph_ave, c, ph, fkx, fky] = cmtmMM(x,y,dt,NW,adj);
%
%Multitaper method coherence using adaptive weighting and correcting
%for the bias inherent to coherence estimates.
%
% Inputs:
% x - Input data matrix.
% y - Input data matrix.
% dt - Sampling interval (default 1)
% NW - data-length bandwidth product (default 4)
% adj - If adj = '1' phase estimates are adjusted by +/- 360 degrees to improve continuity (this is
the default).
%
% Outputs:
% f - frequency vector
% c - matrix of trial-specific coherence magnitudes
% c_ave - vector of trial-averaged coherence magnitudes
% ph - matrix of trial-specific phase
% ph_ave - vector of phase of trial-averaged complex coherence
% fkx - Multitaper fourier transform of data matrix, x
% fky - Multitaper fourier transform of data matrix, y
%
%Required files: cohbias.m and cohbias.mat by Peter Huybers, Matlab Signal Procesing toolbox.
%
```

```
%Adapted from:
%cmtm.m
%Peter Huybers
%MIT, 2003
%phuybers@fas.harvard.edu
%
%Adaptations:
%1) Correction for bias in the coherence is done automatically as opposed to as a user option.
%2) Data format is matrix instead of vector to allowed for repeated measurements.
%3) Incorporation of averaging of spectra, coherence, and phase estimates across trials.
%4) Huybers plotting and statistical calculations, including Monte Carlo estimation, have been
removed.
%5) Statistics are now calculated using: Bootstrap_coherences.m, associated files, and the
Matlab
statistics toolbox.
%6) Plots are generated after the bootstrapping procedure.
%7) Multitaper fourier transforms are included as outputs.
%8) Adjustment of the phase estimates to improve continuity has been included.
%9) Code and commenting have been changed accordingly.
%
%Adapted by:
%Matthew J. McGinley
%Oregon Health & Science University, 2009
%matthew.j.mcginley@gmail.com
function [f, c_ave, ph_ave, c, ph, fkx, fky] = cmtmMM(x,y,dt,NW,adj)
```

cohbiasQ.m

```
%check input
if nargin<2, help cmtmMM; return; end;
if nargin<3, dt=1; end;
if nargin<4, NW=4; end;
if nargin<5, adj=1; end;
if isempty(NW), NW=4;end;
if isempty(dt), dt=1;end;
if NW<1.5, disp('Warning: NW must be greater than or equal to 1.5'); return; end;
if length(x)~=length(y), disp('Warning: the lengths of x and y must be equal.'); return; end;
%define some parameters
[N,m] = size(x);
k = min(round(2*NW),N);
k = max(k-1,1);
f = (0:1/(N*dt):1/dt-1/(N*dt))';
v = (2*NW-1); %approximate degrees of freedom
pls = 2:(N+1)/2+1; %values for 'cut to one-sided' spectra
if rem(size(y,1),2)==1; pls=pls(1:end-1); end;
disp(['Number of tapers: ',num2str(k)]);
%Compute the discrete prolate spheroidal sequences (requires the Matlab Signal Processing
toolbox).
[E,V]=dpss(N,NW,k);
disp('-------------------------');
fkx_uncut = zeros(N,k,m);
fky_uncut = zeros(N,k,m);
```

```
ph_uncut = zeros(N,m);

c_uncut = zeros(N,m);

for i = 1:m

%De-mean for 'vari' calculations. Does not affect DFT estimates (Priestley, 1981; pp. 661-662).

x_temp=x(:,i)-mean(x(:,i),1);

y_temp=y(:,i)-mean(y(:,i),1);

%Compute the windowed DFTs.

fkx_temp=fft(E(:,1:k).*x_temp(:,ones(1,k)),N);

fky_temp=fft(E(:,1:k).*y_temp(:,ones(1,k)),N);

Pkx=abs(fkx_temp).^2;

Pky=abs(fky_temp).^2;

%Iteration to determine adaptive weights:

for i1=1:2,

if i1==1, vari=x_temp'*x_temp/N; Pk=Pkx; end;

if i1==2, vari=y_temp'*y_temp/N; Pk=Pky; end;

P = (Pk(:,1)+Pk(:,2))/2; % initial spectrum estimate

Ptemp= zeros(N,1);

P1 = zeros(N,1);

tol = .0005*vari/N; % usually within 'tol'erance in about three iterations, see equations from [2]

(P&W pp 368-370).

a = vari*(1-V);

while sum(abs(P-P1)/N)>tol

b=(P*ones(1,k))./(P*V'+ones(N,1)*a'); % weights

wk=(b.^2).*(ones(N,1)*V'); % new spectral estimate

P1=(sum(wk'.*Pk')./ sum(wk'))';
```

```
Ptemp=P1; P1=P; P=Ptemp; % swap P and P1
end
if i1==1,
fkx_temp=sqrt(k)*sqrt(wk).*fkx_temp./repmat(sum(sqrt(wk'))',1,k);
Fx(:,i)=P; %Power density spectral estimate of x
fkx_uncut(:,:,i)=fkx_temp;
end;
if i1==2,
fky_temp=sqrt(k)*sqrt(wk).*fky_temp./repmat(sum(sqrt(wk'))',1,k);
Fy(:,i)=P; %Power density spectral estimate of y
fky_uncut(:,:,i)=fky_temp(:,:);
end;
end;
Cxy_temp= sum([fkx_temp.*conj(fky_temp)]');
ph_temp = angle(Cxy_temp)*180/pi;
c_temp = abs(Cxy_temp)./sqrt(sum(abs(fkx_temp').^2).*sum(abs(fky_temp').^2));
c_temp = cohbias(v,c_temp); %correct for the bias of the coherence estimate
ph_uncut(:,i) = ph_temp;
c_uncut(:,i) = c_temp;
end;
c_ave = mean(c_uncut,2);
for i = 1:m
c_complex(:,i)=squeeze(sum(fkx_uncut(:,:,i).*conj(fky_uncut(:,:,i)),2))./sqrt(squeeze(sum(fkx_un
cut(:,:,
i).*conj(fkx_uncut(:,:,i)),2)).*squeeze(sum(fky_uncut(:,:,i).*conj(fky_uncut(:,:,i)),2)));
```

```
end
c_complex = mean(c_complex,2);
ph_ave = angle(c_complex)*180/pi;
%Cut to one-sided estimates
f = f(pls)';
c_ave = c_ave(pls);
ph_ave=ph_ave(pls);
fkx = zeros(size(fkx_uncut(pls,:,:)));
fky = fkx;
for i = 1:m
c(:,i)=c_uncut(pls,i);
ph(:,i)=ph_uncut(pls,i);
for j = 1:v
fkx(:,j,i) = fkx_uncut(pls,j,i);
fky(:,j,i) = fky_uncut(pls,j,i);
end
end
% Adjust phase estimates to avoid 'wraparound'
if adj == 1
ph_ave = phase_smooth(ph_ave);
end
%function [cu]=cohbiasQ(v,cb);
%
%Corrects for the bias inherent to coherence estimates. Note the Matlab
%function cohere.m returns squared-coherence, and the square-root should
```

```
%be used. Coherence below the minimum expected value returns a zero.
%
%Requires the file cohbiasQ.mat. If the file does not exist,
%prompts whether it should be created -- note the calculation
%takes roughly an hour on a 2 GHz machine (i.e. it should be
%easier to get the file from http://web.mit.edu/~phuybers/www/XCM/index.html.)
%
%
%inputs: v - degrees of freedom, single value or vector (2 <= n <= 50)
% cb - biased coherence estimate, single value of vector (0 <= c <= 1).
%
%outputs: cu - unbiased cohernce estimate (always less than cb).
%
%
%Peter Huybers
%phuybes@mit.edu
%MIT, 2003.
function [cu]=cohbiasQ(v,cb)
if nargin<2, help cohbias; return; end;
if v<2, disp('Warning: degress of freedom must be greater or equal to two.'); return; end;
if cb<0 | cb>1, disp('Warning: biased coherence should be between zero and one, inclusive.');
return;
end;
if v>50, disp('using 50 degrees of freedom'); v=50; end;
if nargin==0; help cohbias.m; return; end;
```

```
if exist('cohbiasQ.mat')==0;
%Cohbias.mat file should be down-loaded with cmtm.m and cohbias.m
%The routine is included primarily to show how it was created.
n=2:1:50;
c=.1:.0001:1;
disp('-- The file cohbias.mat does not exist within the path.');
qans=input('-- To create this file now enter ''y'' or to skip ''n''. \n--> ','s');
if strncmpi(qans,'y',1);
z=0:.1:1;
for i3=1:length(n);
disp(n(i3)),
for i2=1:length(c)-1;
for i1=1:length(z),
A(1)=1;
%Calculated according to: Amos and Koopmans, "Tables of the distribution of the
%coefficient of coherence for stationary bivariate Gaussian processes", Sandia
%Corporation, 1963
%
%Also see the manuscript of Wunsch, C. "Time-Series Analysis. A Heuristic Primer".
for k=1:n(i3)-1;
A(k+1)=A(k)*(n(i3)-k)*(2*k-1)/((2*n(i3)-(2*k+1))*k)*((1-c(i2)*z(i1))/(1+c(i2)*z(i1)))^2;
end;
f(i1)=2*(n(i3)-1)*(1-c(i2)^2)^n(i3)*z(i1)*(1-z(i1)^2)^(n(i3)-2)/((1+c(i2)*z(i1))*(1-
c(i2)*z(i1))^(2*n(i3)-1))...
*gamma(n(i3)-.5)/(sqrt(pi)*gamma(n(i3)))*sum(A);
```

```
end;
%Use a quadratic Newton-Cotes methods to determine the cumulative sum
for i1 = 2:length(f)/2;
M(i1) = [f(2*(i1-1)+1) + 4*f(2*i1) + f(2*i1+1)]*z(2*i1);
end
expect(i3,i2)=sum([M 1])/(6*(length(M)));
end;
expect(i3,i2+1)=1;
end;
save cohbiasQ.mat expect n c;
else %if skip cohbias.mat calculation
expect=repmat(c,length(n),1);
end; %stop qans condition
else %if cohbias.mat already exists
load cohbiasQ.mat expect n c;
end; %stop cohbias calculation
cb=cb(:);
c=c(:);
n=n(:);
v=v(:);
ec = zeros(length(c),1);
for i=1:length(c);
ec(i)=interp1q(n,expect(:,i),v);
end;
cu = zeros(length(cb),1);
```

```
for i=1:length(cb);

cu(i)=interp1q(ec,c,cb(i));

end;

cu=cu(:);

pl=find(isnan(cu)==1 & cb<1 & cb>=0); %If cu is NaN while cb is between (0,1)

cu(pl)=0;
```

ph_mean_boot.m

```
function [ph_boot] = ph_mean_boot(fkx_i,fky_i,ph_mean);

fkx_i = fkx_i';

fky_i = fky_i';

Sxy=squeeze(sum(conj(fky_i).*fkx_i,1));

Sx=squeeze(sum(conj(fkx_i).*fkx_i,1));

Sy=squeeze(sum(conj(fky_i).*fky_i,1));

Sxy=squeeze(mean(Sxy));

Sx=squeeze(mean(Sx));

Sy=squeeze(mean(Sy));

ph_boot = angle(Sxy)*180/pi;

[ph_boot] = phase_correct(ph_boot,ph_mean);
```

ph_trial_boot.m

```
function [ph_boot] = ph_trial_boot(fkx_i,fky_i,ph_ave)

fkx_i = fkx_i';

fky_i = fky_i';

m = size(fkx_i,2);

for i = 1:m

Sxy_temp(i)=squeeze(sum(fkx_i(:,i).*conj(fky_i(:,i)),1));

Sx_temp(i)=squeeze(sum(fkx_i(:,i).*conj(fkx_i(:,i)),1));

Sy_temp(i)=squeeze(sum(fky_i(:,i).*conj(fky_i(:,i)),1));

c_complex(i)=Sxy_temp(i)./sqrt(Sx_temp(i).*Sy_temp(i));

end

c_complex = mean(c_complex);

ph_boot = angle(c_complex)*180/pi;

[ph_boot] = phase_correct(ph_boot,ph_ave);
```

phase_correct.m

```
function [ph_new] = phase_correct(ph_old,ph_ref)

length = size(ph_old);

for i = 1:length

value = ph_old(i);

value_high = ph_old(i)+360;

value_highest = ph_old(i)+720;

value_low = ph_old(i)-360;

value_lowest = ph_old(i)-720;

diff = abs(value-ph_ref(i));

diff_high = abs(value_high-ph_ref(i));

diff_highest = abs(value_highest-ph_ref(i));

diff_low = abs(value_low-ph_ref(i));

diff_lowest = abs(value_lowest-ph_ref(i));

if diff_high < diff

ph_old(i) = value_high;

end

if diff_low < diff

ph_old(i) = value_low;

end

if diff_highest < diff_high

ph_old(i) = value_highest;

end

if diff_lowest < diff_low

ph_old(i) = value_lowest;
```

```
end

end

ph_new = ph_old;
```

phase_smooth.m

```
function [ph_new] = phase_smooth(ph_old)

length = size(ph_old);

for i = 1:length-1

value = ph_old(i+1);

value_high = ph_old(i+1)+360;

value_low = ph_old(i+1)-360;

diff = abs(value-ph_old(i));

diff_high = abs(value_high-ph_old(i));

diff_low = abs(value_low-ph_old(i));

if diff_high < diff && diff_high < 180

ph_old(i+1) = value_high;

end

if diff_low < diff && diff_low < 180

ph_old(i+1) = value_low;

end

end

ph_new = ph_old;
```

Simplex_latency_adjust.m

```
% To compute latency corrected currents: load currents and time files into the workspace, then
run
this m file.
tic;
m = 3000;
%x0 = x_init(currentsA);
f = @(x)slide_cov_simplex(x,currentsA,currentsB,time,m);
[x,fval,exitflag,output] = fminsearch(f,x0);
[COR,COV,TwoSD,Lags,AdjCurrA,AdjCurrB] = slide_cov_ts(currentsA,currentsB,time,m,x);
toc
```

slide_cov_simplex.m

```
function [max_corr] = slide_cov_simplex(x,currentsA,currentsB,time,m)

m_full = size(currentsA,1);

n = size(currentsA,2);

x_int = round(x);

x_min = min(x_int);

parfor i = 1:n

x_int(i) = x_int(i)-x_min;

end

x_max = max(x_int);

m_new = m_full-x_max;

parfor i = 1:n

x_rest(i) = x_max - x_int(i);

end

currentsA_long = reshape(currentsA,m_full*n,1);

currentsB_long = reshape(currentsB,m_full*n,1);

for i = 1:n

currentsA_long(1+m_new*(i-1):x_int(i)+m_new*(i-1),:) = [];

currentsA_long(m_full-x_rest(i)-x_int(i)+1+m_new*(i-1):m_full-x_int(i)+m_new*(i-1),:) = [];

currentsB_long(1+m_new*(i-1):x_int(i)+m_new*(i-1),:) = [];

currentsB_long(m_full-x_rest(i)-x_int(i)+1+m_new*(i-1):m_full-x_int(i)+m_new*(i-1),:) = [];

end

shaped_currentsA = reshape(currentsA_long,m_new,n);

shaped_currentsB = reshape(currentsB_long,m_new,n);

shaped_time = time;
```

```
for i = 0:m_new-(m+1)
shaped_currentsA(m_new-i,:) = [];
shaped_currentsB(m_new-i,:) = [];
shaped_time(m_new-i,:) = [];
end
parfor i = 1:n
COR_all(:,i) = xcorr(shaped_currentsA(:,i),shaped_currentsB(:,i));
end
COR = mean(COR_all,2);
AveCurrentA = mean(shaped_currentsA,2);
%AveSqrdA = AveCurrentA.^2;
AveCurrentB = mean(shaped_currentsB,2);
%AveSqrdB = AveCurrentB.^2;
%for i = 1:n
% DeviationA(:,i) = (currentsA(:,i)-AveCurrentA).^2;
% DeviationB(:,i) = (currentsB(:,i)-AveCurrentB).^2;
%end
%VarianceA = (sum(DeviationA,2))./(n-1);
%VarianceB = (sum(DeviationB,2))./(n-1);
%TwoSD =
2*(((xcorr(VarianceA,VarianceB)+xcorr(AveSqrdA,VarianceB)+xcorr(VarianceA,AveSqrdB))/(n
)).^(1/
2));
COV = COR - xcorr(AveCurrentA,AveCurrentB);
%DelTime = (time(m)-time(1))/(m-1);
```

```
%Lags = ([-m+1:1:m-1].*DelTime).';

%plot(Lags,-TwoSD,Lags,TwoSD,Lags,COV)

max_corr = max(abs(COV));
```

slide_cov_ts.m

```
function [COR,COV,TwoSD,Lags,AdjCurrA,AdjCurrB] =
slide_cov_ts(currentsA,currentsB,time,m,x)
m_full = size(currentsA,1);
n = size(currentsA,2);
x_int = round(x);
x_max = max(x_int);
m_new = m_full-x_max;
for i = 1:n
x_rest(i) = x_max - x_int(i);
end
currentsA_long = reshape(currentsA,m_full*n,1);
currentsB_long = reshape(currentsB,m_full*n,1);
for i = 1:n
currentsA_long(1+m_new*(i-1):x_int(i)+m_new*(i-1),:) = [];
currentsA_long(m_full-x_rest(i)-x_int(i)+1+m_new*(i-1):m_full-x_int(i)+m_new*(i-1),:) = [];
currentsB_long(1+m_new*(i-1):x_int(i)+m_new*(i-1),:) = [];
currentsB_long(m_full-x_rest(i)-x_int(i)+1+m_new*(i-1):m_full-x_int(i)+m_new*(i-1),:) = [];
end
currentsA = reshape(currentsA_long,m_new,n);
currentsB = reshape(currentsB_long,m_new,n);
for i = 0:m_new-(m+1)
currentsA(m_new-i,:) = [];
currentsB(m_new-i,:) = [];
time(m_new-i,:) = [];
```

```
end
AdjCurrA = currentsA;
AdjCurrB = currentsB;
for i = 1:n
COR_all(:,i) = xcorr(currentsA(:,i),currentsB(:,i));
end
COR = mean(COR_all,2);
AveCurrentA = mean(currentsA,2);
AveSqrdA = AveCurrentA.^2;
AveCurrentB = mean(currentsB,2);
AveSqrdB = AveCurrentB.^2;
for i = 1:n
DeviationA(:,i) = (currentsA(:,i)-AveCurrentA).^2;
DeviationB(:,i) = (currentsB(:,i)-AveCurrentB).^2;
End
VarianceA = (sum(DeviationA,2))./(n-1);
VarianceB = (sum(DeviationB,2))./(n-1);
TwoSD =
2*(((xcorr(VarianceA,VarianceB)+xcorr(AveSqrdA,VarianceB)+xcorr(VarianceA,AveSqrdB))/(n
)).^(1/
2));
COV = COR - xcorr(AveCurrentA,AveCurrentB);
DelTime = (time(m)-time(1))/(m-1);
Lags = ([-m+1:1:m-1].*DelTime).';
plot(Lags,[-TwoSD,TwoSD,COV]);
```

x_init.m

```
function [x0] = x_init(currentsA)

n = size(currentsA,2);

[C,I] = max(abs(currentsA));

x_min = min(I);

x0 = zeros(1,n);

for i = 1:n

x0(i)= I(i)-x_min;

end

x0 = transpose(x0);
```

XcorrAve.m

```
function [peaks, corrs, corr_ave, lags, amps,tamp] = XcorrAve(currentsA,currentsB,time)

m = size(currentsA,1);

n = size(currentsA,2);

DelTime = time(2)-time(1);

lags = ([-m+1:1:m-1].*DelTime).';

for i=1:n

corrs(:,i)= xcorr(currentsA(:,i),currentsB(:,i));

end

corr_ave = mean(corrs,2);

[C,I] = max(corrs,[],1);

for i=1:n

peaks(i)=lags(I(i));

[amps(i,1),index_amp(i,1)]=min(currentsA(:,i));

[amps(i,2),index_amp(i,2)]=min(currentsB(:,i));

end

for j=1:2

for i=1:n

tamp(i,j)=time(index_amp(i,j))-500;

end

end

subplot(221); plot(currentsA)

subplot(223); plot(currentsB)

subplot(222); plot(corrs)

subplot(224); plot(lags,corr_ave)
```